Run-Around Membrane Energy Exchanger Performance and Operational Control Strategies

A Thesis Submitted to the College of

Graduate Studies and Research

In Partial Fulfillment of the Requirements

For the Degree of Master of Science

In the Department of Mechanical Engineering

University of Saskatchewan

Saskatoon

By

Blake Erb

Permission to Use

In presenting this thesis in partial fulfillment of the requirements for a Postgraduate degree from the University of Saskatchewan, I agree that the Libraries of this University may make it freely available for inspection. I further agree that permission for copying of this thesis in any manner, in whole or in part, for scholarly purposes may be granted by the professor or professors who supervised my thesis work or, in their absence, by the Head of the Department or the Dean of the College in which my thesis work was done. It is understood that any copying or publication or use of this thesis or parts thereof for financial gain shall not be allowed without my written permission. It is also understood that due recognition shall be given to me and to the University of Saskatchewan in any scholarly use which may be made of any material in my thesis.

Requests for permission to copy or to make other use of material in this thesis in whole or part should be addressed to:

Head of the Department of Mechanical Engineering

University of Saskatchewan

Saskatoon, Saskatchewan (S7N 5A9)

ABSTRACT

A run-around membrane energy exchanger (RAMEE) is a novel energy exchanger that is capable of transferring both heat and moisture, which can significantly reduce the energy required to condition outdoor ventilation air. The RAMEE uses a liquid desiccant to transfer both heat and moisture between two remote air streams, making it appropriate for many applications, including building HVAC retro-fits. Both initial system start-up and changing outdoor conditions require time for the desiccant to undergo changes in both temperature and concentration, and can cause significant transient delays in system performance. Under some conditions, these transients may be beneficial by increasing the system performance. However under some conditions, the transient delays can cause a substantial decrease in performance.

This thesis focuses on the development of control strategies that can be used to reduce unwanted transient delays. In order to develop these control strategies, the performance of a RAMEE is first investigated using both experimental and numerical methods. The transient numerical and experimental effectiveness results show satisfactory agreement, with a maximum root mean squared error of 10%. Both the numerical and experimental data show that a long transient time of several hours, or even several days, can occur upon initial system start-up.

The numerical model is used to investigate several control strategies to reduce unwanted transient delays. The control strategies investigated are: solution and air flow control, air flow bypass, solution temperature control, and solution concentration control. The solution and air flow control are shown to reduced the start-up transient time by up to 11%, but require either a reduction in air flow or an increase in solution

pumping costs. Air flow bypass proves to be a better option which provides a 16% reduction in transient time, and only requires that a bypass damper be provided for each exchanger. Solution temperature control is capable of essentially eliminating the thermal transient time (time required for the solution to reach operating temperature), but the thermal transient time is found to be a minor contributor to the overall transient time (time required for the solution to reach operating temperature and concentration) when the initial concentration of the solution is different than the steady-state concentration. When thermal and moisture transients exist, total transient times may be over 18 days. A practical temperature and concentration control strategy is developed, which can reduce transient delays by over 90% and increase performance during variable outdoor weather conditions.

ACKNOWLEDGEMENTS

I would like to express my sincere gratitude to my supervisors Professor C. J. Simonson and Professor Emeritus R.W. Besant. Thank you for your guidance and inspiration throughout this research. It was a pleasure to conduct this research with your support, leadership, and friendship.

I wish to thank Chris James and Dave Deutscher for their assistance throughout the experimental component of this research. I would also like to thank my fellow graduate students who have also worked on this project, either before or during my studies. Their hard work has contributed toward my research in many ways.

I would like to acknowledge the financial assistance from the Department of Mechanical Engineering, National Science and Engineering Research Council of Canada (NSERC), the Russell William Haid Memorial Scholarship, the George Ira Hanson Scholarship, the American Society of Heating, Refrigerating, and Air-Conditioning Engineers (ASHRAE) Grant-In-Aid, and Venmar CES Inc, Saskatoon.

DEDICATION

I dedicate this thesis to my wife, Jackie, and my parents, Ellery and Gloria.

Thank you very much for your love and encouragement throughout my studies.

I could not have succeeded without your support.

TABLE OF CONTENTS

Page

LIST OF TABLES

Table **Page**

LIST OF FIGURES

Figure **Page**

NOMENCLATURE

Acronyms

AHRI	Air-Conditioning, Heating and Refrigeration Institute
ANSI	American National Standards Institute
ASHRAE	American Society of Heating, Refrigerating and Air-Conditioning Engineers
ASME	American Society of Mechanical Engineers
AWG	American Wire Gauge
CRD	Collaborative Research and Development
HVAC	Heating, Ventilation and Air-Conditioning
ISO	International Organization for Standardization
LAMEE	Liquid-to-Air Membrane Energy Exchanger
NSERC	National Science and Engineering Research Council of Canada
PTFE	Polytetrafluoroethylene
RAHE	Run-Around Heat Exchanger
RAMEE	Run-Around Membrane Energy Exchanger
RAMEE-TA	Run-Around Membrane Energy Exchanger Test Apparatus
RH	Relative Humidity
RTD	Resistance Temperature Detector
VOCs	Volatile organic compounds

English Symbols

A	membrane surface area, m^2
AAD	average absolute difference
B	bias error
C	heat capacity rate, W/K

CC_{Cr^*}	Cr* control criterion
C_d	orifice plate discharge coefficient
C_p	specific heat capacity, J/(kg·K)
Cr*	ratio of solution to air heat capacity rates, (W/K)/(W/K)
C_{Salt}	concentration of salt solution (kg of salt per kg of solution), %
D_{pipe}	inside pipe diameter, m
d_{Air}	air channel thickness, m
$d_{orifice}$	orifice plate opening diameter, m
d_{Sol}	solution channel thickness, m
d_x	control volume width, m
d_y	control volume height, m
e_c	energy convergence criterion
H	enthalpy, J/kg
h_{Air}	convective heat transfer coefficient between the air and membrane, W/(m^2·K)
h_{fg}	heat of vaporization, m^2/s^2
h_m	convective mass transfer coefficient, kg/(m^2·s)
$h_{m,Sol}$	convective mass transfer coefficient between the membrane and the solution, kg/(m^2·s)
h_{Sol}	convective heat transfer coefficient between the solution and the membrane, W/(m^2·K)
k	membrane thermal conductivity, W/(m·K)
k_m	membrane water vapor permeability, kg/(m·s)
m_c	mass convergence criterion
$\dot{m}$	mass flow rate, kg/s

$\dot{m}_{addition/removal}$	the rate of water addition/removal using concentration control, kg/s
$\dot{m}_{RAMEE,QSS}$	rate of moisture transfer by the RAMEE at quasi-steady state
$\dot{m}''$	mass flux rate of water, kg/(m^2·s)
$\dot{m}^*$	the ratio of mass flow rate addition/removal to the mass transferred by the RAMEE at quasi-steady state, (kg/s)/(kg/s)
N	the number of independent variables/data points
NTU	number of transfer units
P	pressure, Pa
$q_{concentration,heating}$	the heating/cooling capacity of the external solution concentration control system, W
$q_{External,Sol}$	the heating/cooling capacity of the external solution temperature control system, W
$q_{RAMEE,QSS}$	the amount of energy transferred between the supply and exhaust air streams by the RAMEE at quasi-steady state, W
q''	heat flux rate, W/m^2
q*	ratio of external solution heating/cooling capacity to the RAMEE energy transfer at quasi-steady state, W/W
$q^*_{concentration}$	ratio of heating/cooling capacity of external solution concentration control to the RAMEE energy transfer at quasi-steady state, W/W
R	a variable given for a calculated property
RMSE	root mean square error
RSS	root-sum-squares
S	standard deviation
T	bulk mean temperature, K
$T_{Sol,Mem}$	temperature of the solution at the membrane surface, K

t	time, (seconds, minutes or hours)
$t_{thermal}$	thermal transient time, (seconds, minutes or hours)
t^*	Student-t distribution constant
U	overall heat transfer coefficient, $W/(m^2 \cdot K)$
U_m	overall mass transfer coefficient, $kg/(m^2 \cdot s)$
U_R	uncertainty in property R.
$U_{\bar{x}_i}$	the uncertainty in the independent variable x_i
$U_{95\%}$	95% confidence interval uncertainty
V	velocity, m/s
W_{Air}	air humidity ratio, kg/kg
$W_{Sol,Mem}$	humidity ratio of the air that is in equilibrium with the solution at the membrane surface, kg/kg
x,y,z	coordinates
x_0,y_0,z_0	exchanger dimensions, m
X_{Sol}	solution mass fraction (kg of water per kg of salt), kg/kg
$X_{Sol,Mem}$	solution mass fraction at the membrane surface, kg/kg

Greek Symbols

β	ratio of orifice plate diameter to pipe diameter, m/m
Δ	difference (change in)
δ	membrane thickness, m
ε	effectiveness
ρ	density, kg/m^3
ρ_{Salt}	mass of salt per unit volume of solution, kg/m^3
τ	number of volume circulations of the solution in the exchangers
ψ_i	a sensitivity index

Subscript

Air	air stream
desired	desired supply outlet condition
E	exhaust
FC	with flow control
g	moist air
in	inlet
Indoor	indoor air conditions
Initial	initially at time=0
Lat	latent
Mem	membrane
No FC	no flow control
O	overall
out	outlet
Outdoor	outdoor air conditions
QSS	quasi-steady state
QSS@Cr*=3	quasi-steady state if Cr* is kept at constant 3
RAMEE	Run-Around Membrane Energy Exchanger
S	supply
Salt	pure salt
Sen	sensible
Sol	solution
SS	steady state
Tot	total

CHAPTER 1

INTRODUCTION

1.1 Overview of Building Ventilation

Supplying fresh air into a building is crucial to providing a healthy environment for building occupants who often spend up to 95% of their time indoors (AHSRAE, 1985; and Oakley, 1972). Fresh air reduces the risk of contracting air transmitted illnesses and can reduce the effects of indoor pollutants such as volatile organic compounds (VOCs) which can be found in many products such as cleaners, paints, carpet, office furniture, and computer printers. In addition, providing fresh air has been found to play an important role in worker productivity (Fang et al. 2000; and Kosonen and Tan 2004). The current recommended ventilation rate for an office building is at least 8.5 L/s (18 cfm) per person (ANSI/ASHRAE Std. 62.1, 2004). However, providing this fresh air at comfortable temperature and humidity levels requires a lot of energy, and expensive equipment. In fact, up to 50% of the energy consumed in a building is used to deliver conditioned fresh air (D&R International, 2009). In order to supply fresh air into the building without pressurizing the space, the same volume of air needs to be exhausted out of the building. This exhaust air has already been conditioned to the comfortable or near comfortable temperature and humidity (ANSI/ASHRAE Std. 55, 2004). An air-to-air energy exchanger can be used to recover some of the energy in the exhaust air to pre-condition the supply air.

1.2 Air-to-Air Energy Recovery

An air-to-air energy recovery device transfers energy between the supply and exhaust air streams, resulting in the supply air becoming preconditioned closer to the desired temperature and humidity in the space. During hot and humid outdoor conditions, the air-to-air energy recovery device cools and dehumidifies the supply air. During cold and dry conditions, the air-to-air energy recovery device heats and humidifies the supply air. Figure 1.1 shows an example of how a typical air-to-air energy recovery device can precondition hot and humid outdoor air closer to the desired 24°C temperature and 9.3 g/kg humidity ratio (air moisture content in grams of water per kilogram of dry air)(50% RH) for summer conditions. By preconditioning the supply air, the auxiliary energy needed to fully condition the air is reduced, and the size and capital cost of heating and cooling equipment can be significantly reduced (Fauchoux et al., 2007; Asiedu et al., 2004; and Asiedu et al., 2005).

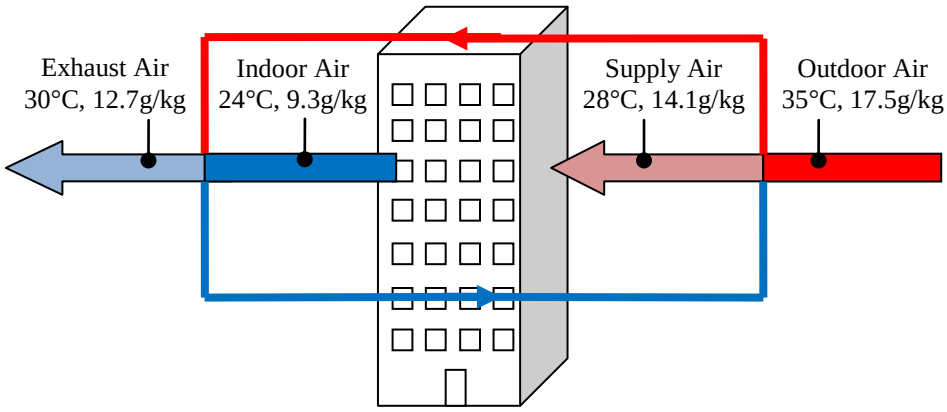

Figure 1.1: Changes in air conditions for an energy exchanger during summer outdoor conditions when the exchanger effectiveness is 50%.

The performance of an air-to-air energy exchanger is typically expressed in terms of the systems effectiveness, which is a measure of how much energy is transferred compared to the maximum possible amount of energy that could be

transferred between the indoor air leaving the building (exhaust air stream) and the outdoor air entering the building (supply air stream). The example given in Figure 1.1 has an effectiveness of 50%, which means that 50% of the available energy is transferred from the supply air stream to the exhaust air stream, and the remaining 50% of this available energy must be removed using cooling equipment The exchanger effectiveness can be calculated based on the temperature and humidity values given in Figure 1.1, and the equations that will be presented in Chapter 2..

There are several different types of air-to-air energy recovery devices currently on the market. Many of them, such as heat pipes (Wu et al., 1997), flat plate heat exchangers (Romie, 1983; Mishra et al., 2004; Spiga and Spiga, 1987; and Srihari and Das, 2008), and glycol run-around loops (Johnson et al., 1995; and Fan et al., 2005) are capable of transferring heat (sensible energy) only. Others such as enthalpy wheels (Simonson, 2007), enthalpy plates (Zhang and Niu, 2002), and twin tower enthalpy recovery loops (Ali et al., 2004; Mesquita et al., 2006; and Park et al., 1994) are capable of transferring both heat and moisture (sensible and latent energy).

Larson (2006) defined a new method to classify the current types of air-to-air energy recovery devices. Larson not only divided them based on whether they transfer heat only or heat and moisture, but also based on their required duct configuration. Some devices require the supply and exhaust air ducts to be located adjacent to each other, while others allow for remote location of the air streams. Requiring adjacent supply and exhaust air ducts is often a problem for retrofit applications, where re-ducting the supply and exhaust air streams to be adjacent is either very costly or impossible due to space constraints. However, the retro-fit application market is large

due to a building replacement rate of less than 3%. Figure 1.2 shows some of the most common air-to-air energy recovery devices divided into these four classifications.

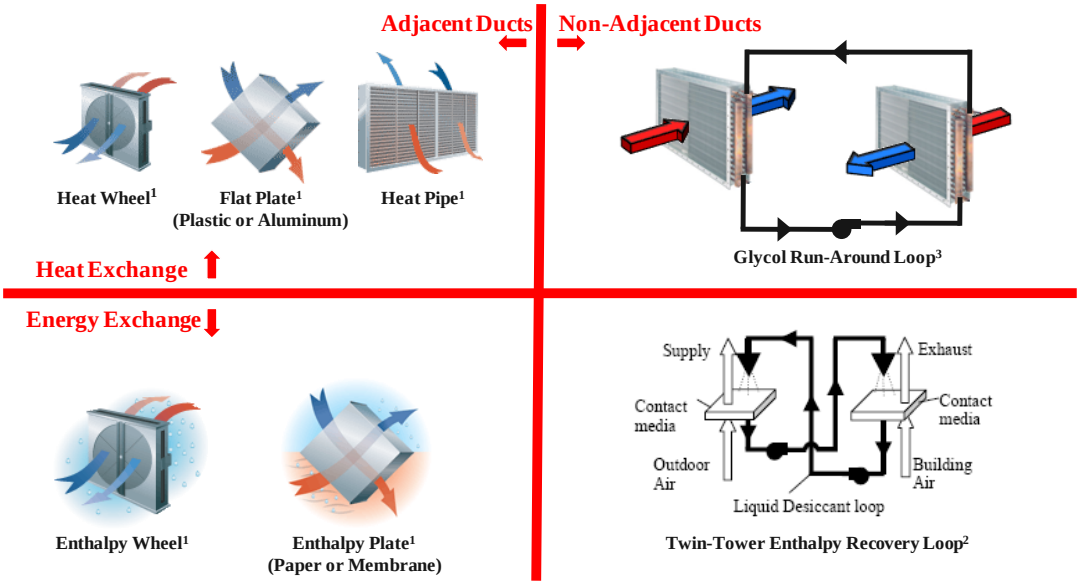

Figure 1.2: Four main categories of air-to-air energy exchange technology and examples for each. ([1]Venmar CES (2009); [2]Larson (2006); [3]Keep Right Refrigeration (2009))

The ideal method of energy recovery is one that is capable of transferring both heat and moisture (ASHRAE, 2004). During hot and humid conditions such an exchanger is capable of transferring up to four times more energy than an exchanger capable of sensible heat transfer only. Therefore, energy recovery devices such as enthalpy wheels, enthalpy plates, and twin tower enthalpy recovery loops have the best performance and are often chosen over sensible only exchangers. However, each method of air-to-air energy recovery has both benefits and disadvantages, and selection requires careful consideration of the application.

1.2.1 Flat Plate Heat Exchangers

Flat plate heat exchangers are the most basic type of energy recovery equipment, based on their simple design and inexpensive cost. The exchanger is comprised of thin plates that separate the supply and exhaust air streams into closely spaced flow channels.

The air streams typically flow through these channels in a cross-flow orientation, where the supply air stream flows perpendicular relative to the exhaust air stream. Heat is transferred from one air stream, through the thin plate, to the other air stream. These thin plates are often made from aluminum or plastic. Plastic plates are made from corrugated material to provide consistent flow channels for each air stream ranging from 2.5 mm to 12.5 mm wide, depending on the desired air flow rate (ASHRAE, 2000). Aluminum plates are dimpled to achieve the same spacing. Figure 1.3 shows a typical flat plate heat exchanger.

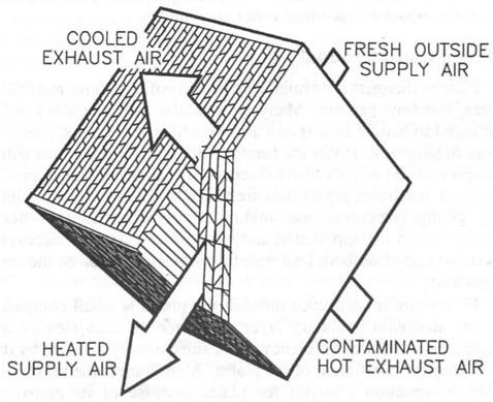

Figure 1.3: Flat plate heat exchanger (ASHRAE, 2000)

Flat plate heat exchangers are widely used in both residential and commercial ventilation air-to-air energy recovery markets, and therefore have a predictable performance established by research and testing. Most heat and mass transfer text books contain correlations that quantify the steady-state performance of flat plate heat exchangers (Incropera and Dewitt, 2002). Research has also been completed on the transient performance of flat plate heat exchangers. Romie (1983) developed an analytical solution for the transient response of flat plate exchangers, while Srihari and Das (2008) used a finite difference method to numerically determine the transient behavior of these exchangers. Srihari and Das (2008) also compared their results with

experimental data and were able to accurately predict the expected time required to reach steady state, as well as changes in response time for non-uniform flow conditions.

Flat plate heat exchangers have the advantage of high heat transfer performance (50-80% sensible effectiveness), while causing a relatively low airflow pressure drop (ASHRAE, 2000). These exchangers contain no moving parts and are therefore virtually maintenance free, except for filter replacements and the occasional cleaning. Flat plate heat exchangers have the drawback of only providing heat transfer, and require the supply and exhaust air ducts to be adjacent to each other. Therefore, flat plate exchangers are best suited for newly constructed buildings. Flat plate exchangers are also best suited for climates where there is a low moisture transfer potential. Residential air-to-air energy recovery units often utilize the flat plate exchanger for its simplicity and inexpensive construction.

1.2.2 Enthalpy Plate Exchangers (Hygroscopic Flat Plate)

Enthalpy plate exchangers are identical in construction and orientation as the previously mentioned flat plate heat exchanger. The only difference is the thin flat plate is replaced with a hygroscopic membrane that allows both moisture and heat transfer between the two air streams. Some common hygroscopic materials include cellulose, polymers, and synthetic membranes. The addition of moisture transfer can cause a large increase in energy transfer performance. However, having a very porous membrane can also introduce cross-leakage of air between the two air streams, increasing the amount of cross-contamination (up to 5% (ASHRAE 2000)). Cross-leakage may limit the application of the enthalpy plate exchanger, but can be minimized by choosing the proper hygroscopic material.

1.2.3 Heat Pipes

Heat pipes are sensible heat transfer devices that consist of one or several evacuated tubes which are filled with a working fluid such as a refrigerant and use a capillary wick structure (Wu et al., 1997). The supply air stream passes over one half of the tube, while the exhaust air stream passes over the other half. The warmer air causes the fluid inside the tube to evaporate on the one end of the tube (evaporator end). The resulting vapor pressure gradient inside the tube causes the vapor to travel to the other end of the tube (condenser end), where the colder air stream passes over causing the vapor to condense, releasing the latent energy of vaporization. The condensed fluid is then wicked back to the evaporator end to complete the cycle. This continuous phase change cycle can continue even when the temperature difference between the supply and exhaust air stream is small. Typical heat transfer (sensible energy) performance is moderate (45-65% sensible effectiveness (ASHRAE, 2000)) compared to the fixed-plate exchanger. Many heat pipes are equipped with a tilting option, in which the evaporator end of the tube can be lowered/raised below/above the horizontal in order to improve/impede the condensate flow back to the evaporator, to control the heat transfer rate. The heat pipe's lower performance and higher air stream pressure drop make it an unlikely choice over other methods of energy recovery. However, heat pipes are still used for special applications.

1.2.4 Thermosiphon Exchangers

Thermosiphon heat exchangers are very similar to heat pipes, except that they have no wicking structure and rely on gravity to return the condensate to the evaporator (ASHRAE, 2000). Generally, thermosiphons use a series of pipes to form an exchanger

for each air stream. The two exchangers are then coupled to each other with piping, which allows for the vapor to travel through one pipe above the coils, and condensate to travel in a pipe below the coils. This allows for separation between the exhaust and supply air streams, and requires no pumping to move either the vapor or condensate. Thermosiphon exchangers depend on nucleate boiling, and therefore require much higher temperature differences between the supply and exhaust air streams to operate compared to heat pipes (McDonald and Shivprasad, 1989). Thermosiphons are often used for solar water heating (Mathur 1990), but they do not provide a high enough performance relative to the capital cost to become commonly used HVAC equipment.

1.2.5 Heat and Enthalpy Wheels

Heat wheels and enthalpy wheels are currently the most commonly used energy exchangers for new commercial buildings, since they combine high performance with low airflow pressure drop (Shang and Besant, 2008). Both heat and enthalpy wheels are generally made from corrugated aluminum, plastic, or synthetic fiber which is wrapped around a center hub to form a wheel. This wheel is then placed so that one half is in the supply air stream and the other half is in the exhaust air stream. A small electric motor rotates the wheel, transferring the available energy between the two air streams. The heat wheel transfers only sensible energy, while the enthalpy wheel is capable of transferring both sensible and latent energy between the two air streams. The enthalpy wheel is capable of moisture transfer because the corrugated material is coated with a desiccant of either silica gel or molecular sieve, which stores/releases moisture as the humidity increases/decreases.

One disadvantage of heat and enthalpy wheels is that they require the supply and exhaust air ducts to be adjacent to each other. As stated before, this configuration may not be practical for many retro-fit applications. Both the supply and exhaust air streams must both flow through the rotating wheel. Therefore, flow channel seals must be used to separate the two air streams, and an outer peripheral seal must be used on the outer rim of the wheel while still allowing the wheel to rotate. These seals are generally made of a flexible plastic or brush material, and often result in cross-leakage if the pressure on the supply and exhaust sides are different from one another. This cross-leakage can be up to 10% (ASHRAE, 2000) which can cause unwanted contamination of the supply air. A certain amount of cross-contamination will occur due to wheel rotation carryover or by particles becoming adsorbed on the adsorbed water, desiccant material, or in the corrugated material (Zhang et al., 2008). This cross-contamination must be avoided for some HVAC applications such as hospitals, laboratories, and manufacturing facilities, where slight cross contamination can cause occupant health effects.

1.2.6 Run-Around Heat Exchanger

Run-around heat exchangers (RAHEs) consist of two liquid to air heat exchangers; one of which is placed in the supply air stream and one which is placed in the exhaust air stream. The exchangers are coupled using an aqueous glycol-water solution, and are therefore often called a glycol run-around loop. This system is capable of sensible energy transfer only, because the exchangers are made from impermeable materials such as copper or aluminum. Their performance is typically lower (55-65% sensible effectiveness (ASHRAE, 2000)) than other technologies such as the enthalpy wheel. A RAHE permits the supply and exhaust air streams to be located either

adjacent to one another, or remotely, allowing for design flexibility for both new buildings and retro-fits. The complete separation of the supply and exhaust air streams eliminates the chance of cross-contamination.

Research on RAHE systems began with a study by London and Kays (1951) who found the optimum operating condition for a RAHE. Several studies followed this pioneering effort, and the research field began to rapidly grow in the 1980's when Forsyth and Besant (1988a and 1988b) developed a procedure for analyzing and optimizing the design of the coils of a two coil RAHE system. Bennett et al. (1994a and 1994b) continued to study the RAHE system by considering a liquid bypass for part load conditions, and developed a life cycle cost procedure.

Run-around heat exchangers are often used if the supply and exhaust air streams must be located remotely, or if zero cross contamination is required. Otherwise, the run-around heat exchanger is often rejected for the better performing and lower cost enthalpy wheel or hygroscopic fixed plate.

1.2.7 Twin-Tower Enthalpy Recovery Loop

Currently there is only one type of commercial energy exchanger that is capable of transferring both sensible and latent energy, while allowing for remote supply and exhaust air ducts. This system is the twin-tower enthalpy recovery loop, and has not been a popular choice since its inception in the 1980's, due to several disadvantages resulting from using direct contact between the air streams and a liquid desiccant (ASHRAE, 2004). Allowing the liquid desiccant to come in direct contact with the air allows for high moisture transfer rates (Ali et al., 2004; Mesquita et al., 2006; and Park et al., 1994). However, a small fraction of the desiccant salt becomes entrained in the

air and is transported downstream through the air ducts. This results in poor indoor air quality and corrosion problems. Demister pads, which are porous blankets of knitted metal or plastic wire, can be used to reduce the desiccant carryover. However, they are not 100% effective and increase the capital cost of the system.

Another disadvantage of the open twin-tower enthalpy recovery loop is that the desiccant fluid is gravity fed through the air stream, which does not allow for a wide range of control over the desiccant flow rate. The result is very little control over the energy transfer rate. If desiccant solution flow rates become too large, the flow channels (pores) in the contact media become filled or nearly filled with desiccant, causing the pressure drop on the air side to increase, resulting in higher fan power to maintain adequate ventilation rates.

1.2.8 Run-Around Membrane Energy Exchanger (RAMEE) System

A novel run-around membrane energy exchanger (RAMEE) system has been proposed to eliminate the disadvantages associated with the twin-tower enthalpy recovery loop (Fan et al., 2006). The RAMEE is suited to both new building designs and the large retro-fit market, as it is able to transfer both heat and moisture (sensible and latent energy) between remote supply and exhaust air ducts, without the risk of cross contamination. In addition, the RAMEE is projected to perform competitively with other high performing devices such as enthalpy wheels and plates currently used in HVAC systems in commercial buildings. A schematic of the RAMEE system is shown in Figure 1.4.

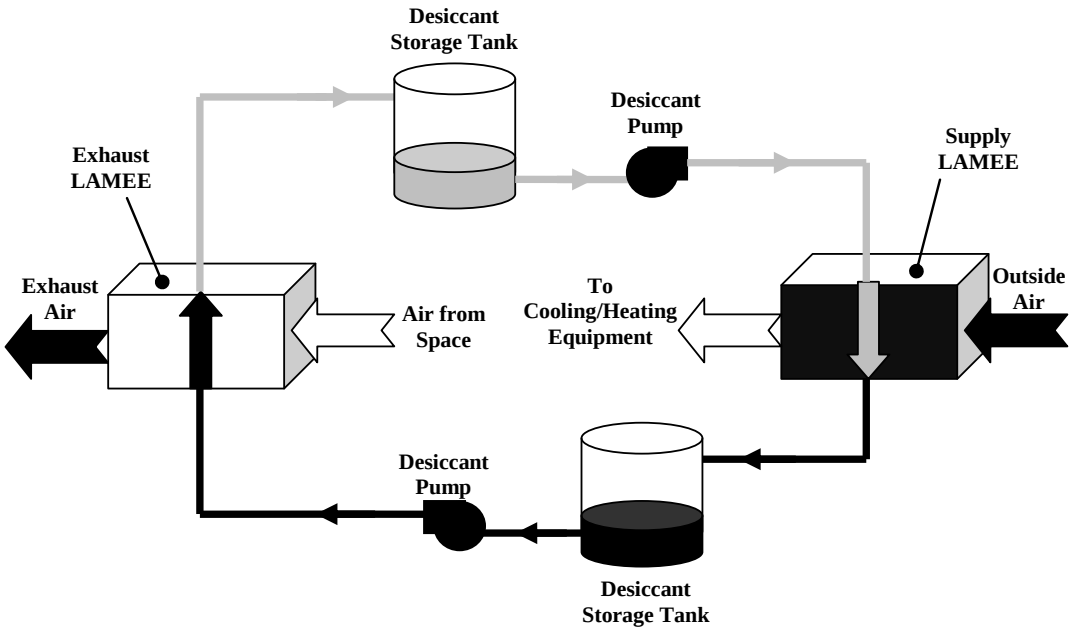

Figure 1.4: Schematic of a run-around membrane energy exchanger (RAMEE) system.

The RAMEE system is comprised of two remote liquid-to-air membrane energy exchangers (LAMEEs) coupled by a pumped liquid desiccant loop. One LAMEE is located in the supply air duct entering the building, while a second LAMEE is located in the exhaust air duct leaving the building. Each LAMEE is constructed using semi-permeable membranes that are permeable to water vapor, but impermeable to liquid water. These types of membranes include popular commercial products such as Gore-Tex®, DuPont's™ Tyvek® and 3M's™ Propore™, as well as many other polytetrafluoroethylene (PTFE), polypropylene and polyethylene membranes. The LAMEEs are coupled by a liquid desiccant loop, which transports the heat and moisture between the two exchangers. The membrane separates the liquid desiccant from the air, while still allowing both heat and water vapour transfer. Two small centrifugal pumps are used to move the desiccant-water solution through small piping between the two

exchangers. A small solution storage tank is placed upstream of the pump in each desiccant line to allow room for volume changes as the desiccant gains/losses moisture.

1.3 Past RAMEE Research

Research on the run-around membrane energy exchanger (RAMEE) began in 2002, when Professors Besant and Simonson, Department of Mechanical Engineering, University of Saskatchewan, partnered with a local HVAC company, Venmar CES Inc., to research and develop a novel system that can transfer both heat and moisture between remote supply and exhaust air streams. A NSERC Collaborative Research and Development (CRD) Grant was awarded in 2002 to fund the project, and a second CRD grant was awarded in 2008 for continuation of the project. The goal of these CRD projects was to not only research and develop an innovative product that could be sold by Venmar CES, but also to train several graduate students as will be described in the following sections.

1.3.1 First Stage Numerical Modeling (Fan, 2005)

Fan (2005) numerically modeled a RAMEE system consisting of two cross flow energy exchangers, coupled by a lithium bromide solution. The numerical model was used to determine the performance of the RAMEE system at various design conditions (e.g. exchanger size, operating flow rates). Fan found that a total effectiveness of over 70% was possible if the proper design conditions were chosen. However, Fan chose a very permeable membrane, which resulted in higher performance than may be actually achievable using cross flow exchangers.

1.3.2 Prototype #1 (Hemingson, 2005)

Hemingson (2005) tested the first prototype of the RAMEE system in order to compare experimental results with Fan's (2005) numerical work. Two cross flow exchangers were made from a high density polyethylene membrane manufactured by DuPont™ named Tyvek®, and coupled together using a lithium bromide solution. Unfortunately, this prototype could not be successfully tested, as the membrane deformed under the pressure of the solution and caused the airflow channels to become substantially blocked. There were also some issues with some of the lithium bromide solution leaking through the membrane.

1.3.3 Membrane Research (Larson, 2006)

The structural and membrane problems associated with prototype #1 together with the aim of finding a practical membrane to obtain the performance predicted by Fan (2005) initiated the membrane study of Larson (2006). Various semi-permeable membranes were considered and tested for properties such as water vapor permeability, air permeability, liquid water penetration pressure, and elastic structural properties. The ideal membrane was defined as one that had a high water vapor permeability, a high liquid penetration pressure, and a high modulus of elasticity to minimize deflections. Larson chose a polypropylene membrane and substrate composite from 3M™ called Propore™. Propore™ not only had a semi-permeable membrane with high water vapor permeability, but also contained a structural support layer. When implemented in an exchanger, Larson also recommended using an outer support screen to maintain minimum membrane deflections.

1.3.4 Counter/Cross Flow LAMEE (Vali, 2009 and Mahmud, 2009)

The performance of an energy exchanger is highly dependent on the flow configuration of the air and desiccant solution. Typically, there are two different flow configurations, cross and counter flow, as illustrated in Figure 1.5. In the cross flow configuration the desiccant solution flows perpendicular to the air (Figure 1.5a), while in the counter flow configuration the desiccant flows parallel to the air (Figure 1.5b), but in the opposite direction. The counter flow configuration can produce higher performance than the cross flow configuration (up to 15% higher effectiveness) (Vali, 2009). However, having the solution and air flow in a counter flow arrangement requires the air and solution to enter/leave at the same end of the exchanger, which causes a practical difficulty in separating the air and solution at each exchanger end. Therefore, a new configuration was studied by Vali (2009) which used a small cross flow inlet and outlet at opposite ends of the exchanger, causing the flow to be nearly counter flow, while retaining separate air and solution entrances/exits (Figure 1.5c).

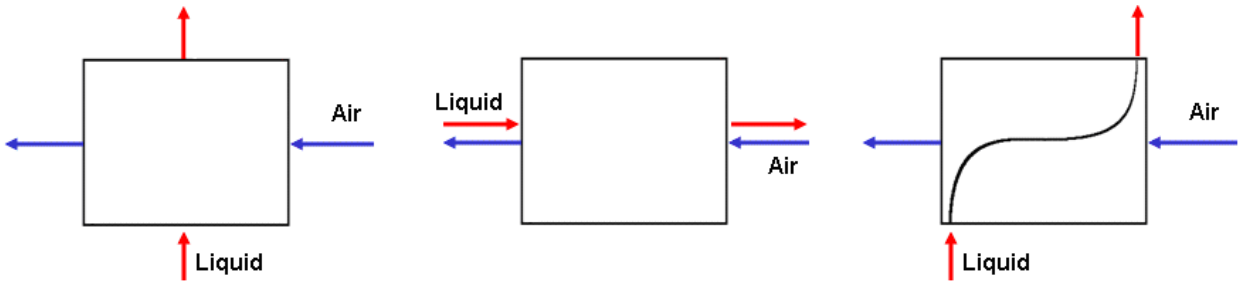

Figure 1.5: Air and solution flow configurations: (a) cross flow, (b) counter flow, and (c) counter/cross flow. (Vali, 2009)

Vali (2009) showed numerically that a RAMEE which uses the counter/cross configuration in each of the two exchangers was capable of providing an increase of 6% and decrease of 1.5% in effectiveness compared to the cross flow and counter flow configurations, respectively. Vali (2009) also found that the performance of a

counter/cross flow configuration was heavily influenced by the ratio of the solution entrance size, and the overall length of the exchanger. Vali's (2009) results were also compared to the experimental results of Mahmud (2009). The agreement between the numerical and experimental data was found to be between 1% and 17% absolute in total effectiveness.

1.3.5 Transient Numerical Modeling (Seyed-Ahmadi, 2008)

The transient response of a RAMEE system was studied numerically by Seyed-Ahmadi (2008). Seyed-Ahmadi found the impact of various parameters on the RAMEE system response including the number of heat transfer units, thermal capacity ratio, and solution storage volume. Seyed-Ahmadi found that large transient times of up to several days can occur during the initial start up of the system. The amount of solution in the RAMEE system was found to have a large impact on the response time of the system. Therefore, for a fast response to changing conditions, Seyed-Ahmadi recommended minimizing the amount of solution in the system. Seyed-Ahmadi also considered the impact of heat loss/gains between the RAMEE system and its surroundings and found that heat loss/gains not only impacted the time response of the system, but also the system performance at quasi-steady state. Understanding the transient performance of the RAMEE system is important in order to control the system under different operating conditions, and maximize its performance.

1.4 Research Objectives

This study will be in both conjunction with, and in continuation of, the work of Seyed-Ahmadi (2008) and focuses on the transient performance of the RAMEE system.

Experiments will be conducted to validate Seyed-Ahmadi's numerical transient model. The main objective of this thesis is to:

1. Develop control strategies that can minimize transient time delays and improve the performance of the RAMEE system.

Sub-objectives are to:

2. Experimentally test a RAMEE system and determine both its transient behavior as well as its steady-state performance.
3. Compare the experimental results with the numerical model of Seyed-Ahmadi (2008).
4. Use the numerical model to investigate and determine the operating parameters of the developed control strategies.
5. Use the developed control strategies to study how the RAMEE system behaves during variable operating conditions that exist in a practical installation in a building HVAC system.

1.5 Thesis Overview

The RAMEE prototype and evaluation methods (numerical and experiemental) are presented in Chapter 2 (**Objective 2**). The prototype design, along with membrane and desiccant solution, are discussed. In addition, the experimental test apparatus and test condition uncertainties are presented. The numerical model developed by Seyed-Ahmadi (2008) is also introduced in Chapter 2. This model assumes conservation of energy and mass for both the air and solution flows. A finite difference method of solution is used with an implicit time discretization to provide a two dimensional transient model of the complete RAMEE system, including the well mixed storage

tanks. The numerical model is compared to the experimental data in Chapter 3 (**Objective 3**). Both transient and quasi-steady-state results are presented, and any differences are justified.

Control strategies that can be used to minimize the transient delays of the RAMEE system, while maintaining system performance (**Objective 1 and Objective 4**) of the RAMEE system are developed and investigated in Chapter 4. The control variables studied are the flow rate, temperature, and concentration of the desiccant solution. Section 4.6 examines how well these control strategies perform when the system encounters variable operating conditions, such as changing weather conditions during operation in a building (**Objective 5**).

The results of this study are summarized in Chapter 5, and the conclusions found throughout are explicitly stated. Recommendations for future RAMEE research are also presented.

CHAPTER 2

RAMEE PROTOTYPE DEVELOPMENT, TESTING AND MODELING

2.1 Introduction

The purpose of this chapter is to describe the LAMEE prototype, including the membrane heat and mass transfer properties and the desiccant solution chosen. The RAMEE testing apparatus (RAMEE-TA) will also be described including all of the sensors, and the testing conditions. This chapter will also present the numerical model including the governing equations and assumptions used, as well as convergence criteria that are used to determine when the RAMEE system has reached constant (steady-state) operating conditions.

2.2 LAMEE Prototype Design

The RAMEE system investigated in this thesis consists of two separate liquid-to-air energy exchangers (LAMEEs); one located in the supply air stream, and the other in the exhaust air stream. The LAMEEs are designed as cross flow exchangers, where the air and desiccant solution flow perpendicular to each other. A cross flow configuration is chosen for both simplicity and for direct comparison to the cross flow numerical model developed by Seyed-Ahmadi (2008), even though a counter flow or cross/counter flow design has been proven to provide higher performance (Vali, 2009; Mahmud, 2009). The cross flow model developed by Seyed-Ahmadi (2008) is the only transient model, while the counter flow and cross/counter flow models are steady state only. The

LAMEEs constructed for laboratory testing are 10 cm wide, 60 cm long, and 40 cm high and contain 10 desiccant channels (1.70 mm thick) and 11 air channels (4.76 mm thick), as shown in Figure 2.1. A small desiccant reservoir is located on both the top and bottom of each LAMEE to facilitate the entrance and exit of the desiccant solution.

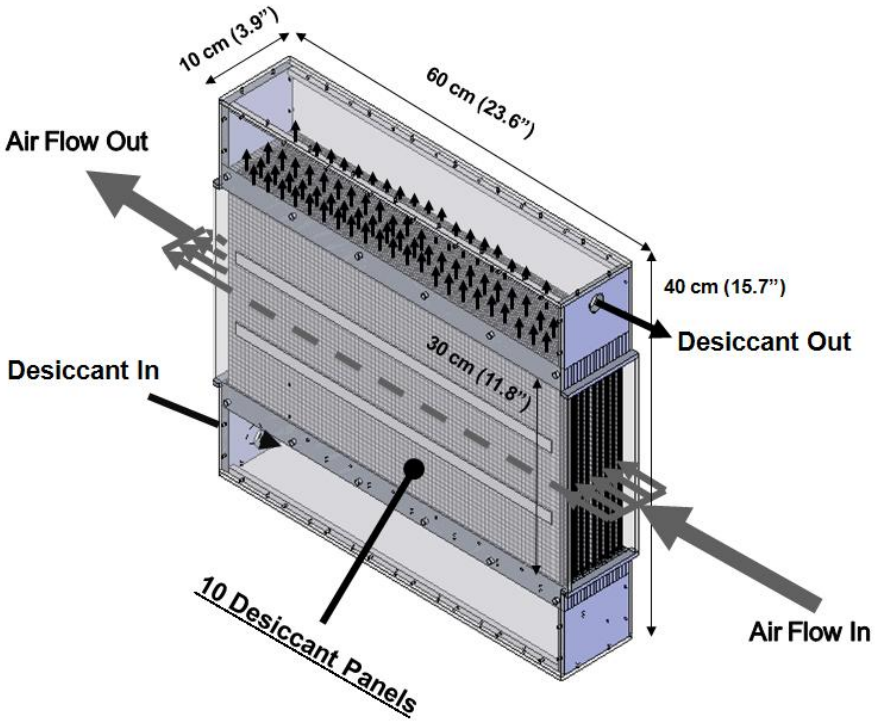

Figure 2.1: The liquid-to-air membrane energy exchanger (LAMEE) prototype.

Each LAMEE consists of ten desiccant panels (Figure 2.2), which are first assembled separately and then combined with an outer aluminum casing to produce the exchanger (Figure 2.1). Each desiccant panel is constructed using a semi-permeable membrane. This membrane allows for the transmission of water vapor between the solution inside the panel and the air that flows on the outside of the panel. However, the surface tension of the solution in the small microscopic membrane pores does not allow the solution to pass through, therefore retaining the liquid inside the solution channel. There are several different semi-permeable membranes available including common ones such as Tyvek® and Gore-Tex®. Larson et al. (2007) found that a polypropylene

composite made by 3M™ called Propore™ was a good choice for use in a LAMEE. This composite material contains a thin semi-permeable membrane bonded to a non-woven fabric for structural support. This non-woven fabric is also made from polypropylene, but is permeable to both liquids and vapors. The thin polypropylene membrane is permeable to water vapor, but impermeable to liquid water except at very high pressures (above 20 psi (138 kPa) which is well above the expected operating pressures of a RAMEE system). Figure 2.2 shows an atomic force microscopic image of Propore™.

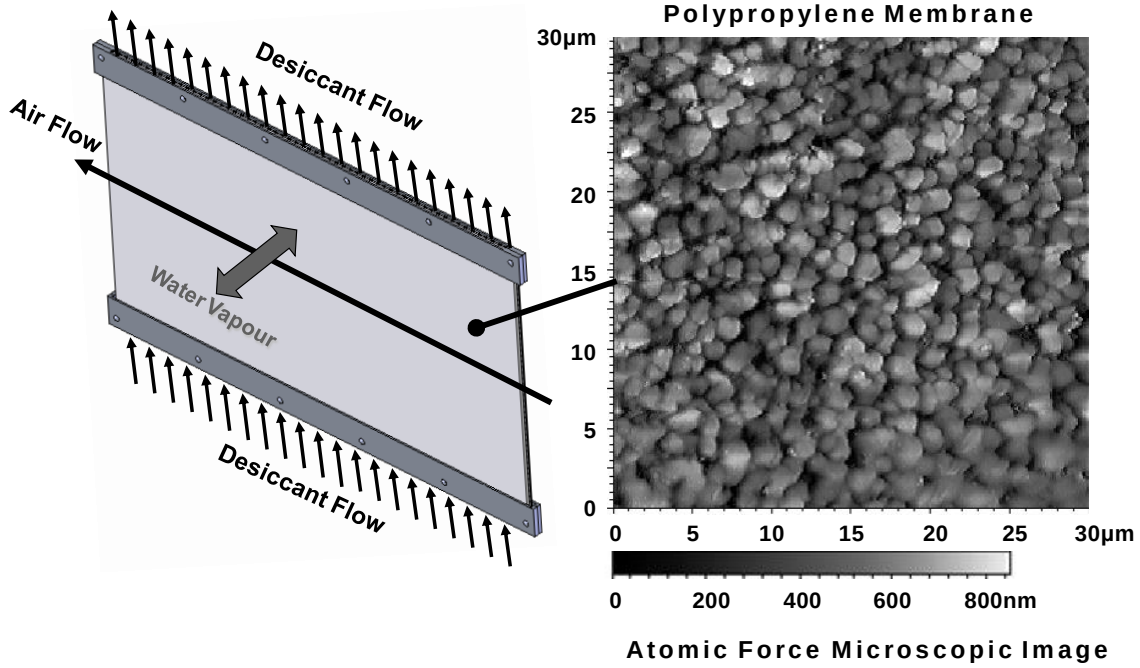

Figure 2.2: A single membrane panel and atomic force microscope image (courtesy of Larson, 2006) of Propore™ used in the LAMEE prototype.

Each desiccant panel is made by wrapping Propore™ around a thin, plastic coated, fiberglass screen with square pores that are 1 mm x 2 mm (0.039 in. x 0.079 in.). This fiberglass screen provides a 1.70 mm (0.067 in.) wide channel for the desiccant solution to flow through. The screen also improves the distribution and mixing of the

desiccant solution inside the panel and promotes solution contact with the membrane wall. The Propore™ that is wrapped around the fiberglass screen is orientated such that the membrane side is on the inside of the envelope and in contact with the liquid desiccant, and the non-woven fabric is located on the outside of the envelope and in contact with the air flow. The Propore™ is glued to itself to provide a sealed seam in the panel. A metal screen is placed on the outside of each panel in order to provide further structural support, and reduce membrane bulging under pressure. This support is important because the bulging of the Propore™ under pressure will reduce the size of the air flow channels and decrease performance (Larson et al., 2008). A 12.7 mm (1/2 in.) square screen with a wire thickness of 1 mm (0.04 in.) was found to provide adequate support (Larson, 2006). Finally, the entire membrane and screen assembly is glued between two aluminum header plates on both the top and bottom of each panel. These header plates provide the proper spacing for the desiccant flow channel and provide a 4.76 mm (3/16 in.) air flow channel between the desiccant panels. Two additional rectangular aluminum spacers are placed between each desiccant panel to further reduce the outer metal screen bulging, and maintain a somewhat uniform air flow channel. These spacers can be seen at heights of 1/3 and 2/3 between the bottom and top headers in the picture of the two fully assembled LAMEEs shown in Figure 2.3. As Figure 2.3 shows, the panels are assembled inside the outer aluminum casing using bolts through the aluminum header plates.

Figure 2.3: Photograph of the two fully assembled LAMEEs.

The two LAMEEs are coupled together with a desiccant solution running between the two exchangers in a closed loop. There are several desiccants that are suitable for use in the RAMEE system including magnesium chloride, lithium chloride, calcium chloride, and lithium bromide. Selecting a proper desiccant solution involves considering cost, performance, and safety. Afshin et al. (2009) studied the use of desiccants in a RAMEE application and found that the most cost effective desiccant was magnesium chloride, which should perform well in most climates.

The performance of a desiccant is primarily based on the potential for moisture transfer between the air and the solution. Therefore the air humidity that exists when air is in contact with the desiccant must be considered for various climates and operating conditions. This can be visualized by plotting the desiccant solution equilibrium concentration lines on the psychrometric chart, using the correlations developed by Cisternas and Lam (1991) (Afshin et al., 2009). Figure 2.4 shows the equilibrium concentration lines for magnesium chloride ($MgCl_2$) superimposed on the psychrometric

chart. These concentration lines indicate what the equilibrium concentration of the desiccant will be if the desiccant is in contact with air at the corresponding temperature and humidity, represented by the horizontal and vertical axis on the psychrometric chart. The concentration of the desiccant is defined as,

$$C_{Salt} = \frac{\text{mass of salt}}{\text{mass of salt} + \text{mass of water}} = \frac{1}{1 + X_{Sol}} \ , \tag{2.1}$$

where:

X_{Sol} is the solution mass fraction [kg/kg] and can be expressed as,

$$X_{Sol} = \frac{\text{mass of water}}{\text{mass of salt}} . \tag{2.2}$$

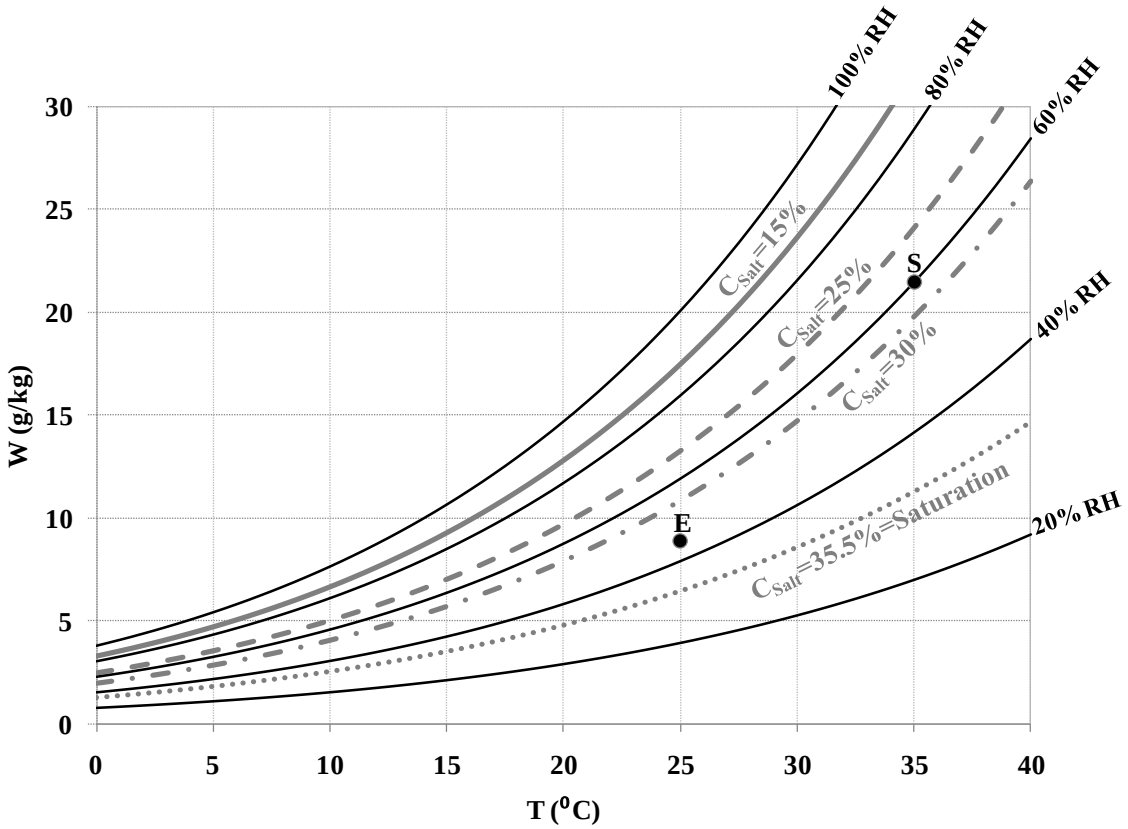

Figure 2.4: Magnesium chloride equilibrium concentration lines superimposed on a psychrometric chart showing operating conditions for the RAMEE system inlet air. Points S and E correspond to the AHRI summer test condition for inlet supply and exhaust air.

From Figure 2.4, it can be seen that the $MgCl_2$ equilibrium concentration lines nearly follow the constant relative humidity lines on the psychrometric chart. This modified psychrometric chart provides the desiccant equilibrium concentration at any air temperature and humidity. Therefore as the operating conditions of the RAMEE change, the desiccant will lose/gain moisture in order to move towards the equilibrium concentration. For example, if the supply outdoor air conditions are 35°C and 60% RH (Point S in Figure 2.4), then the desiccant will try to maintain a concentration of approximately 28% in the supply LAMEE. However, the exhaust air may be leaving the building and entering the exhaust LAMEE at 25°C and 45% RH (Point E in Figure 2.4), in which the desiccant would try to maintain a concentration of approximately 34% in the exhaust LAMEE. Therefore, the desiccant concentration will end up somewhere between 28% and 34% depending where it is in the run-around loop. As the desiccant travels through the supply LAMEE, its concentration decreases as it absorbs water vapor from the supply air. The supply air will be therefore dehumidified. The desiccant continues through the RAMEE to the exhaust LAMEE, where its concentration increases by releasing moisture into the exhaust air. Therefore, the exhaust air will be humidified.

Also shown in Figure 2.4 is the saturation concentration of $MgCl_2$ which was found to be 35.5% (Linke, 1965), and occurs at approximately 33% RH (Greenspan, 1977). This is the maximum allowable concentration of $MgCl_2$ in the RAMEE system because crystallization of the salt begins at this concentration. Crystallization can cause many problems including blockage of flow channels, pump problems, and decreased heat and moisture transfer characteristics of the semi-permeable membrane (Charles and

Johnson, 2008; and Gryta, 2007). Therefore, it is critical to not operate the system close to, or only slightly above, the desiccant saturation limit. For conditions that require such concentrations, an alternative desiccant should be chosen. Afshin et al. (2009) also considered using mixtures of different desiccants in order to lower the saturation concentration, while keeping the cost of the desiccant to a minimum.

2.3 Experimental Testing Apparatus

The run-around membrane energy exchanger test apparatus (RAMEE-TA) used to test the RAMEE prototype was designed to meet ANSI/ASHRAE Standard 84 Method of Testing Air-to-Air Heat Exchangers (ANSI/ASHRAE, 2008). The RAMEE-TA consists of two separate air streams, both of which contain a single LAMEE, as shown in Figure 2.5. One air stream represents the outdoor air being supplied to the building. This air stream is conditioned using an environmental chamber, which can simulate an outdoor air temperature between -40°C (-40°F) and 40°C (104°F), and an outdoor air humidity up to 90% RH. The other air stream represents the indoor air being exhausted out of the building. The RAMEE-TA uses the laboratory room air for this purpose. Both air ducts are made of 50.8 mm (2 in.) diameter round PVC pipe, which are insulated with 12.7 mm (1/2 in.) thick fiberglass insulation to reduce heat transfer with the surroundings. Each duct is supplied with air by two variable speed 5 hp (3.73 kW) fans (vacuum pumps). One fan is located on each side of the LAMEE in order to minimize the pressure difference between the air stream and the ambient pressure at each exchanger. This reduces the membrane deflections inside the exchanger, and air leakage at the exchanger and ductwork connections.

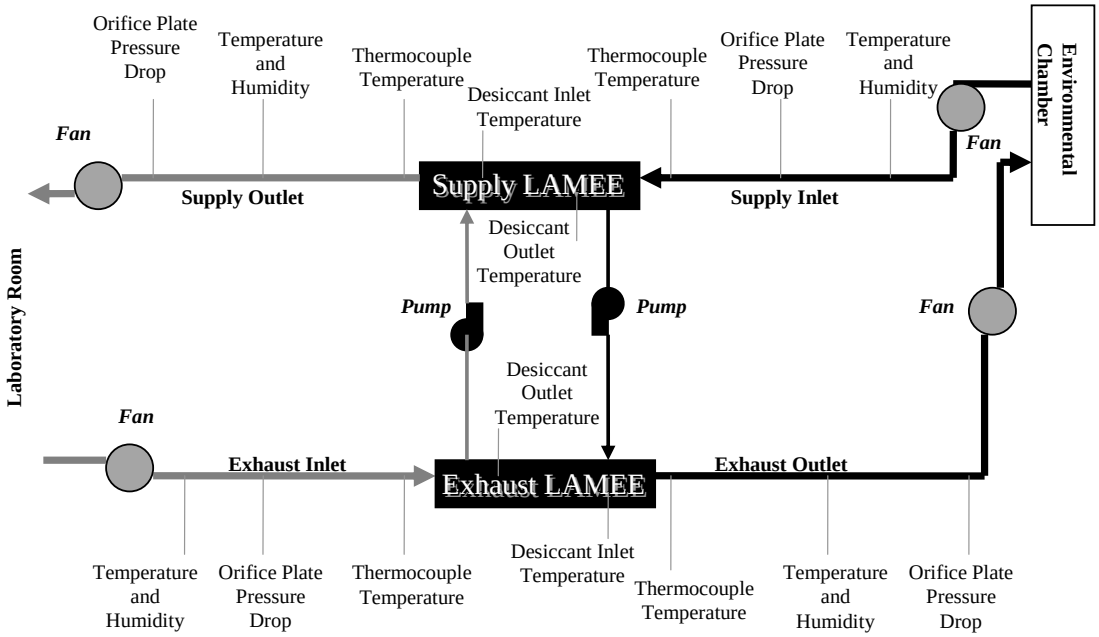

Figure 2.5: Run-Around Membrane Energy Exchanger Testing Apparatus (RAMEE-TA) showing the sensor locations.

The LAMEEs installed in each air stream are coupled together with a liquid desiccant piping network. All piping is 1 in. diameter flexible plastic pipe and is insulated with 9.53 mm (3/8 in.) thick foam insulation to reduce heat loss/gain. The desiccant flow to each LAMEE is provided by a 93.2 W ($1/8^{th}$ hp) magnetic drive pump, and the flow rate is controlled using a rotometer capable of flow rates between 0.2 and 2.2 US gallons per minute (0.013 L/s and 0.140 L/s). A storage tank is placed before each pump to allow for the expansion or contraction of the solution volume with changes in solution concentration and to provide a small positive pressure on each pump inlet.

In order to determine the performance or energy transfer rates in the RAMEE system, the RAMEE-TA must be able to accurately measure the properties of the air before and after each LAMEE. Air stream temperatures are measured using 0.51 mm (24 AWG, 0.02 in.) wire diameter T-type thermocouples. Three thermocouples are

placed before and after each LAMEE and are connected in parallel to provide a spatial average temperature for each air flow. Resistance temperature detectors (RTDs) are also placed in each air stream. RTDs are more accurate than thermocouples, but have slower response times to transient changes. Therefore, thermocouples are used for transient testing, while RTDs provide more accurate steady-state temperatures. Integrated capacitive humidity sensors measure the humidity of the air entering and leaving both exchangers.

The mass flow rate of air through each LAMEE is measured using an orifice plate located before and after each exchanger. The orifice plates create a pressure drop which is measured with a differential pressure transducer. From this pressure drop, the mass flow rate, $\dot{m}_{Air}$, is calculated by using the standard orifice equation (ISO, 1991)

$$\dot{m}_{Air} = C_d \frac{\pi}{4} d_{orifice}^2 \left[\frac{2\rho_{Air}(\Delta P)}{(1-\beta^4)} \right]^{\frac{1}{2}} \tag{2.3}$$

where:

C_d is the discharge coefficient (obtained from ISO, 1991),

$d_{orifice}$ is the diameter of the orifice plate opening [m],

$\beta = \frac{d_{orifice}}{D_{pipe}}$,

D_{pipe} is the inside pipe diameter [m],

ΔP is the measured pressure drop across the orifice plate [Pa], and

ρ_{Air} is the density of the air at the orifice [kg/m^3].

The orifices used and the length of each pipe section are designed to follow ISO Standard 5167-1 for proper flow rate measurements using orifice plates (ISO, 1991).

Also important are the desiccant temperatures before and after each LAMEE, which allows for the determination of heat gains/losses from the desiccant piping and pumps. The desiccant temperature entering and leaving each exchanger are measured using 30 AWG (0.01 in., 0.25 mm diameter) T-type thermocouples which are placed inside a well to avoid contact with the conductive desiccant. Data acquisition is handled with the use of data acquisition boards controlled by custom LabView software which collects and stores the readings of all twenty sensors in 10 second intervals. Data are acquired at a speed of 2.8 MHz, and in 16 bit format.

2.4 Experimental Calibration and Uncertainties

Calibration of all the sensors used is necessary in order to reduce the uncertainty in the measured properties. Carefully calibrating each measurement device to a traceable standard reduces the bias so that it is close to the bias in the calibration equipment, which is often very low. All T-type thermocouples and resistance temperature detectors (RTDs) were calibrated using a Dry Block Calibrator prior to testing. Each humidity sensor was calibrated using a Humidity Generator which provides several different levels of relative humidity for calibration over the entire range of operating conditions. Calibration of the pressure transducers was done with a precision pressure generator and a micromanometer. All of these calibration devices allow for the generation of calibration curve fits, which are directly implemented into the data acquisition program.

The precision and bias errors for each sensor can be combined to produce an overall uncertainty by considering the combination of these errors following the ASME

performance test code 19.1 (ASME, 1998) which says that the overall uncertainty for any set of readings is given by,

$$U_{95\%} = \sqrt{(B)^2 + (t^* \cdot S)^2}\ , \tag{2.4}$$

where:

$U_{95\%}$ is the 95% confidence interval uncertainty,

B is the bias error,

S is the standard deviation of the random fluctuations, and

t^* is the Student-t distribution constant.

This assumes that the uncertainty follows Student's t-distribution developed by William Gosset (Student, 1908) which is used for cases where a small number of measurements are made and the ideal Gaussian distribution cannot be assumed. The Student-t distribution constant depends on how many data points are considered, and was therefore different for each sensor calibrated. Most values of t^* are around 2. Although the sensors used at different measurement locations in the RAMEE-TA have slightly different uncertainties for each sensor type, the worst case (i.e., highest uncertainty) was chosen for each measurement device and applied to all sensors of the same type for simplicity. Using the worst case uncertainties resulted in less than 1% higher uncertainty in the overall performance of the system, than if the uncertainty of each sensor was considered separately. The precision, bias, and uncertainty associated with each individual measurement are shown in Table 2.1.

Table 2.1: Worst case standard deviations, t-distribution constants, bias errors and overall uncertainties for each type of sensor.

Measurement	Standard Deviation	t*	Bias Error	$U_{95\%}$	Units
Air Temperature-RTD	0.02 [0.04]	2.1	0.10 [0.18]	0.11 [0.20]	K [°F]
Air Temperature	0.08 [0.14]	2.0	0.10 [0.18]	0.19 [0.34]	K [°F]
Air Humidity	0.3%	2.1	1.0%	1.2%	(% R.H.)
Air Flow Rate	0.8%	2.6	0.9%	2.2%	% of Flow
Desiccant Temperature	0.03 [0.05]	2.0	0.10 [0.18]	0.12 [0.22]	K [°F]
Desiccant Flow Rate	2.0 [0.27]	2.1	2.1 [0.28]	4.8 [0.63]	g/s [lb/min]

The uncertainty in the air temperature is found to be 0.11 K (0.20 °F) when using an RTD compared to 0.19 K (0.34 °F) when using a thermocouple. This is why the data from the RTD is used where response time is not as critical. However as mentioned earlier, the thermocouples have a faster response for transient situations. The uncertainty in the desiccant temperature measurement is 0.12 K (0.22 °F) which is smaller than the thermocouple uncertainty used to measure the air temperature. This is because the desiccant thermocouples are of better grade and contain a smaller diameter wire which aid in their sensitivity and reduces the standard deviation of the random fluctuations measured during calibration. It should be noted that the bias error is somewhat in doubt for the bulk desiccant temperature because mixing of the liquid desiccant may not be complete near the thermocouple well. The uncertainty in the air humidity measurement is 1.2% RH, and the uncertainty in the air mass flow rate measurement is 2.2% of the mass flow rate. The desiccant mass flow rate has a constant uncertainty of 4.8 g/s (0.63 lb/min). Since the rotometer is capable of measuring flows from 0.2 to 2.2 US gallons per minute (0.013 L/s to 0.14 L/s), the percent uncertainty ranges from approximately 26% at the lowest flow rate to 2% at the highest flow rate. It should be noted that although these liquid flow uncertainties are high, the performance of the RAMEE will be determined from the air properties, and not the desiccant properties.

The uncertainties in the measured values are included in all calculated properties by uncertainty propagation and summation using the root-sum-squares (RSS) method, which ensures 95% confidence intervals (Figliola and Beasley, 2006). The uncertainty propagation is derived from the linearized approximation of the Taylor series for a multivariable function given by,

$$R = f\{x_1, x_2, ..., x_N\}, \tag{2.5}$$

where:

R is the calculated property, and

N is the number of independent variables.

A sensitivity index, ψ_i, can be defined to relate how changes in each x_i affect R, and is given by,

$$\psi_i = \frac{\partial R}{\partial x_i} \quad i = 1,2,...,N. \tag{2.6}$$

Therefore, the total RSS uncertainty becomes,

$$U_R = \pm\left[\sum_{i=1}^{N}\left(\psi_i U_{\bar{x}_i}\right)^2\right]^{1/2}, \tag{2.7}$$

where:

$U_{\bar{x}_i}$ is the uncertainty in the independent variable x_i (obtained from eq. (2.4)).

Each data point collected and each property calculated was analyzed using this uncertainty analysis technique, and will be included with the test results.

2.5 Numerical Modeling

The numerical model was created and validated by Seyed-Ahmadi (2008) using the Fortran programming language. This model was developed from physical principles

for transient and two-dimensional simultaneous heat and moisture transfer in the RAMEE system and is formulated using the finite difference method with an implicit time step method. The model solves the coupled energy and moisture balance equations and considers the desiccant reservoirs and their affect on the dynamic performance of the system, as well as heat gains/losses between the RAMEE system and ambient air. The assumptions used in the analysis are as follows:

1. The liquid desiccant and air flows are assumed to be laminar and fully developed. The entrance regions of air and desiccant flows were found to occur in less than 6% of the exchanger length, and laminar flow was found to occur during all normal operating conditions (Seyed-Ahmadi, 2008).
2. The heat and mass transfer processes occur only normal to each membrane and the membrane properties are constant. This assumption is valid because the membrane is very thin (0.5 mm) and has a low thermal and moisture transfer resistance, compared to the convective heat and mass transfer resistance in the two flows. Therefore convection heat and mass transfer normal to the membrane surface dominates, while axial heat and mass transfer in the membrane is negligible.
3. Axial heat conduction and water vapor molecular diffusion in the two fluids in the flow directions are negligible. This was found to be valid since the Peclet number is above 20 for normal operating conditions (Seyed-Ahmadi, 2008).
4. Heat gain or loss due to adsorption/desorption of water vapor at the membrane surface occurs only in the liquid component. This is due to the phase change between the liquid and vapor states occurring at the interface between the

membrane and the solution. This is true for hydrophobic membranes which do not allow liquid to enter the membrane structure.

5. The membrane thermal and mass transfer capacitance effects are negligible. This assumption is valid since the thermal and mass transfer capacitance of the membrane is much smaller than the mass transfer capacitance of the desiccant solution (Iskra, 2007).
6. The desiccant liquid in the storage tanks is well mixed at all times. This assumption is valid since the solution flows into the top of the tank, and free falls approximately 0.3 m (12 in.) before striking the liquid surface causing large disturbances and mixing in the fluid. The salt solution leaves the bottom of each tank, resulting in a constant mixing and exchange of solution in the tanks.
7. Condensation in the air stream and crystallization in the liquid stream are neglected.
8. Channel thickness is assumed uniform everywhere, and maldistributions of flow streams are not considered.
9. Velocity distributions in both the air and liquid channels are assumed to be uniform.

The governing equations for coupled heat and moisture transfer in each LAMEE based on the above assumptions were developed (Seyed-Ahmadi, 2008) based on the control volume and coordinate system shown in Figure 2.6.

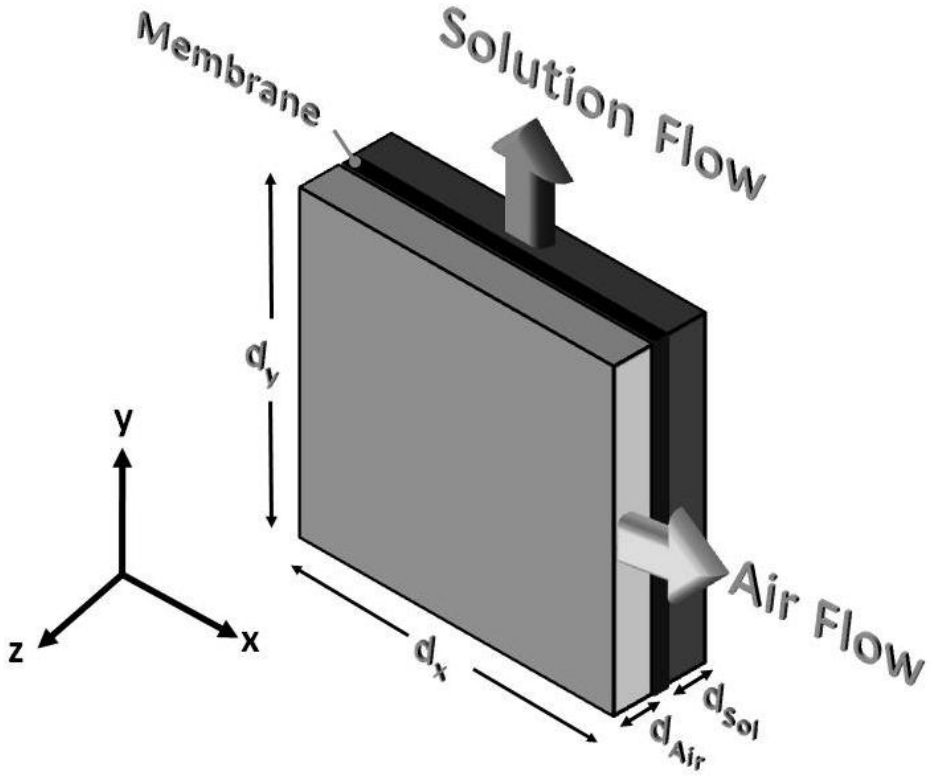

Figure 2.6: Governing equation control volume and coordinate system.

2.5.1 Conservation of Mass in the Air Stream

The change in water vapor content in the air at any point (x,y) at any time (t) can be determined knowing the mass gain/loss in the air flowing in the x direction and the amount of mass transferred across the membrane in the z direction, and can be expressed as:

$$\rho_{Air} d_{Air} \frac{\partial W_{Air}}{\partial t} + \frac{\dot{m}_{Air}}{y_0} \frac{\partial W_{Air}}{\partial x} + 2U_m (W_{Air} - W_{Sol,Mem}) = 0, \qquad (2.8)$$

where:

ρ_{Air} is the density of air [kg/m^3],

d_{Air} is the air channel width [m],

$\dot{m}_{Air}$ is the air mass flow rate [kg/s],

y_0 is the exchanger height [m],

W_{Air} is the air humidity ratio [kg/kg],

$W_{Sol,Mem}$ is the humidity ratio of the air that is in equilibrium with the solution at the membrane surface [kg/kg], and

U_m is the overall mass transfer coefficient [kg/(m^2·s)].

The overall mass transfer coefficient, U_m, is defined as:

$$U_m = \left[\frac{1}{h_{m,Air}} + \frac{\delta}{k_m} \right]^{-1}, \tag{2.9}$$

where:

$h_{m,Air}$ is the convective mass transfer coefficient between the membrane and the air [kg/(m^2·s)],

δ is the membrane thickness [m], and

k_m is the water vapor permeability of the membrane [kg/(m·s)].

The membrane is assumed to be uniform throughout, and therefore has a constant thickness and water vapor permeability. The resistance of the solution ($1/h_{m,Sol}$) is not included in Eq. 2.9 for the overall mass transfer coefficient. However, the resistance of the solution is smaller than the air resistance but it is not neglected, as it is considered in the determination of the humidity ratio of the air at the membrane surface ($W_{Sol,Mem}$) which is used in the governing equation (Eq. 2.8). The humidity ratio of the air at the membrane surface accounts for the solution resistance by considering the mass flux between the solution and the air, and is a function of the temperature ($T_{Sol,Mem}$) and the mass fraction ($X_{Sol,Mem}$) of the desiccant at the membrane surface (Cisternas and Lam, 1991):

$$W_{Sol,Mem} = f\left(T_{Sol,Mem}, X_{Sol,Mem}\right), \tag{2.10}$$

The temperature and the concentration of the solution at the membrane surface is found by considering a heat and mass flux balance at the solution-membrane interface. The mass flux balance is expressed as,

$$\dot{m}'' = \frac{W_{Air} - W_{Sol,Mem}}{\left(h_{m,Air}\right)^{-1} + \left(k_m / \delta\right)^{-1}} = h_{m,Sol}\left(\frac{1}{1+X_{Sol}} - \frac{1}{1+X_{Sol,Mem}}\right), \tag{2.11}$$

and the energy balance is given by the equation,

$$q'' = \frac{T_{Air} - T_{Sol,Mem}}{\left(h_{Air}\right)^{-1} + \left(k/\delta\right)^{-1}} + \frac{W_{Air} - W_{Sol,Mem}}{\left(h_{m,Air}\right)^{-1} + \left(k_m/\delta\right)^{-1}} h_{fg} = h_{Sol}\left(T_{Sol,Mem} - T_{Sol}\right), \tag{2.12}$$

where:

$\dot{m}''$ is the mass flux rate of water [kg/m^2·s],

q'' is the heat flux rate [W/m^2],

h_{Air} is the convective heat transfer coefficient between the air and the membrane [W/(m^2·K)],

h_{Sol} is the convective heat transfer coefficient between the solution and the membrane [W/(m^2·K)],

$h_{m,Sol}$ is the convective mass transfer coefficient between the membrane and the solution [kg/(m^2·s)],

k is the thermal conductivity of the membrane [W/(m·K)],

T_{Air} is the bulk mean temperature of the air [K],

T_{Sol} is the bulk mean temperature of the solution [K],

$T_{Sol,Mem}$ is the temperature of the solution at the membrane surface [K],

X_{Sol} is the bulk mean mass fraction of the solution [kg/kg],

$X_{Sol,Mem}$ is the mass fraction of the solution at the membrane surface [kg/kg], and

h_{fg} is the heat of vaporization [m^2/s^2].

Equations 2.10, 2.11 and 2.12 are solved iteratively for $T_{Sol,Mem}$, $X_{Sol,Mem}$, and $W_{Sol,Mem}$.

2.5.2 Conservation of Mass in the Solution Stream

The change in water content with time in the desiccant solution at any point (x,y) and at any time (t) can be determined by considering the moisture gain/loss in the solution flowing in the y direction, and the amount of mass transferred across the membrane in the z direction (Figure 2.6). Therefore, the conservation of mass for the solution can be expressed as,

$$\rho_{Salt} d_{Sol} \frac{\partial X_{Sol}}{\partial t} + \frac{\dot{m}_{Salt}}{x_0} \frac{\partial X_{Sol}}{\partial y} - 2U_m (W_{Air} - W_{Sol,Mem}) = 0, \qquad (2.13)$$

where:

ρ_{Salt} is the density of the salt [kg/m^3],

d_{Sol} is the solution channel thickness [m],

x_0 is the overall length of the exchanger [m], and

$\dot{m}_{Salt}$ is the mass flow rate of the salt [kg/s].

2.5.3 Conservation of Energy in the Air Stream

The conservation of energy equation for the air stream includes energy storage, convection energy transfer, and energy transferred across the membrane, and is expressed as,

$$\rho_g C_{p,Air} d_{Air} \frac{\partial T_{Air}}{\partial t} + \frac{\dot{m}_{Air}}{y_0} C_{p,Air} \frac{\partial T_{Air}}{\partial x} + 2U(T_{Air} - T_{Sol}) = 0 \quad (2.14)$$

where:

ρ_g is the density of moist air [kg/m^3],

$C_{p,Air}$ is the specific heat capacity of moist air [J/(kg·K)], and

U is the overall heat transfer coefficient [W/(m^2·K)].

The overall heat transfer coefficient can be found by taking the inverse of the sum of the thermal resistance due to the solution, the membrane, and the air.

$$U = \left[\frac{1}{h_{Sol}} + \frac{\delta}{k} + \frac{1}{h_{Air}} \right]^{-1}, \quad (2.15)$$

2.5.4 Conservation of Energy in the Solution Stream

The conservation of energy equation for the solution stream includes energy storage, convective energy transfer, energy due to the heat of vaporization (phase change energy), and energy transferred across the membrane.

$$\rho_{Sol} C_{p,Sol} d_{Sol} \frac{\partial T_{Sol}}{\partial t} + \frac{\dot{m}_{Sol}}{x_0} C_{p,Sol} \frac{\partial T_{Sol}}{\partial y} - 2U_m (W_{Air} - W_{Sol,Mem}) h_{fg} - 2U(T_{Air} - T_{Sol}) = 0 \quad (2.16)$$

Where:

ρ_{Sol} is the density of the solution [kg/m^3],

$C_{p,Sol}$ is the specific heat capacity of the solution [J/(kg·K)],

$\dot{m}_{Sol}$ is the mass flow rate of the solution [kg/s], and

The solution to the governing equations together with equations that describe the heat and energy balances for the coupling piping and storage tanks (Seyed-Ahmadi, 2008) gives two dimensional temperature and humidity ratio distributions within both the air

and salt solution throughout the exchangers as a function of time. The properties of air can be found from tables and/or equations in Incropera and DeWitt (2002) and the properties of the desiccant solution can be found from tables and/or equations in Zaytsev and Aseyev (1992). The membrane properties of Propore™ that were used are shown in Table 2.2 and were given by Seyed-Ahmadi (2008).

Table 2.2: Membrane properties for Propore™.

Property	Symbol	Value
Membrane Thickness	δ	0.5 mm
Membrane Thermal Conductivity	k	0.334 kg/(m·s)
Membrane water vapor permeability	k_m	1.66×10^{-6} kg/(m·s)

2.6 Performance Indicators

The most common way to evaluate the performance of the RAMEE system is to determine the sensible, latent, and total effectivenesses (ASHRAE, 2008). The sensible effectiveness (ε_{Sen}) defines the exchanger's ability to transfer heat and, for the case where the mass flow rates of air in the supply and exhaust air streams are equal, is defined as:

$$\varepsilon_{S,Sen} = \frac{T_{Air,S,in} - T_{Air,S,out}}{T_{Air,S,in} - T_{Air,E,in}}, \tag{2.17}$$

on the supply side, and

$$\varepsilon_{E,Sen} = \frac{T_{Air,E,out} - T_{Air,E,in}}{T_{Air,S,in} - T_{Air,E,in}}, \tag{2.18}$$

on the exhaust side, where subscripts:

S are for the supply air stream,

E are for the exhaust air stream,

"in" are for the inlet leading to the energy exchanger,

"out" are for the outlet from the energy exchanger, and

"Sen" are for sensible.

The latent effectiveness (ε_{Lat}) measures the exchanger's ability to transfer moisture and, for the case of balance supply and exhaust air flow rates, can be calculated with:

$$\varepsilon_{S,Lat} = \frac{W_{Air,S,in} - W_{Air,S,out}}{W_{Air,S,in} - W_{Air,E,in}}, \tag{2.19}$$

on the supply side, and

$$\varepsilon_{E,Lat} = \frac{W_{Air,E,out} - W_{Air,E,in}}{W_{Air,S,in} - W_{Air,E,in}}, \tag{2.20}$$

on the exhaust side, where subscripts:

"Lat" are for latent.

The total effectiveness (ε_{Tot}) measures the exchanger's ability to transfer both heat and moisture. For balanced supply and exhaust air flow rates, the total effectiveness is found by

$$\varepsilon_{S,Tot} = \frac{H_{Air,S,in} - H_{Air,S,out}}{H_{Air,S,in} - H_{Air,E,in}}, \tag{2.21}$$

on the supply side, and

$$\varepsilon_{E,Tot} = \frac{H_{Air,E,out} - H_{Air,E,in}}{H_{Air,S,in} - H_{Air,E,in}}, \tag{2.22}$$

on the exhaust side, where:

H is the air stream enthalpy [J/kg], and subscripts

"Tot" are for total.

If there are no external heat gains/losses, the amount of heat and moisture exchanged on the supply side should equal the amount exchanged on the exhaust side at steady state.

Therefore, both conservation of mass,

$$\sum \dot{m}_{Air} W_{Air} = 0, \tag{2.23}$$

and conservation of energy,

$$\sum \dot{m}_{Air} H_{Air} = 0, \tag{2.24}$$

should be satisfied when considering all air streams entering and leaving each exchanger at steady state. This also means that the effectiveness values on both sides of the system should be equal once the system has reached steady state. Therefore, for steady-state conditions, the average of the supply and exhaust effectiveness values is taken to give an overall system effectiveness for the sensible, latent, and total energy ($\varepsilon_{O,Sen}, \varepsilon_{O,Lat}, \varepsilon_{O,Tot}$) (Johnson et al., 1995).

$$\varepsilon_O = \frac{\varepsilon_S + \varepsilon_E}{2}. \tag{2.25}$$

The effectiveness is dependent on two dimensionless parameters (Fan, 2005). The first is the ratio of heat capacity rates which is defined as:

$$Cr^* = \frac{C_{Sol}}{C_{Air}} = \frac{\dot{m}_{Sol} C_{P,Sol}}{\dot{m}_{Air} C_{P,Air}}, \tag{2.26}$$

where:

C is the heat capacity rate [W/K].

The ratio of heat capacity rates can therefore be varied by altering either the solution or air mass flow rates. The second parameter is the number of transfer units (NTU), which for the run-around system can be defined as:

$$NTU = MAX\left\{\left(\frac{2UA}{C_{Air}}\right)_S, \left(\frac{2UA}{C_{Air}}\right)_E\right\}, \tag{2.27}$$

where:

A is the membrane surface area [m^2].

Since the overall heat transfer coefficient and the area are usually fixed for a given exchanger design, NTU can be varied by adjusting the air mass flow rate. It should be noted that this definition of NTU is slightly different from the one presented by Fan (2005), in that it does not consider the NTU based on the solution heat capacity rate. For Cr* values less than 1, the heat capacity rate of the solution becomes less than that of the air, and therefore the NTU becomes the maximum between the supply and exhaust solution properties in Eq. 2.27. The definition based solely on the air heat capacity rate is chosen so that the NTU is always based on the air, regardless of the value of Cr*.

2.7 Testing Conditions

The RAMEE is tested and modeled during both heating and cooling conditions as guided by AHRI Standard 1060 (AHRI, 2005). The experimental test conditions used are as close as possible to the summer and winter test conditions outlined in the AHRI standard. However, the test apparatus limits some of the conditions. For example, the AHRI winter supply inlet humidity is not able to be obtained due to limitations in the environmental chamber humidification equipment at low temperatures. Table 2.3 shows both the AHRI test conditions and one of the experimental test conditions. Each experimental test has slight variations in the temperature and humidity conditions compared to the values given in Table 2.3. The AHRI conditions are used for the numerical model when experimental data is not being used for comparison. However

for all cases where the numerical model is being compared to experimental data, the numerical model uses the specific conditions for each individual experimental test.

Table 2.3: AHRI and experimental test conditions.

		AHRI Conditions	Experimental Test Conditions
Summer	Supply Inlet Temperature: $T_{Air,S,in}$	35 ºC (95 ºF)	34.8 ºC (94.6ºF)
	Supply Inlet Humidity Ratio: $W_{Air,S,in}$	17.5 g/kg (0.0175 lb/lb)	18.9 g/kg (0.0189 lb/lb)
	Exhaust Inlet Temperature: $T_{Air,E,in}$	24 ºC (75.2 ºF)	24.5 ºC (76.1ºF)
	Exhaust Inlet Humidity Ratio: $W_{Air,E,in}$	9.3 g/kg (0.0093 lb/lb)	8.9 g/kg (0.0089 lb/lb)
Winter	Supply Inlet Temperature: $T_{Air,S,in}$	1.7 ºC (35.1 ºF)	4.1 ºC (39.4ºF)
	Supply Inlet Humidity Ratio: $W_{Air,S,in}$	3.5 g/kg (0.0035 lb/lb)	0.36 g/kg (0.00036 lb/lb)
	Exhaust Inlet Temperature: $T_{Air,E,in}$	21 ºC (69.8 ºF)	23.2 ºC (73.8ºF)
	Exhaust Inlet Humidity Ratio: $W_{Air,E,in}$	7.1 g/kg (0.0071lb/lb)	8.1 g/kg (0.0081lb/lb)

The initial conditions of desiccant are correspond to the exhaust inlet, since the solution is stored at room temperature and humidity. Therefore, the solution is initially at the exhaust inlet temperature, and a concentration corresponding to the air exhaust inlet temperature and humidity ratio. For the AHRI conditions in Table 2.2, the solution would be at an initial concentration of 31.8% during summer and 33.8% during winter.

2.8 Heat Losses and Gains

In order to ensure that the numerical model accurately simulates the experimental setup, heat losses/gains are estimated for each AHRI test condition. These heat loss and gains were estimated using one dimensional heat transfer theory including the heat transferred between the surroundings and the following components of the RAMEE system: the sides of each LAMEE, the small top and bottom desiccant reservoirs, the storage tanks, the pumps, and all piping. Table 2.4 shows the total amount of estimated heat gain/loss for the summer and winter testing conditions and the fraction of the total that comes from each component. As Table 2.4 shows, there is a net heat loss (-) during summer testing conditions and a net heat gain (+) during the winter

testing conditions. The winter heat gain is larger than the summer heat loss due to the larger difference between the outdoor and indoor air temperatures. The large heat gain/loss contribution by the LAMEE side walls can influence the performance of the smaller experimental prototype more substantially than a typical commercial unit because there are so few panels in the prototype, providing only a small amount of energy transfer which can be influenced by the heat loss/gains.

Table 2.4: Estimated heat gains/losses for the RAMEE system along with corresponding makeup from each component.

	Summer Test Condition		Winter Test Condition	
	Supply LAMEE	**Exhaust LAMEE**	**Supply LAMEE**	**Exhaust LAMEE**
Total Estimated Heat Gain (-Loss)	-59 Watts (-201 Btu/h)	-30 Watts (-102 Btu/h)	+102 Watts (348 Btu/h)	+53 Watts (181 Btu/h)
Percentages of Total Gain (-Loss):				
LAMEE Side Walls	-61%	-53%	+66%	+38%
Air Ducts	-3%	-3%	+3%	+2%
LAMEE Desiccant Reservoirs	-33%	-56%	+26%	+50%
Desiccant Storage Tank	-2%	-3%	+1%	+2%
Pump	+2%	+5%	+1%	+3%
Desiccant Piping	-3%	+10%	+3%	+5%

2.9 Quasi-Steady-State Convergence Criteria

In order to investigate the transient behavior of the system, the dynamic performance of the RAMEE system is studied for a sufficient time duration so that quasi-steady state is obtained for each operating condition. Quasi-steady state is defined as the time when the energy and moisture that is lost by one air stream is taken up by the other air stream. Mass and energy conservation for balanced air flow rates exist when:

$$\left|\frac{(W_{Air,S,in} - W_{Air,S,out}) - (W_{Air,E,in} - W_{Air,E,out})}{(W_{Air,S,in} - W_{Air,E,in})}\right| \leq \text{Mass criterion (m\_c)} \qquad (2.28)$$

and,

$$\left|\frac{(H_{Air,S,in} - H_{Air,S,out}) - (H_{Air,S,in} - H_{Air,E,out})}{(H_{Air,S,in} - H_{Air,E,in})}\right| \leq \text{Energy criterion (e\_c).} \qquad (2.29)$$

Selecting the proper mass and energy criteria is based on the resulting supply air conditions leaving the exchanger. Selecting more stringent criteria will cause the air

conditions at the outlet of the supply exchanger to be closer to the steady-state values. Setting very stringent criteria is appealing; however, in a practical HVAC system it is only necessary for the outlet conditions to be equal to the steady-state conditions within the uncertainty bounds of the measurement sensors. Therefore, setting too strict of criteria will result in unrealistically long or unpractical transient times and long computational times for the numerical model. The goal of this section is to select appropriate quasi-steady-state convergence criteria for equations (2.28) and (2.29). These will then be used throughout the remainder of the thesis.

During summer AHRI conditions, the system is started with the solution initially at the indoor room temperature which is assumed to be the same as the exhaust air entering the exchanger. The solution in the storage tanks is open to the environment (vented) and therefore begins in equilibrium with the room conditions. Therefore, the solution begins at 24°C and a concentration of approximately 31.8% (corresponding to 24°C and 9.3 g/kg air conditions). As the system runs, the solution warms up, and becomes slightly lower in concentration (higher equilibrium relative humidity). Therefore, the supply air leaving the exchanger is initially cooled and dehumidified at a maximum rate (resulting in the maximum effectiveness). As the solution warms up and decreases concentration, the amount of energy transferred reduces, resulting in a slightly higher temperature and humidity of the supply air at steady state. Therefore, depending on which criterion is chosen, the temperature and humidity exiting the supply exchanger will be different than the steady-state values. The intent is to select a quasi-steady-state mass and energy convergence criteria that provide accurate enough temperature and humidity results, without being computationally extensive.

Figure 2.7 shows the time required to reach quasi-steady state for various criteria for both mass and energy convergence. For the AHRI summer start-up conditions, the mass and energy balances become satisfied at nearly the same time, except for cases with very low criteria. For criteria above 5%, the mass balance occurs first, so the energy balance governs the time required to reach quasi-steady state. However, for criteria under 5%, the energy balance occurs first, so the mass balance dictates when quasi-steady state is reached. Using different initial starting conditions or different outdoor conditions will result in differences in this trend. For example, if the solution began at a concentration that is further away from the steady-state concentration, then the mass balance would take much longer than the energy balance and would govern the quasi-steady state determination for all criteria, even for convergence criteria above 10%. Similarly, if the temperature of the solution was initially further away from the steady-state temperature, the energy balance would take longer, and could govern over a wider range of criteria.

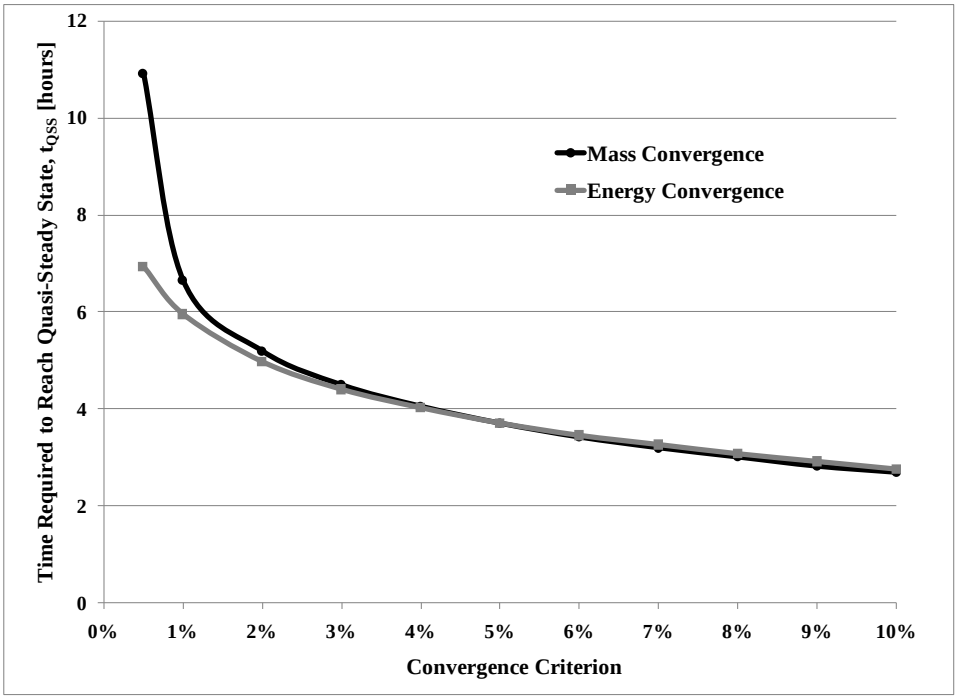

Figure 2.7: Time required to reach quasi-steady state for various mass and energy convergence criteria (AHRI Summer Conditions, NTU=11.4, Cr*=3).

The difference between the quasi-steady-state and the steady-state air temperatures leaving the supply exchanger ($\Delta T_{QSS,SS}$) can be represented by the equation,

$$\Delta T_{QSS,SS} = \left| T_{QSS} - T_{SS} \right|, \tag{2.30}$$

where:

T_{QSS} is the temperature at quasi-steady state [K], and

T_{SS} is the temperature at steady state [K].

The steady-state air temperature is determined by considering the trend in the outlet temperature at multiple convergence criteria, as shown in Figure 2.8. From the linear trend developed, the steady-state temperature can be determined by extrapolating backwards until the convergence criteria are set to zero. For the case shown in Figure 2.8, the steady-state outlet temperature is found to be 301.64 K.

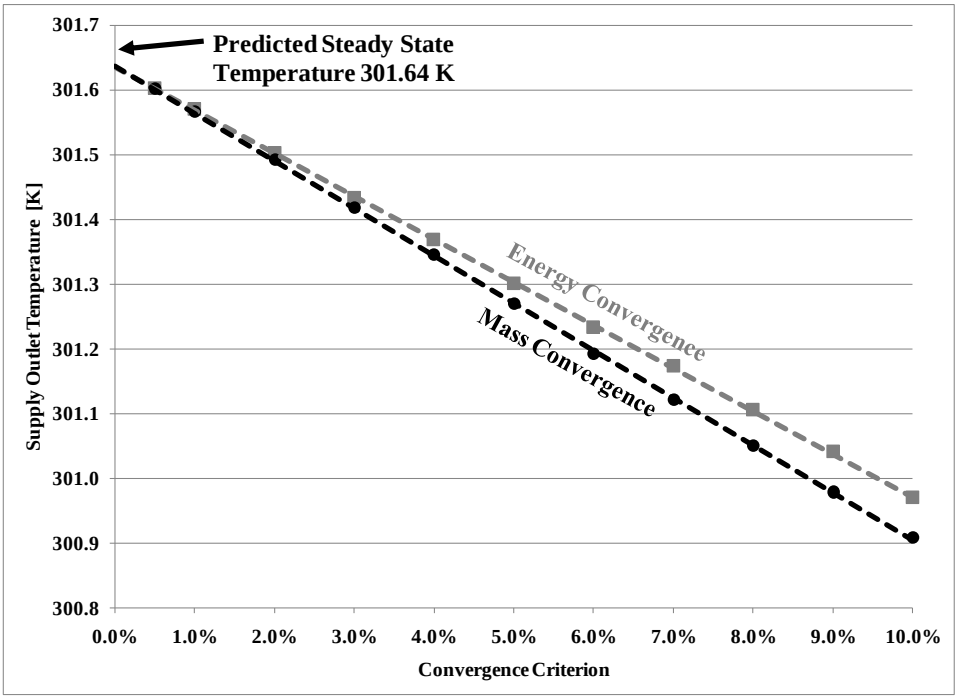

Figure 2.8: Supply outlet temperature for various mass and energy convergence criteria (AHRI Summer Conditions, NTU=11.4, Cr*=3).

The difference between the quasi-steady-state and the steady-state supply air temperatures leaving the exchanger is shown in Figure 2.9 for the different mass and energy convergence criteria. This figure shows that as the convergence criteria is made more strict the difference between the quasi-steady-state and the steady-state supply outlet temperature decreases. Recall that the RTDs used in the experimental testing apparatus were capable of measuring the temperature to ±0.11 K, while the thermocouples were capable of measuring the temperature to ±0.19 K. In most practical applications, a temperature uncertainty of ±0.20 K is deemed as adequate. Therefore, to achieve a quasi-steady-state supply outlet temperature that is within ±0.20 K of the steady-state value requires a mass convergence criterion lower than 2.7% and an energy convergence criterion lower than 3.0%.

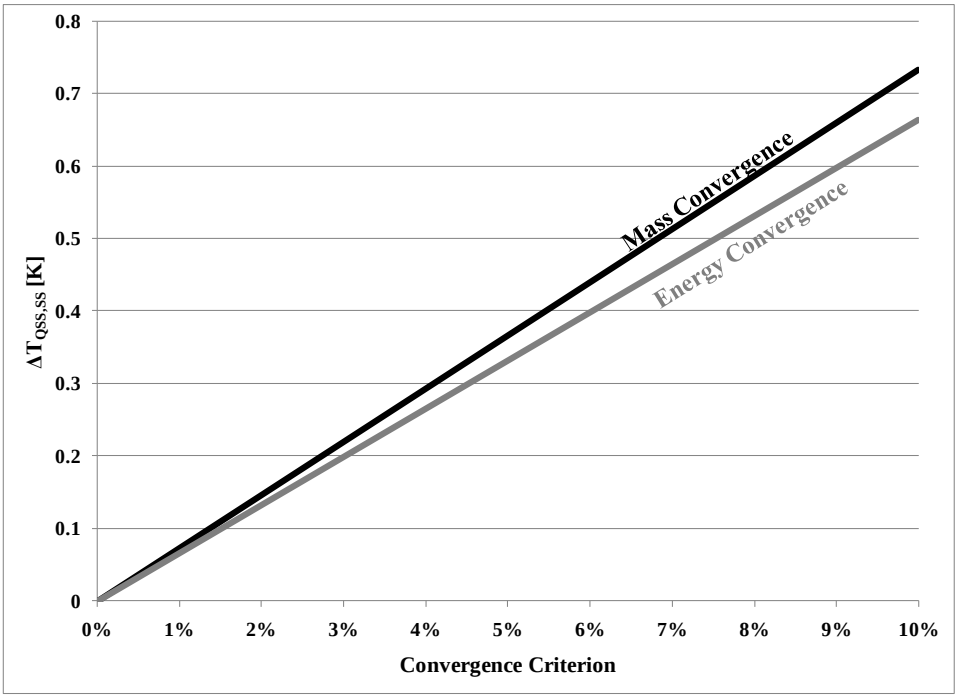

Figure 2.9: Difference between quasi-steady-state and steady-state outlet temperatures of the supply exchanger for different mass and energy convergence criteria (AHRI Summer Conditions, NTU=11.4, Cr*=3).

The other important property of the supply outlet air leaving the exchanger is the relative humidity. Although, not as important as temperature, the relative humidity is usually desired to be within 1% to 2% of the desired value. The difference between the quasi-steady-state and the steady-state relative humidity leaving the supply exchanger ($\Delta RH_{QSS,SS}$) can be represented by the equation,

$$\Delta RH_{QSS,SS} = \left| RH_{QSS} - RH_{SS} \right|, \tag{2.31}$$

where:

RH_{QSS} is the relative humidity at quasi-steady state, and

RH_{SS} is the relative humidity at steady state.

The steady-state relative humidity can be found using the same method that was used to determine the steady-state temperature. The steady-state relative humidity of the air leaving the supply exchanger is 58.1% for AHRI summer testing conditions. The

difference between the quasi-steady-state and the steady-state relative humidity leaving the supply exchanger is shown in Figure 2.10 for the different mass and energy convergence criteria. As Figure 2.10 shows, the quasi-steady-state supply outlet relative humidity is within 1% RH of the steady-state value for all convergence criteria less than 10%.

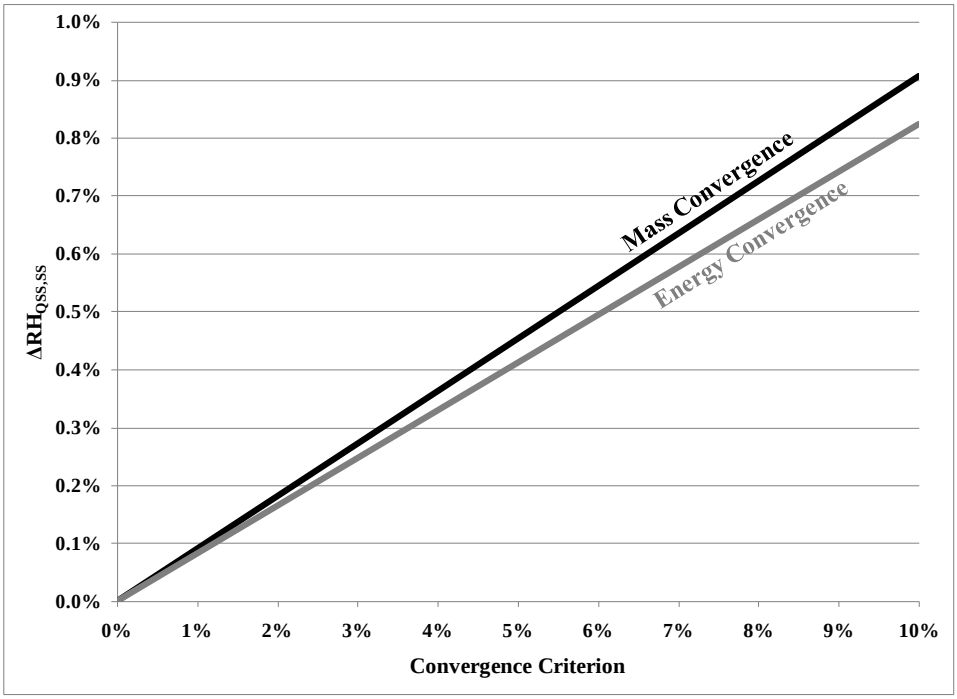

Figure 2.10: Difference between quasi-steady-state and steady-state outlet relative humidity of the supply exchanger for different mass and energy convergence criteria (AHRI Summer Conditions, NTU=11.4, Cr*=3).

Based on the air properties leaving the supply exchanger, a mass convergence criterion of 2.7%, and an energy convergence criterion of 3.0% would produce accurate results. For these conditions, energy convergence would occur after 4.4 hours, while mass convergence would take 4.7 hours (Figure 2.7), and govern the overall system convergence.

While the temperature and humidity leaving the supply exchanger are the most important properties for practical operation, the systems performance is based on the

effectiveness. Therefore, the accuracy of the effectiveness must also be considered when choosing a proper convergence criterion. The difference between the quasi-steady-state and the steady-state overall (average between supply and exhaust exchangers) total effectiveness ($\Delta\varepsilon_{O,Tot,QSS,SS}$) is shown in Figure 2.11, and represented by the equation,

$$\Delta\varepsilon_{O,Tot,QSS,SS} = \left| \varepsilon_{O,Tot,QSS} - \varepsilon_{O,Tot,SS} \right|, \tag{2.32}$$

where:

$\varepsilon_{O,Tot,QSS}$ is the overall total effectiveness at quasi-steady state, and

$\varepsilon_{O,Tot,SS}$ is the overall total effectiveness at steady state.

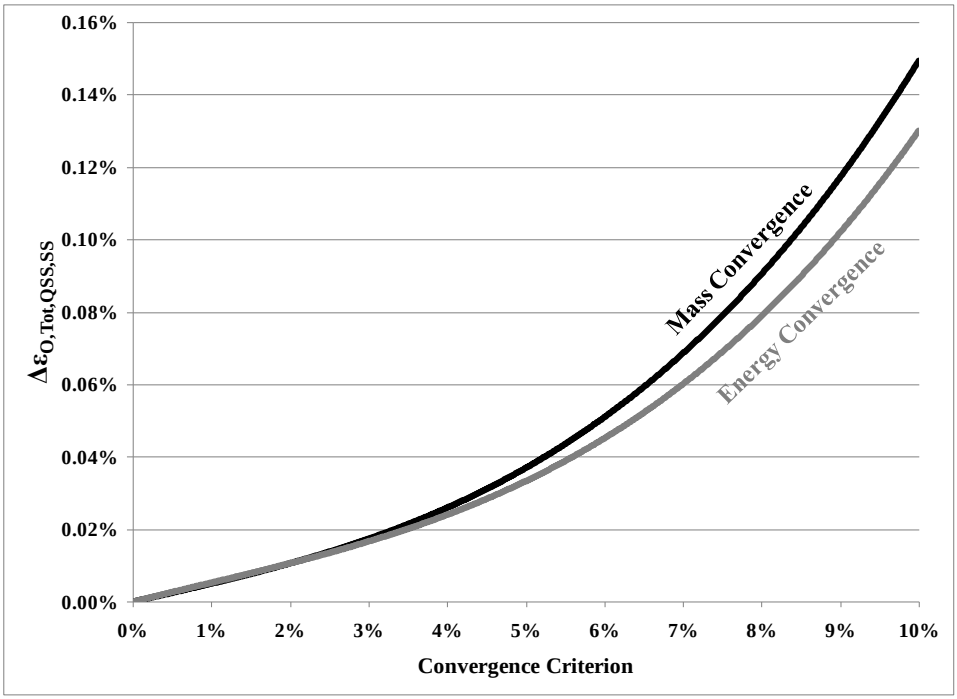

Figure 2.11: Difference between quasi-steady-state and steady-state overall total effectiveness for different mass and energy convergence criteria (AHRI Summer Conditions, NTU=11.4, Cr*=3).

Figure 2.11 shows that a mass and energy convergence criteria below 8% will still provide a quasi-steady-state overall total effectiveness within 0.1% of the steady-state value. However, if the individual exchanger performance is desired instead of the

overall system performance, then the difference between the quasi-steady-state and the steady-state total effectiveness for both the supply ($\Delta\varepsilon_{S,Tot,QSS,SS}$) and the exhaust ($\Delta\varepsilon_{E,Tot,QSS,SS}$) exchangers must be considered, and are shown in Figures 2.12 and 2.13. From Figures 2.12 and 2.13 it can be seen that if the individual exchanger effectiveness for either the supply exhaust exchanger is desired a more stringent criteria must be chosen. In order for both the supply and exhaust exchanger effectiveness to be within 1% of the steady-state effectiveness requires a mass convergence criterion lower than 1.7% and an energy convergence criterion lower than 1.9% .

Based on the discussed results for summer AHRI conditions, a mass and energy balance of 1% will be used when studying the steady-state effectiveness of the system, but more relaxed mass and energy balances of 2.5% and 3%, respectively, will be used to accurately determine when a system has reached quasi-steady-state in a practical application, when the supply outlet temperature and humidity properties are the important properties.

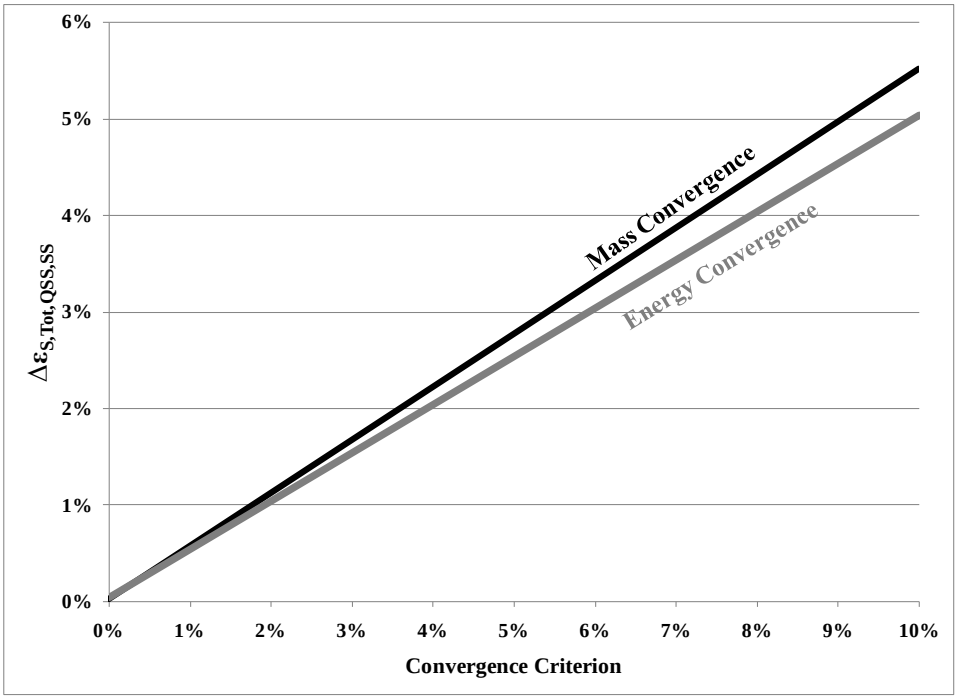

Figure 2.12: Difference between quasi-steady-state and steady-state total effectiveness for the supply exchanger for different mass and energy convergence criteria (AHRI Summer Conditions, NTU=11.4, Cr*=3).

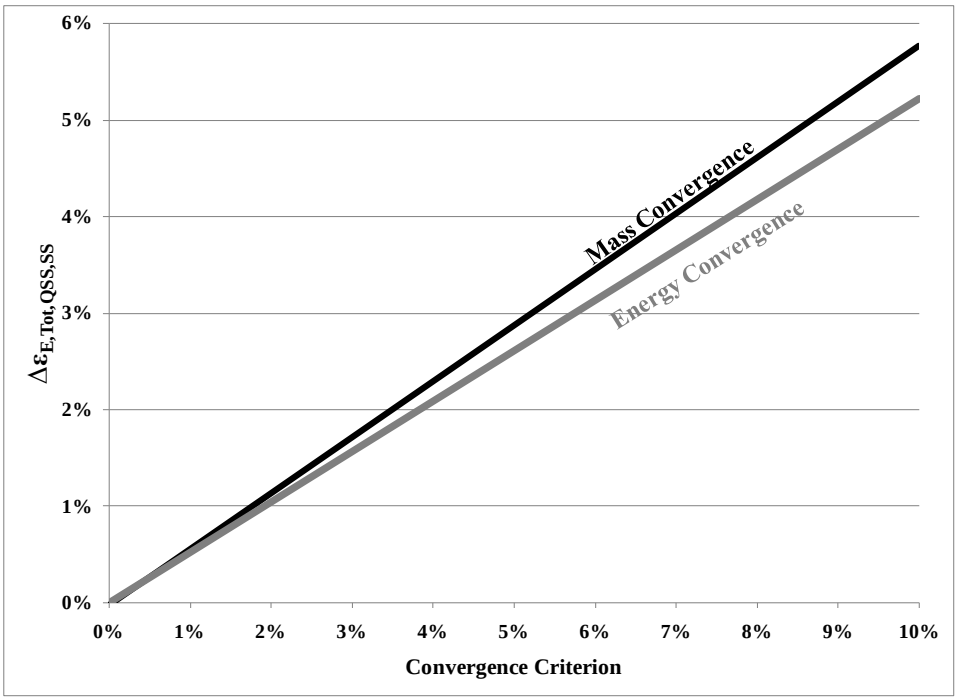

Figure 2.13: Difference between quasi-steady-state and steady-state total effectiveness for the exhaust exchanger for different mass and energy convergence criteria (AHRI Summer Conditions, NTU=11.4, Cr*=3).

During winter AHRI conditions, the system is started with the solution initially at the indoor room temperature of 21°C and at equilibrium with air at a humidity ratio of 7.1 g/kg. Therefore, the desiccant solution begins at 21°C and a concentration of 33.8%. As the system runs, the solution cools down and the concentration decreases to approximately 27%. The large change in concentration required to reach steady state takes significantly longer than the change in temperature. Therefore, the mass convergence criterion takes much longer to be satisfied compared to the energy convergence criterion, as shown in Figure 2.14.

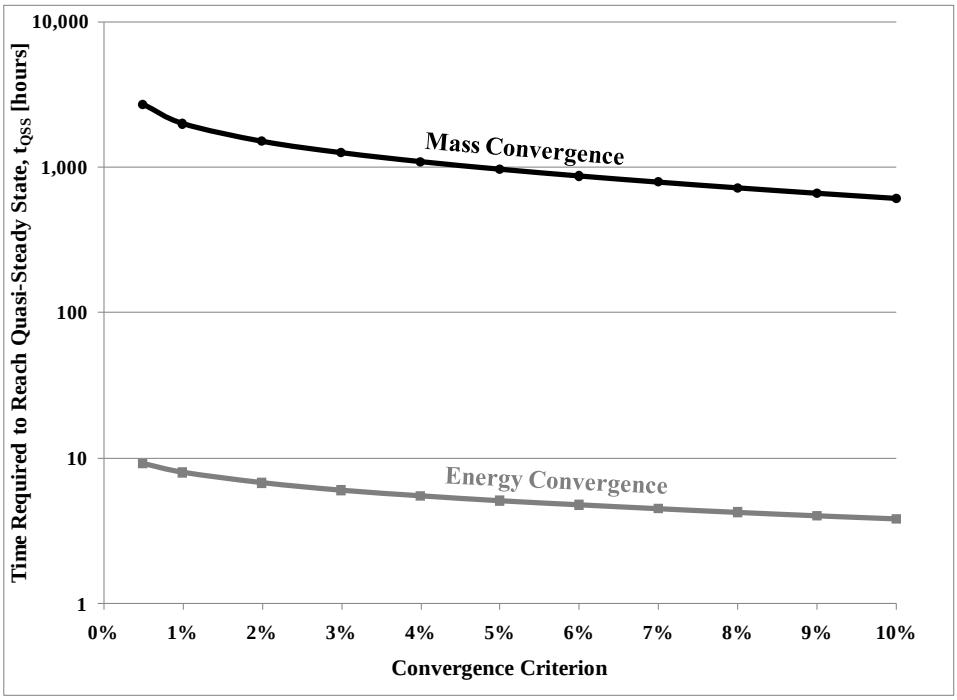

Figure 2.14: Time required to reach quasi-steady state for various criterion for both mass and energy convergence (AHRI Winter Conditions, NTU=11.4, Cr*=3).

The desired accuracy for temperature, humidity, and effectiveness are given in Table 2.5, along with the mass and energy convergence criterion required to reach these accuracies under AHRI winter conditions. Also presented are the times required for the system to reach quasi-steady state for the corresponding mass and energy convergence criteria. As Table 2.5 shows a mass convergence criterion of 2.8% and an energy

convergence criterion of 2.1% would provide accurate quasi-steady-state supply outlet temperature and humidity values. However, the mass and energy convergence criteria could be relaxed to 10.8% and 8.9% respectively to obtain accurate quasi-steady-state overall effectiveness values.

Table 2.5: Desired quasi-steady state accuracy with corresponding required mass and energy convergence criteria and time required to reach quasi-steady state.

	Desired Accuracy	Required Mass Convergence Criterion [%]	Time to Reach Mass Criterion [hours]	Required Energy Convergence Criterion [%]	Time to Reach Energy Criterion [hours]
Temperature [°C]	±0.20	4.3	1056	2.1	6.7
Humidity [% RH]	±1.00	2.8	1309	15.0	3.1
Supply/Exhaust Total Effectiveness	±1.00	88.5	227	1.1	7.8
Overall (average) Total Effectiveness	±0.10	10.8	570	8.9	4.1

Based on the discussed results for winter AHRI conditions, a mass balance of 10% and an energy balance of 1% will be used when studying the steady-state effectiveness of the system. However for the study of practical applications, a 2.5% mass balance and a 2% energy balance will be used.

A special convergence case occurs when heat gains/losses between the RAMEE and the surroundings are taken into account in the numerical model. When heat gains or losses occur, the energy transferred on the supply side will not be the same as the energy transferred on the exhaust side. Therefore, the convergence criteria selected using equation (2.29) will not be met at quasi-steady state. The effects of the heat gains/losses can be taken into account by adding/subtracting the additional energy transfer in the energy convergence equation,

$$\left| \frac{(H_{Air,S,in} - H_{Air,S,out}) - (H_{Air,S,in} - H_{Air,E,out}) + \sum \text{Heat Gains(+)/Losses(-)}}{(H_{Air,S,in} - H_{Air,E,in})} \right| \leq e\_c. \quad (2.33)$$

Similarly if there are any moisture gains/losses in the system, they must be considered in the mass convergence criterion of equation (2.28). An example of when this may occur is if the solution concentration is changed by the addition of water. For the case when there are moisture gains/losses in the system, the mass convergence criterion becomes,

$$\left|\frac{(W_{Air,S,in} - W_{Air,S,out}) - (W_{Air,E,in} - W_{Air,E,out}) + \sum \text{MoistureGains(+)/Losses(-)}}{(W_{Air,S,in} - W_{Air,E,in})}\right| \leq \text{m\_c.} \quad (2.34)$$

An alternate method of determination of quasi-steady state is used for experimental testing in this thesis because quasi-steady state is difficult to determine experimentally using equation (2.33) because heat gains and losses are not known prior to testing. The alternate method is based on the rate of change of the overall (average between the supply and exhaust) effectiveness (Seyed-Ahmadi, 2008). The alternate quasi-steady-state criterion states that quasi-steady state is achieved when the dimensionless rate of change in the sensible, latent, and total overall system effectivenesses are each less than 5 x 10^{-6} during the transient period, and is represented by the equation,

$$\left|\frac{\partial \varepsilon_O}{\partial \tau}\right| \leq 5 \times 10^{-6} \quad (2.35)$$

where:

τ is the number of volume circulations of the solution in the exchangers.

The dimensionless number, τ, is a function of the volume flow rate in each exchanger as well as the length of the exchangers in the solution flow direction, and is given by,

$$\tau = \frac{1}{\left(\frac{tV_{Sol,S}}{y_0}\right)^{-1} + \left(\frac{tV_{Sol,E}}{y_0}\right)^{-1}}, \tag{2.36}$$

where:

t is time required for the solution to travel through the exchanger [s], and

V_{Sol} is the velocity of the solution as it travels through the exchanger [m/s].

A 5 x 10^{-6} rate of change corresponds to an approximate (depends on flow rate) change of less than 0.005% per hour in overall effectiveness (for sensible, latent, and total), and a change of less than 0.5% per hour in supply and exhaust effectiveness (for sensible, latent, and total). Numerical results show that decreasing this value from 5 x 10^{-6} to 1 x 10^{-6} changes the predicted individual (supply or exhaust) effectiveness by less than 2%, and the overall (average of supply and exhaust) effectiveness by less than 0.05%. However, the time required to reach quasi-steady state would increase by 1.5 times.

All experimental tests as well as all numerical simulations that are to be compared to experimental tests (results presented in Chapter 3) will use the convergence criteria given by equation (2.35). The preferred method of determining quasi-steady state is the energy and mass balance and if this method was used for the experimental comparisons instead of equation (2.35) the quasi-steady-state supply and exhaust effectiveness values would change by less than 2% and the overall effectiveness would change by less than 0.03%.

All numerical simulations that are not directly compared to experimental data (results presented in Chapter 4) will assume that the system is well insulated and

therefore will neglect heat loss/gains and use the convergence criteria given by equations (2.28) and (2.29), unless the control strategies developed require the addition of either heat or moisture, in which case equations (2.33) and (2.34) will be used.

2.10 Impact of Quasi-Steady-State Convergence Criteria on Concentration

Section 2.9 showed how the quasi-steady-state air temperature and humidity are impacted by the mass and energy convergence criteria chosen. Similarly, the quasi-steady-state solution mass fraction $\left(X_{Sol,QSS}\right)$ is also impacted by the chosen mass convergence criterion, as well as the initial average mass fraction of the solution $\left(X_{Sol,Initial}\right)$ at system start-up. Since the mass fraction of the solution varies slightly throughout the system (i.e. at the inlet and outlet of each exchanger), the quasi-steady-state solution mass fraction is defined as the average mass fraction in each LAMEE given by,

$$X_{Sol,QSS} = \frac{X_{Sol,S,in} + X_{Sol,S,out}}{2} = \frac{X_{Sol,E,in} + X_{Sol,E,out}}{2}. \qquad (2.37)$$

Figure 2.15 shows the quasi-steady-state solution mass fraction $\left(X_{Sol,QSS}\right)$ for different values of the initial solution mass fraction $\left(X_{Sol,Initial}\right)$ and two different mass convergence criteria (2.5% and 1%).

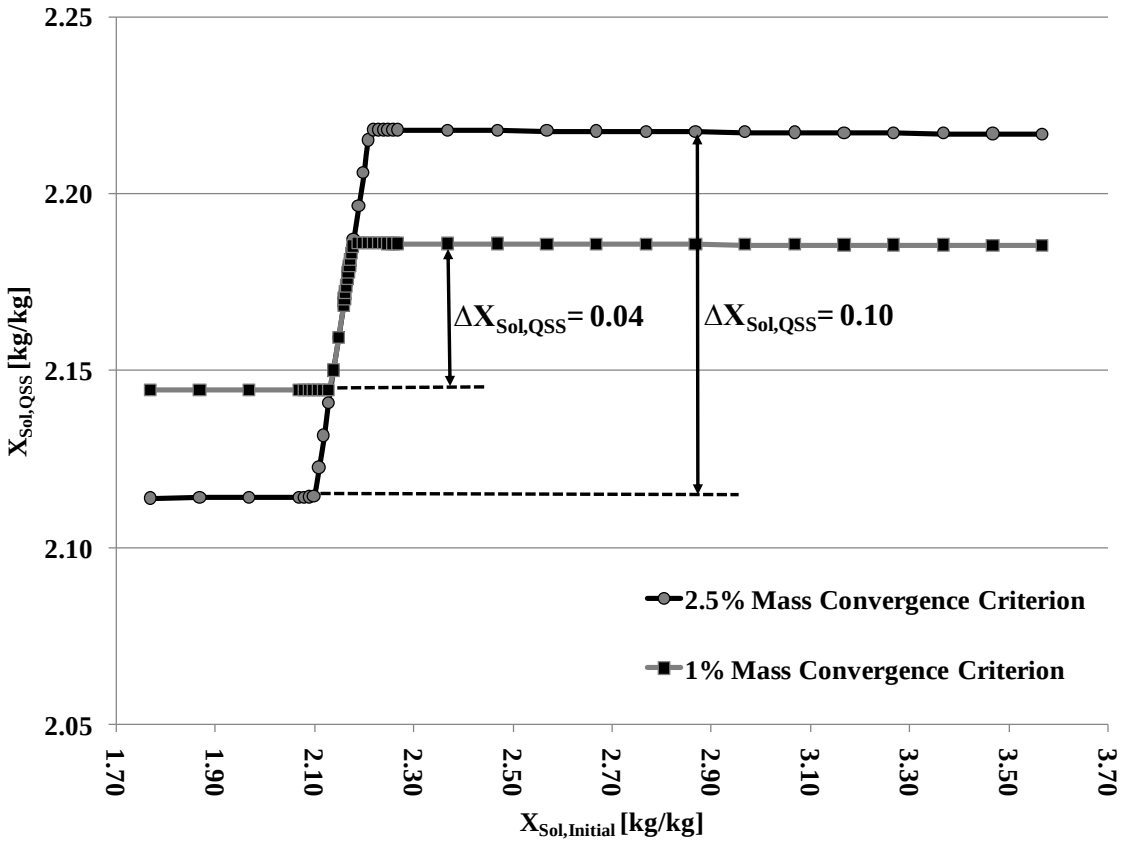

Figure 2.15: The resulting quasi-steady-state solution mass fraction for multiple different initial mass fractions and two different mass convergence criteria (NTU=11.4, Cr*=3, summer AHRI conditions).

As shown in Figure 2.15, for a mass convergence criterion of 2.5% all initial solution mass fraction values below $X_{Sol,Initial} = 2.09$ converge to a quasi-state-state value of $X_{Sol,QSS} = 2.12$, while all initial mass fraction values above $X_{Sol,Initial} = 2.22$ converge to a quasi-steady-state value of $X_{Sol,QSS} = 2.22$. However between these values, the model converges to a value somewhere on the linear line between the two $X_{Sol,QSS}$ values. This occurs because the model is unable to resolve small changes in X_{Sol} when the mass convergence is not strict enough. Therefore, the model is insensitive to the change in X_{Sol} if $X_{Sol,Initial}$ is too close to $X_{Sol,QSS}$ for the chosen mass convergence criterion. As Figure 2.15 shows, this range of insensitivity $(\Delta X_{Sol,QSS})$ is

reduced if the mass convergence criterion is made more stringent. For example reducing the mass convergence criterion from 2.5% to 1% reduces the range of insensitivity from 0.10 to 0.04. Figure 2.16 shows how the range of insensitivity decreases linearly as the mass convergence criterion is reduced. The range of insensitivity could be reduced and essentially eliminated with a very small mass convergence criterion. With such a small mass convergence criterion, the numerical model would be able to accurately predict $X_{Sol,QSS}$, but the resulting transient times would be large, impractical, and inconsistent with the realistic development of the mass convergence criterion in section 2.9 based on a practical HVAC system.

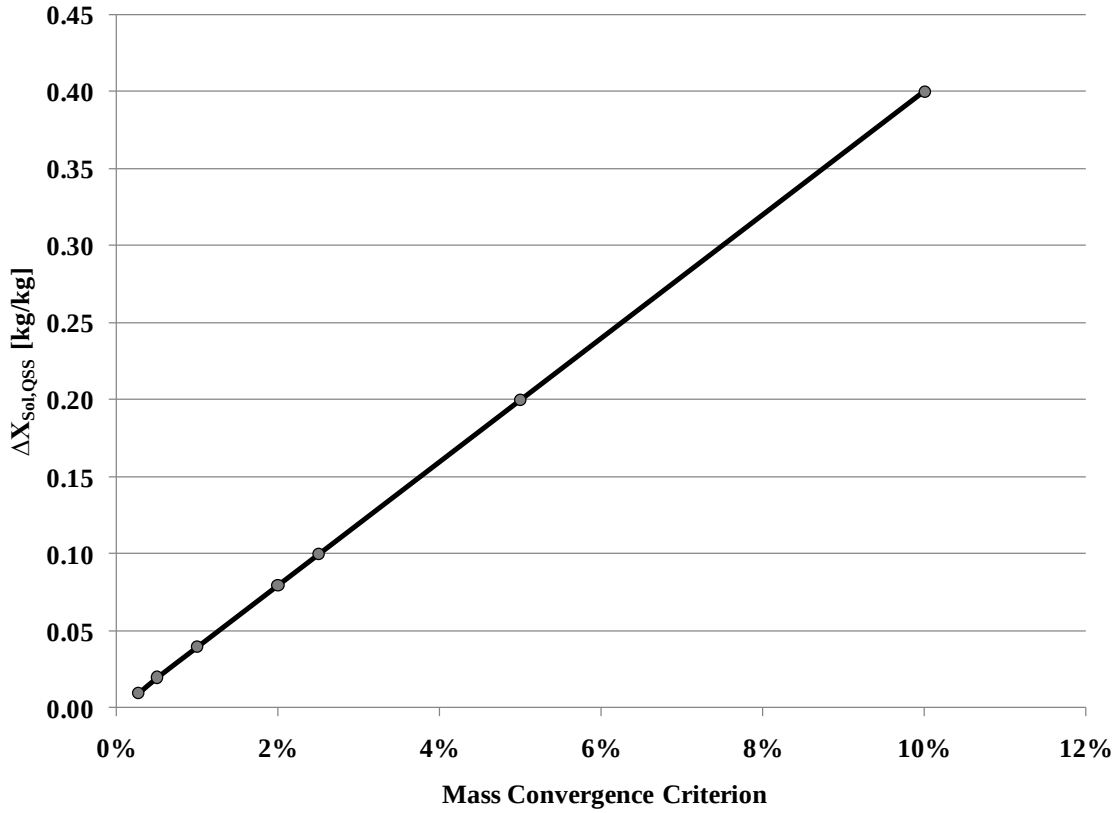

Figure 2.16: Insensitivity range for different mass convergence criterion (NTU=11.4, Cr*=3, summer AHRI conditions).

The insensitivity range decreases as the mass convergence criterion is reduced. Therefore the two constant $X_{Sol,QSS}$ values found outside of the insensitivity range

become closer together as the mass convergence criterion is reduced. However, for any mass convergence criterion, the average between the two $X_{Sol,QSS}$ values outside the insensitivity range remains constant. For the conditions shown in Figure 2.15, the average for a mass convergence criterion of either 2.5% or 1%, results in an average quasi-steady-state mass fraction of 2.17 kg/kg. This average is the quasi-steady-state mass fraction that would occur if the mass convergence criterion were set to zero, and no insensitivity occurred. Therefore, for summer AHRI conditions, NTU=11.4 and Cr*=3, a quasi-steady-state mass fraction of 2.17 kg/kg will be used throughout the remainder of the thesis.

Transient times are increased if the mass fraction of the solution does not begin at the quasi-steady-state mass fraction, but rather at some difference given by,

$$\Delta X_{Sol} = X_{Sol,Initial} - X_{Sol,QSS}. \tag{2.38}$$

Figure 2.17 gives the time required to reach quasi-steady state (t_{QSS}) at different conditions of ΔX_{Sol}. Large values of ΔX_{Sol} result in very large transient times of up to 475 hours (approx. 20 days). It should be noted that a value of $\Delta X_{Sol} = -0.4\,kg/kg$ corresponds to the saturation condition of the salt solution. Therefore, mass fractions below this point will not be considered.

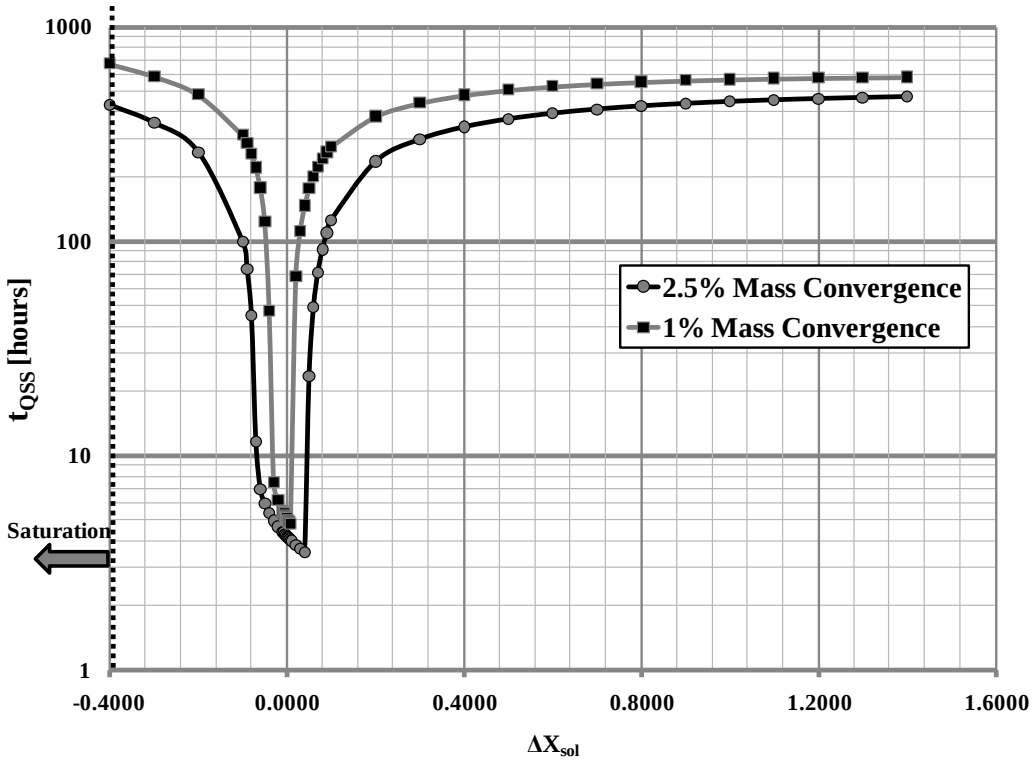

Figure 2.17: Time required to reach quasi-steady state at various initial solution concentrations that are ΔX_{Sol} away from the quasi-steady-state concentration, for mass convergence criteria of 1% and 2.5% (NTU=11.4, Cr*=3, summer AHRI conditions, $X_{Sol,QSS}$=2.1692).

As shown in Figure 2.17, the transient times at concentrations just above $\Delta X_{Sol} = 0$ are actually lower than when $\Delta X_{Sol} = 0$. A discontinuity also occurs at $\Delta X_{Sol} = +0.05$, which is inside the insensitivity range of the numerical model, where it is unable to resolve the small changes in X_{Sol} when it begins too close to $\Delta X_{Sol} = 0$. Figure 2.18 shows the transient time at different values of ΔX_{Sol}, for different mass convergence criteria when the zones of insensitivity are replaced with a smooth transitioning curve fit (dotted lines) instead of data points. These curves are assumed to better represent the actual transient time trends if the insensitivity did not exist.

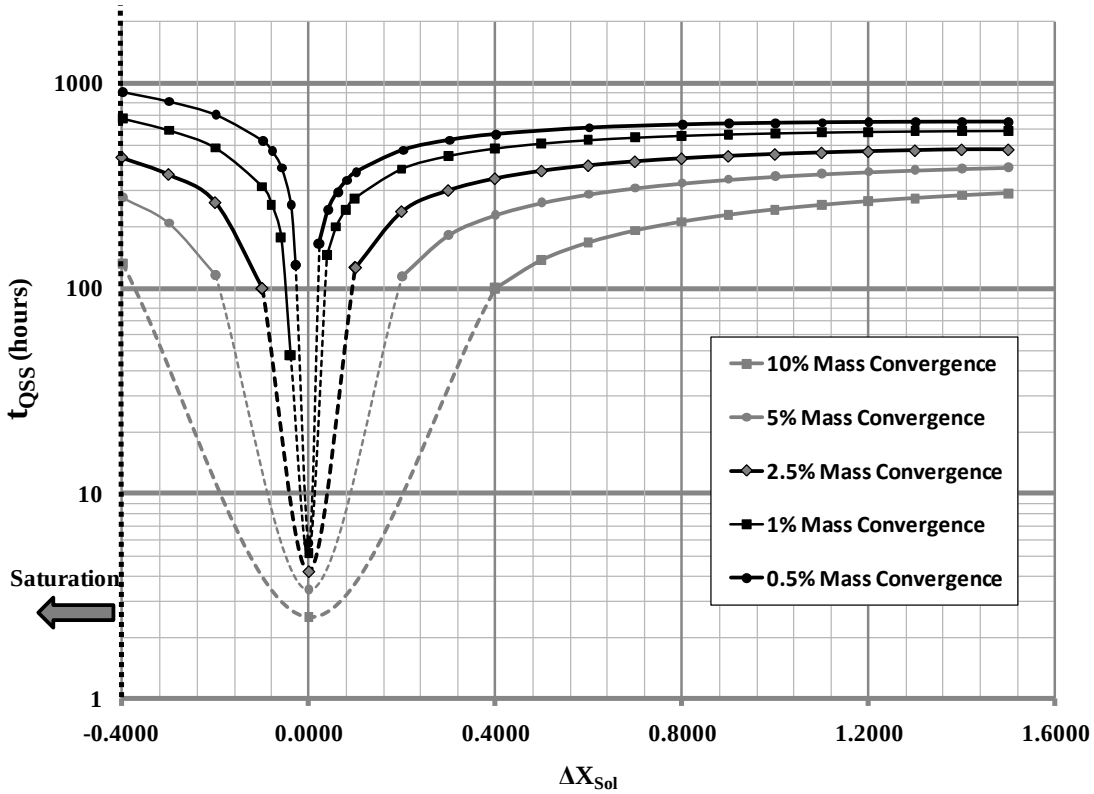

Figure 2.18: Time required to reach quasi-steady state at different ΔX_{Sol} values for five different mass convergence criterion values (NTU=11.4, Cr*=3, summer AHRI conditions).

As Figure 2.18 shows, the areas of insensitivity decrease when the mass convergence criterion is decreased. Again, it is shown that a very low mass convergence criterion would result in a very accurate determination of the transient time over the entire range of ΔX_{Sol}, but would result in much larger transient times compared to the transient times predicted when the mass convergence criterion is chosen as 2.5% for a practical HVAC system (corresponding to the supply outlet air temperature and humidity being within ±0.2 K and ±1%, respectively). Therefore, the curve developed for a mass convergence criterion of 2.5% will be assumed to more accurately represent the transient time for a practical HVAC application, and will be used throughout the remainder of this thesis.

2.11 Chapter 2 Summary

In this chapter the LAMEE prototype was described including the physical characteristics as well as the membrane's heat and mass transfer properties. The RAMEE testing apparatus (RAMEE-TA) was described, including all of the sensors and their corresponding measurement uncertainties. The numerical model was presented along with the assumptions made and the governing equations used. The testing conditions recommended by AHRI for air-to-air energy exchangers were given. However due to limitations in laboratory equipment, the actual experimental testing conditions were slightly different than the AHRI testing conditions. Therefore, the numerical model will use the AHRI testing conditions, except for cases where it is being compared with experimental data, in which the numerical model will then use the conditions associated with each individual experimental test.

Proper criteria for the determination of when quasi-steady state occurs were developed for both summer and winter testing conditions. These criteria were selected based on both the accuracy of the performance factors describing the system, as well as the accuracy in the determination of the air properties leaving the supply exchanger. For summer AHRI conditions, a mass and energy balance of 1% will be used when studying the quasi-steady-state effectiveness of the system, but more relaxed mass and energy balances of 2.5% and 3% will be used to accurately determine when a system has reached quasi-steady state in a practical application. For winter AHRI conditions, a mass balance of 10% and an energy balance of 1% will be used when studying the quasi-steady-state effectiveness of the system, but a 2.5% mass balance and a 2% energy balance will be used when studying the practical application of the RAMEE.

The quasi-steady-state solution mass fraction $\left(X_{Sol,QSS}\right)$ was found to be influenced by both the mass convergence criterion chosen as well as the initial concentration of the solution $\left(X_{Sol,Initial}\right)$ at system start-up. However, the numerical model was found to be insensitive to small changes in X_{Sol} (if $X_{Sol,Initial}$ is too close to $X_{Sol,QSS}$) for the chosen mass convergence criterion. Selecting a more stringent mass convergence criterion was found to reduce and essentially eliminated the range of insensitivity, but the resulting transient times would be large, impractical, and inconsistent with the realistic development of the mass convergence criterion for a practical HVAC system. Therefore a mass convergence criterion of 2.5% will be used throughout the thesis when studying the practical application of the RAMEE, and the quasi-steady-state mass fraction $\left(X_{Sol,QSS}\right)$ will be given by the average between the two constant $X_{Sol,QSS}$ values found at $X_{Sol,Initial}$ values outside the insensitivity range. The quasi-steady-state mass fraction $\left(X_{Sol,QSS}\right)$ was found to be 2.17 kg/kg for summer AHRI conditions, NTU=11.4 and Cr*=3.

The time required to reach quasi-steady-state was found to largely depend on the difference between the initial and the quasi-steady-state mass fractions $\left(\Delta X_{Sol}\right)$. Larger ΔX_{Sol} values result in much larger transient times, which can be as long as several weeks (over 20 days). Reducing these transient times will be the focus of Chapter 4.

CHAPTER 3

EXPERIMENTAL AND NUMERICAL COMPARISON

3.1 Introduction

In this chapter, the performance of the RAMEE system is investigated both numerically and experimentally by considering the experimental setup, numerical model, LAMEEs, and RAMEE described in Chapter 2. The experimental test results are determined by first allowing the supply and exhaust inlet air stream conditions to be as close as possible to AHRI test conditions. Then, the desiccant pumps are turned on, and data acquisition is started. Experimental transient data is collected throughout the test, until quasi-steady state is reached as determined by the criteria described in Chapter 2. Data is collected for various NTU and Cr* values by varying the air and desiccant flow rates. To obtain several data points with the same NTU and varying Cr*, the air flow rate is held constant, and the desiccant flow rate is varied.

3.2 Transient Comparison

The transient performance of the RAMEE system becomes important during both system start-up as well as with changes in the outdoor and exhaust air inlet conditions. It is important for this system to be able to react quickly in conditions where the climate can change drastically in only a few hours. Failure to adjust quickly could result in decreased performance, and may even put extra load on auxiliary heating and cooling equipment in practical applications.

3.2.1 Summer Transient Comparison

The summer experimental testing conditions described in Chapter 2 were used to compare the experimental data and the numerical model. Figures 3.1, 3.2, and 3.3 show the transient total, sensible, and latent effectiveness results for NTU=11.5 and Cr*=18 at summer experimental test conditions.

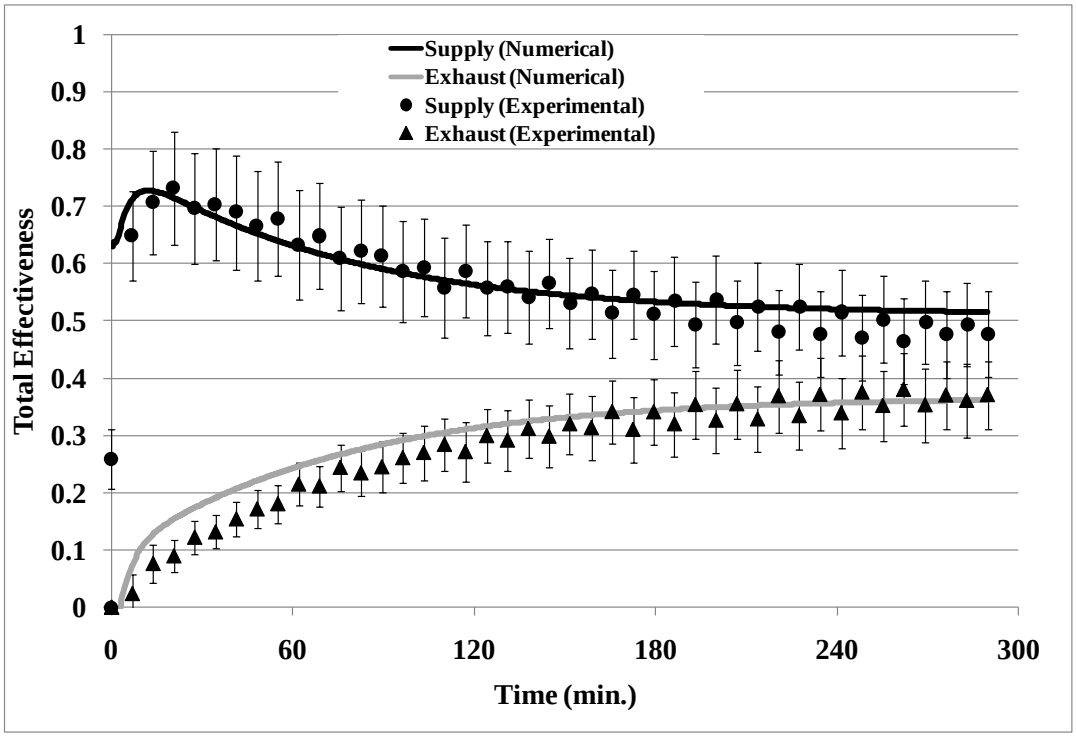

Figure 3.1: Total effectiveness transient results for NTU=11.5 and Cr*=18 (experimental summer test conditions).

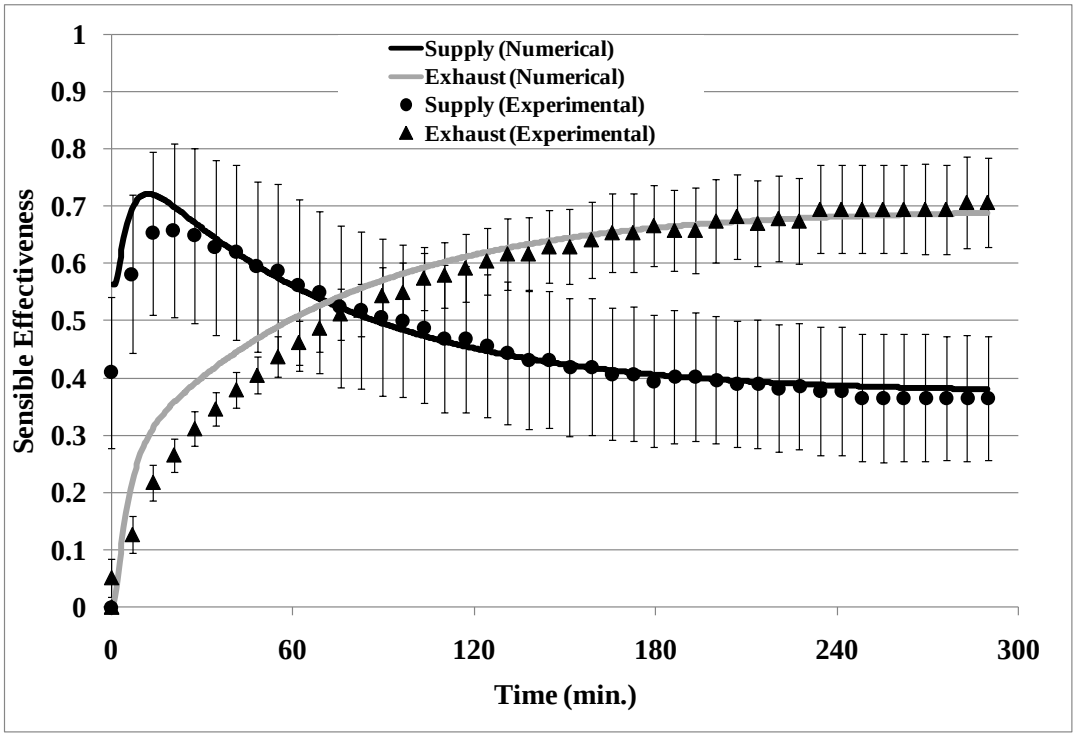

Figure 3.2: Sensible effectiveness transient results for NTU=11.5 and Cr*=18 (experimental summer test conditions).

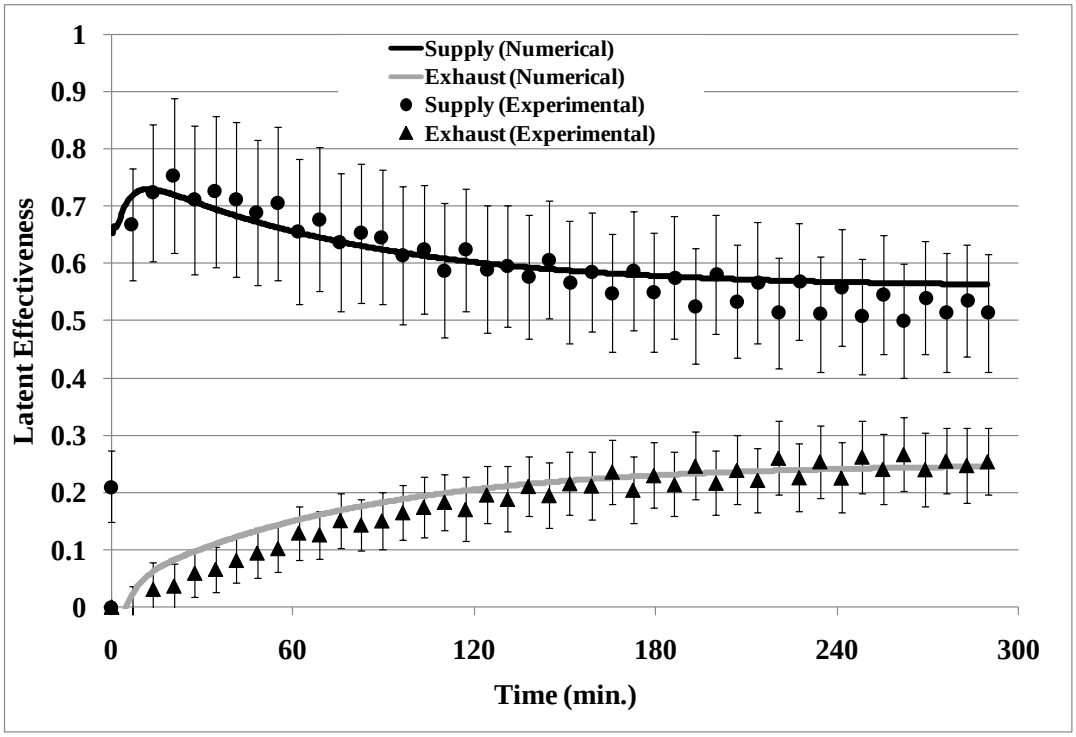

Figure 3.3: Latent effectiveness transient results for NTU=11.5 and Cr*=18 (experimental summer test conditions).

As mentioned earlier, the numerical model considers the heat loss from the RAMEE system to the environment. Figures 3.1, 3.2 and 3.3 show good agreement between the experimental and numerical results for total, sensible, and latent effectiveness, when this heat loss is considered. If there were no heat losses/gains in the system, the effectiveness on the supply side would equal the effectiveness on the exhaust side at steady state, since heat and moisture transfer in both exchangers would be equal. Therefore, the heat loss from the system causes a lower sensible and a higher latent effectiveness on the supply side compared to the exhaust side. For this case, the quasi-steady-state total effectiveness on the supply side is about 15% higher than the exhaust side. Better insulation could reduce this difference.

Figure 3.4 shows the transient change in the sensible, latent, and total effectiveness quasi-steady-state convergence criteria for this test. For this test condition, the overall sensible effectiveness was the last one (out of sensible, latent and total effectiveness) to meet the governing quasi-steady-state convergence criteria from equation (2.35). The transient response of the system is very slow. For the test condition it takes almost five hours to reach quasi-steady state. This is simply too long for practical use during weather that changes rapidly from hour to hour, or even overnight. If the outdoor conditions change faster than the system can react, then the system will always lag behind.

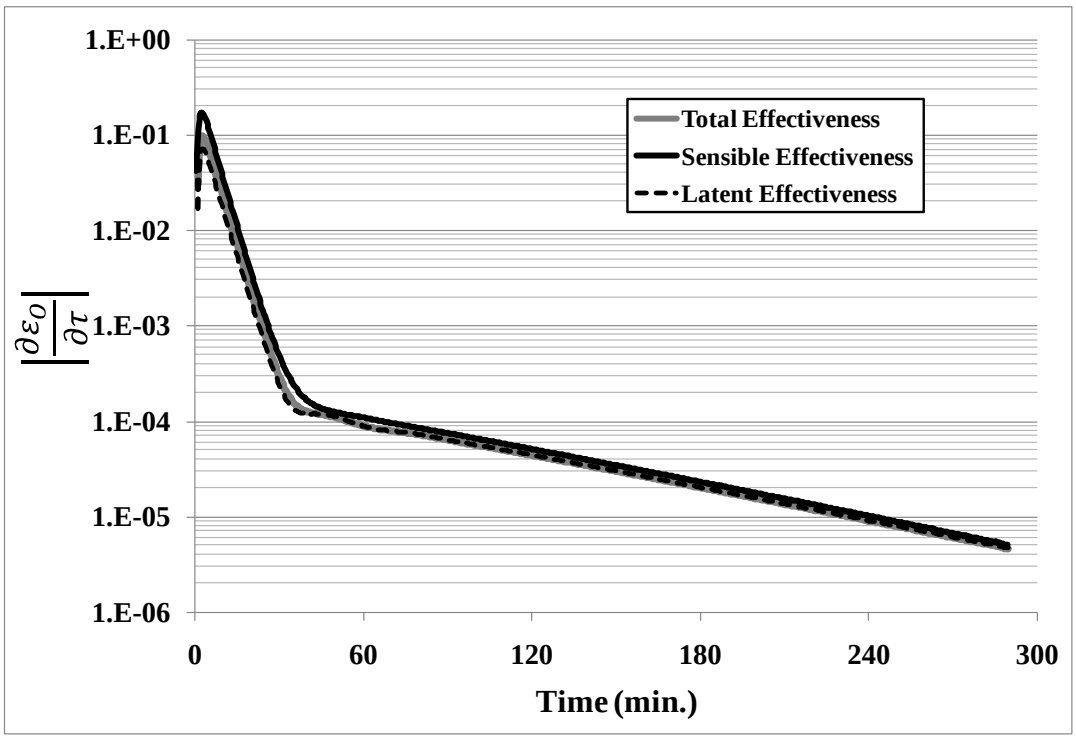

Figure 3.4: The sensible, latent, and total quasi-steady-state convergence criteria for NTU=11.5 and Cr*=18 (experimental summer test conditions).

One interesting thing to note from Figure 3.1 is that during this transient period the supply side effectiveness (which is most important) is actually higher. This means that the RAMEE system actually performs better during the transient period, and under some conditions it would be beneficial to lengthen the transient time. The transient time could be further lengthened by simply increasing the amount of desiccant solution in the system, which will increase the time it takes for the desiccant to reach equilibrium temperature and concentration. Transient times should be reduced when they have a negative impact on the supply side effectiveness. If the supply side effectiveness is higher during the transient period, then the transient time should not be reduced, but rather kept as long as possible.

From Figures 3.1, 3.2 and 3.3 it can be seen that the experimental effectiveness slightly lags the numerical effectiveness. This is thought to be partly due to the flow

maldistribution within each exchanger. Upon assembly of each LAMEE, it was noted that the header plates squeezed the desiccant channels too tight. Spacers were inserted to ensure an adequate desiccant flow could be obtained, but the result was an inconsistent inlet and outlet size for the desiccant flow. As a result, a channeling flow was created at each spacer rather than a well distributed flow, especially at low liquid flow rates. A maldistributed flow would cause a lower effectiveness since the desiccant is not in uniform contact with the membrane and does not provide a uniform heat and moisture transfer throughout each module. Since the numerical model assumes uniform desiccant distribution within each channel, it reaches equilibrium faster by transferring more heat and moisture in a shorter time period. Improving the flow distribution in the experimental design is an important topic for future research. These results indicate that it will not only improve the effectiveness value, but also the transient times of the system.

In order to assess the comparison between the numerical and experimental data, the root mean square error (RMSE) can be calculated by,

$$\mathrm{RMSE} = \sqrt{\frac{\sum_{1}^{N}\left(\varepsilon_{\mathrm{Numerical}} - \varepsilon_{\mathrm{Experimental}}\right)^2}{\mathrm{N}}}, \tag{3.1}$$

where:

N is the number of data points used to compare the results.

Alternatively, the average absolute difference (AAD) can be used to quantify the comparison between the numerical and experimental data, and is given by the equation,

$$\mathrm{AAD} = \frac{\sum_{1}^{N}\left|\varepsilon_{\mathrm{Numerical}} - \varepsilon_{\mathrm{Experimental}}\right|}{\mathrm{N}}. \tag{3.2}$$

Table 3.1 shows the RMSE and AAD of the various effectiveness values for the summer transient comparison between numerical and experimental data.

Table 3.1: The root mean square error (RMSE) and the average absolute difference (AAD) of effectiveness values from the summer transient comparison between numerical and experimental data.

	Supply			Exhaust		
	Sensible	**Latent**	**Total**	**Sensible**	**Latent**	**Total**
RMSE	3.3%	7.4%	6.2%	3.8%	2.4%	3.1%
AAD	1.7%	3.4%	2.9%	2.7%	2.0%	2.6%

The maximum RMSE is 7.4%, and the maximum AAD is 3.4%, which are both well within the experimental uncertainties. Therefore, the numerical model is in good agreement with the experimental data.

3.2.2 Winter Transient Comparison

The numerical model is also compared to the experimental results for winter testing and values of NTU=11.3 and Cr*=10.2. The external heat gain from the environment to the RAMEE system is taken into account in the numerical model, and has a significant influence on the performance of the RAMEE system as shown in Figures 3.5, 3.6 and 3.7. The result is a diverging trend in the sensible effectiveness on the supply and exhaust sides. The supply side retains a very high effectiveness, while the exhaust side has a very low effectiveness. In order to avoid the effects of heat losses/gains on the performance, the system must be better insulated to reduce the amount of external heat transferred to the RAMEE system, especially the desiccant solution.

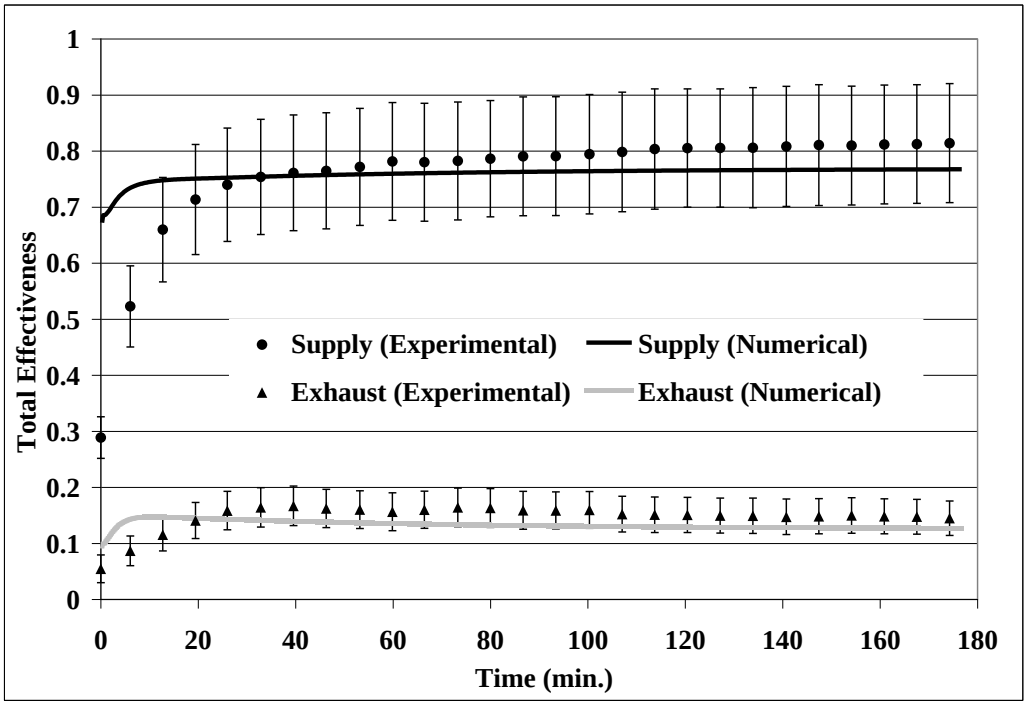

Figure 3.5: Total effectiveness transient results for NTU=11.3 and Cr*=10.2 (experimental winter test conditions).

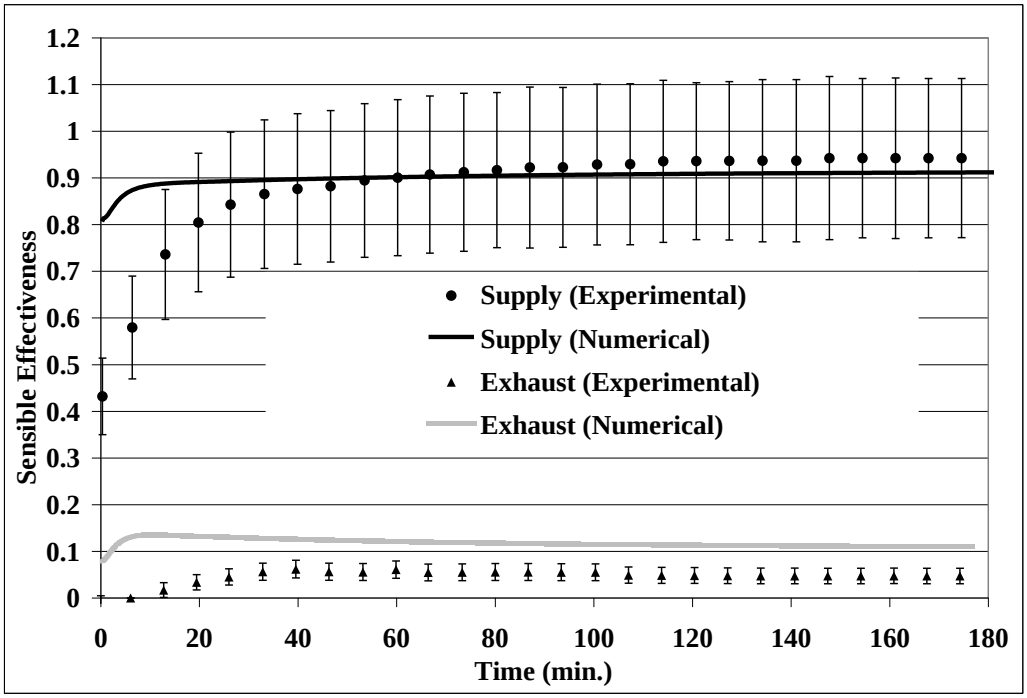

Figure 3.6: Sensible effectiveness transient results for NTU=11.3 and Cr*=10.2 (experimental winter test conditions).

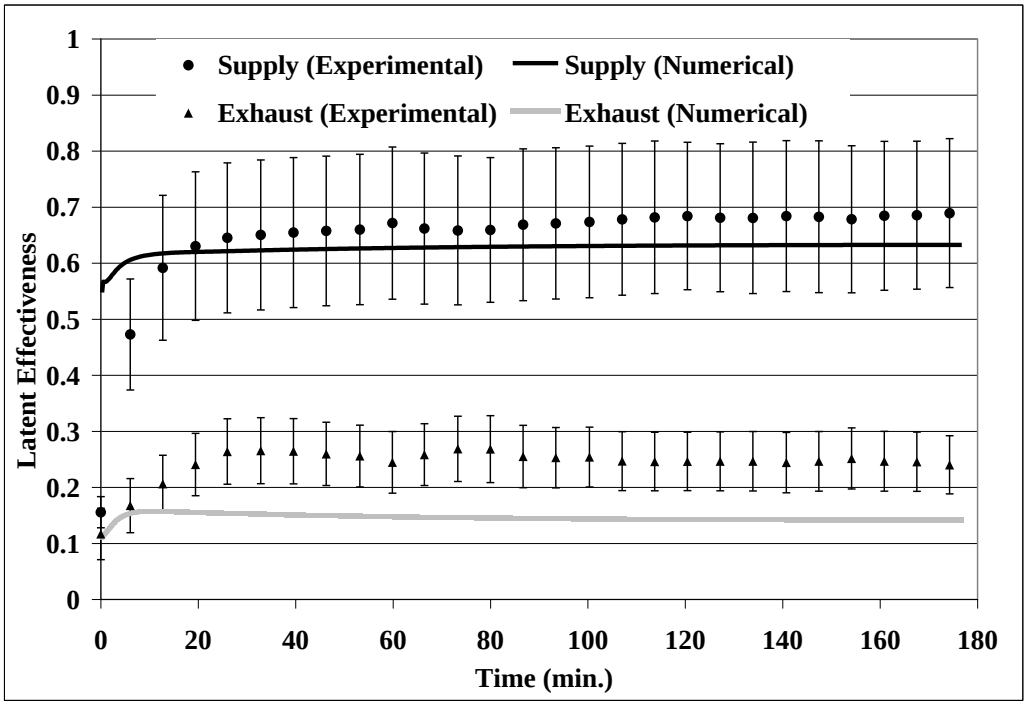

Figure 3.7: Latent effectiveness transient results for NTU=11.3 and Cr*=10.2 (experimental winter test conditions).

Taking the overall (average between the supply and exhaust) effectiveness results in the system achieving quasi-steady state as shown in Figure 3.8. However averaging the supply and exhaust effectiveness values to obtain an overall system performance is misleading, since the supply and exhaust effectiveness results are up to 80% different form one another and are diverging. Therefore, the overall effectiveness should be used for determining quasi-steady state, but not to indicate the performance of the system during these operating conditions.

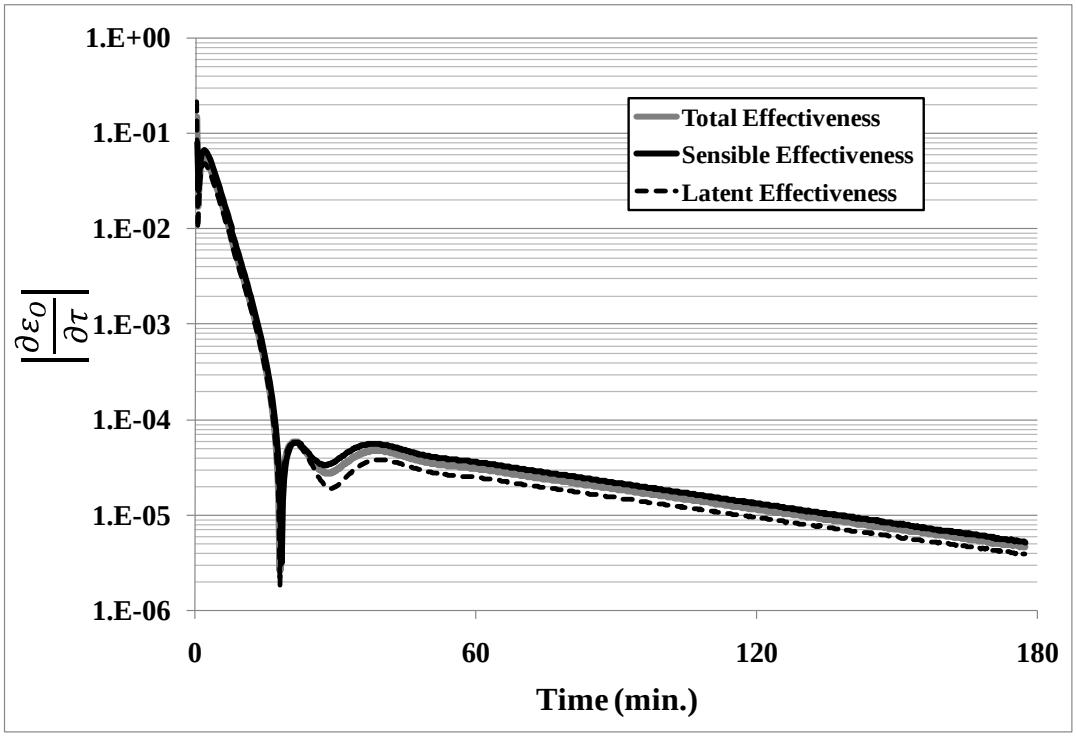

Figure 3.8: The sensible, latent, and total quasi-steady-state convergence criteria for NTU=11.3 and Cr*=10.2 (experimental winter test conditions).

In order to assess the comparison between the numerical and experimental data, the root mean square error (RMSE) and the average absolute difference (AAD) are calculated based on equations (3.1) and (3.2). Table 3.2 shows the RMSE and AAD of the various effectiveness values for the winter transient comparison between numerical and experimental data.

Table 3.2: The root mean square error (RMSE) and the average absolute difference (AAD) of effectiveness values from the summer transient comparison between numerical and experimental data.

	Supply			Exhaust		
	Sensible	**Latent**	**Total**	**Sensible**	**Latent**	**Total**
RMSE	6.9%	3.7%	5.1%	6.5%	10.0%	3.0%
AAD	3.7%	2.5%	3.0%	6.2%	10.3%	2.9%

The maximum RMSE is 10%, and the maximum AAD is 10.3%. Therefore, the numerical model is in good agreement with the experimental data.

Comparing the test data taken during summer test conditions (Figures 3.1, 3.2 and 3.3) to the test data taken during winter conditions (Figures 3.5, 3.6 and 3.7) shows that the difference between the supply and exhaust effectivenesses are larger during winter conditions than during summer conditions. This difference is partly due to the increased heat gains during winter conditions, which are much higher than the heat losses during summer conditions. Another reason, besides heat loss/gain, for this large difference between the supply and exhaust effectivenesses is that the desiccant solution is far from its equilibrium concentration upon initial start-up. Winter condition testing occurred after summer condition testing, without changing the initial desiccant concentration. However, each time the air temperature and humidity change, the desiccant must change both temperature and concentration in order to balance the systems heat and mass transfer. The 32% desiccant concentration used during summer conditions testing is not high enough for winter conditions testing, which requires a concentration of 34%. Therefore, the desiccant solution must change its concentration by expelling moisture into the air stream. From Figure 3.9, it can be seen that the humidity ratio increases on the supply side from inlet to outlet by a substantial amount, much greater than the decrease on the exhaust side. Therefore, the desiccant solution is expelling water into the supply air stream, which humidifies the air exiting the supply exchanger and increases the concentration of the desiccant solution.

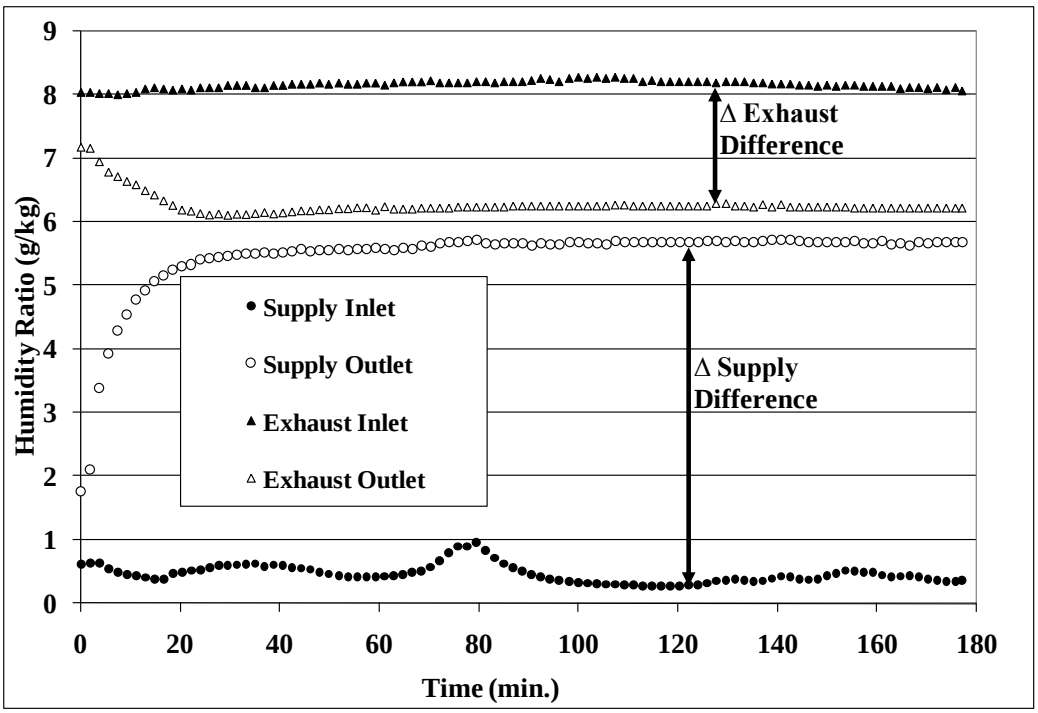

Figure 3.9: Changes in humidity ratios across the supply and exhaust LAMEEs for NTU=11.3 and Cr*=10.2 (experimental winter test conditions).

In order to expedite the change in desiccant concentration an additional heater can be placed in the desiccant loop to evaporate some of the moisture. If the concentration has to be decreased, additional water may be added to the loop. Another way to decrease transient times is to minimize the volume of desiccant in the system. A smaller desiccant volume allows the desiccant to react quicker to temperature and concentration changes.

Another interesting thing to note from Figure 3.9 is the ability of the RAMEE system to provide constant supply outlet humidity even when supply inlet humidity is fluctuating. This is due to the desiccant's ability to dampen fluctuations in the humidity ratio of the air stream. This becomes very important, as outdoor humidity values can often change very rapidly during a rain shower. Even with extreme changes in outdoor humidity, the RAMEE system will be able to provide a more constant indoor humidity to occupants.

3.3 Quasi-Steady-State Comparison

Typically the most important performance value used when assessing the economic feasibility of an air-to-air energy exchanger is the steady-state effectiveness of the system. The overall system effectiveness (average of supply and exhaust) is found for each test by considering the effectiveness once the convergence criterion (determined from equation (2.35)) is met. Since the transient results for winter test conditions had up to a 80% difference between supply and exhaust effectiveness, and diverged, this quasi-steady-state analysis was only completed for experimental summer test conditions. Figure 3.10 shows the experimental results as well as the numerical results for the overall total system effectiveness at several Cr* values for different NTU values.

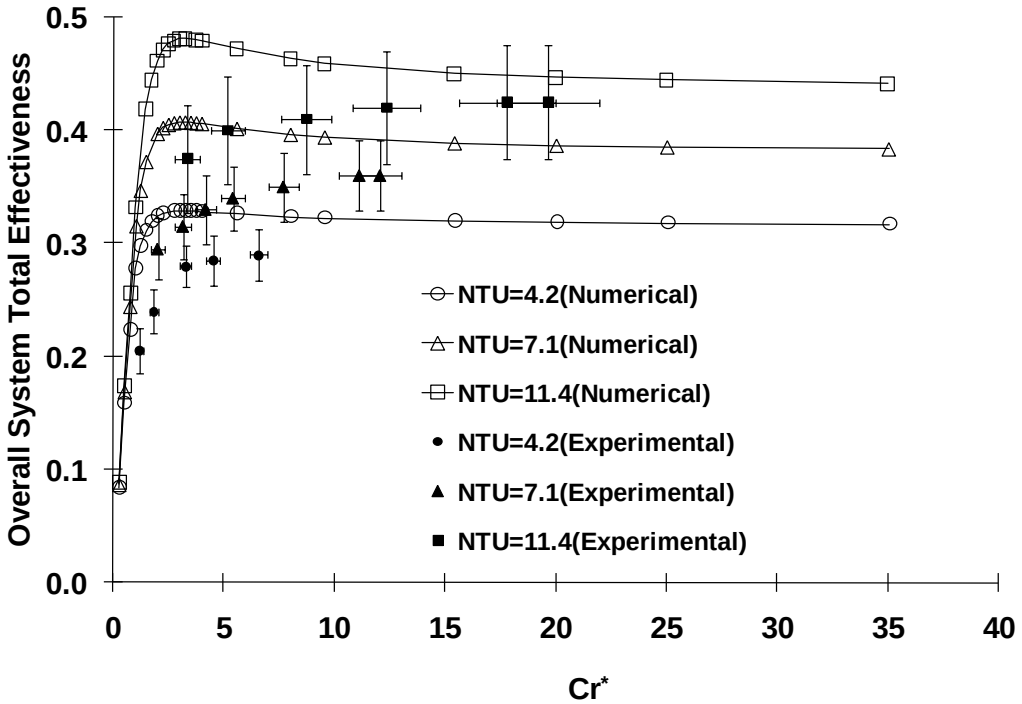

Figure 3.10: Comparison of simulated and measured overall system total effectiveness versus Cr* at three NTU values (experimental summer test conditions).

The experimental data shows that an increase in NTU results in an increase in the total (heat and moisture) system effectiveness, which is also confirmed by the numerical data. Although the experimental and numerical data show the same sensitivity to changes in NTU, they show somewhat different sensitivities to Cr*. The experimental data shows a consistent increase in effectiveness as Cr* increases over the entire range of Cr*, while the numerical data predicts that the effectiveness should increase as Cr* increases from 0 to 3 and then decrease slightly as Cr* increases above 3. Both the experimental and numerical data show that the effectiveness will approach an asymptotic value for large values of Cr*. At very high Cr* values, the numerical and experimental effectiveness values are close enough to agree within the experimental uncertainty bounds. In fact, at the highest Cr* values tested (Cr*=19.6 and NTU=11.4), the numerical and experimental effectiveness values agree within 2.2% of each other. The reason for the different Cr* dependence is believed to be due to desiccant flow distribution problems at low Cr* values (low liquid flow rates). Recall that a maldistributed flow would cause a lower effectiveness since the desiccant is not in uniform contact with the membrane and does not provide uniform heat and moisture transfer throughout each module. Since Cr* is increased by increasing the flow rate of the liquid desiccant, a higher Cr* results in a higher pressure inside of each desiccant channel. This higher pressure appears to reduce the maldistribution, and enhances fluid mixing. This is thought to be why the effectiveness values continue to increase with Cr*, and only begin to reach the numerical results when Cr* is very high.

Also shown in Figure 3.10 are the uncertainties in the experimental measurements. The uncertainties in effectiveness range from 1.8% at NTU=4.2 and low

Cr* values, to 5.1% at NTU=11.4 and high Cr* values. Higher NTU values create a higher uncertainty due to the lower air flow rate. The majority of the uncertainty in the effectiveness comes from measuring the air flow rate using a pressure differential orifice plate. At low flow rates, the uncertainty in flow rate measurements grow, causing an increase in the uncertainty of the effectiveness. The uncertainties in Cr* range from 0.2 at the lowest Cr* value to 2.3 at the highest Cr* value.

When quantifying the performance of an air-to-air energy exchanger, it is important to determine the sensible and latent effectiveness values individually, so that heat and moisture transfer can be examined somewhat independently. Figures 3.11 and 3.12 compare the numerical and experimental sensible and latent effectiveness for tests with summer experimental test conditions.

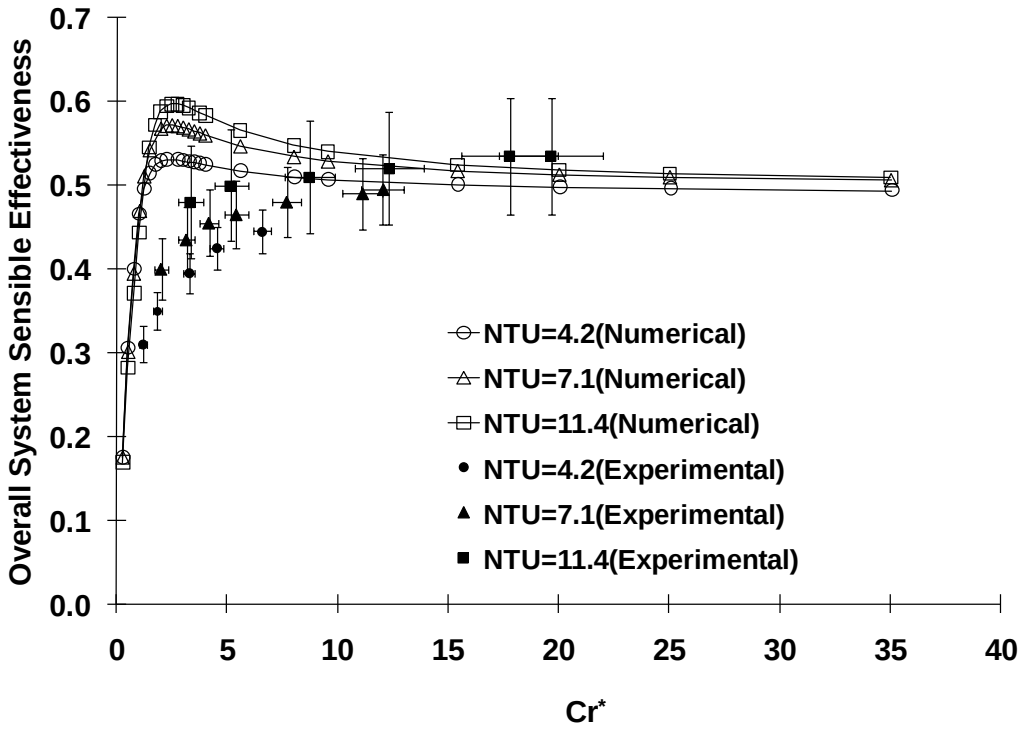

Figure 3.11: Comparison of simulated and measured overall system sensible effectiveness versus Cr* at three NTU values (experimental summer test conditions).

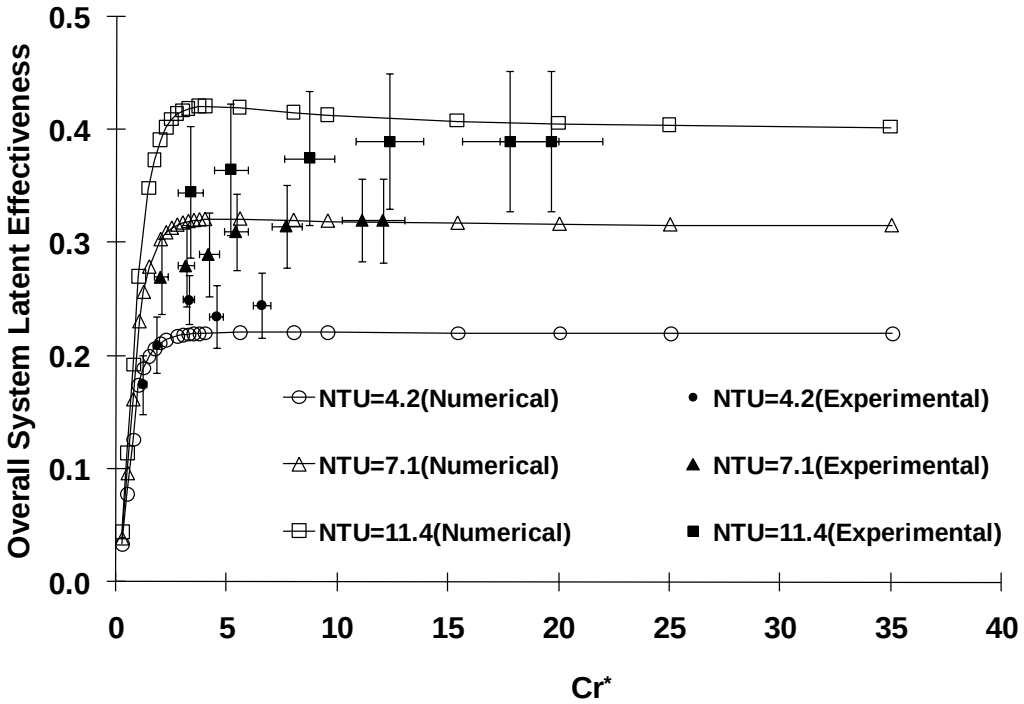

Figure 3.12: Comparison of simulated and measured overall system latent effectiveness versus Cr* at three NTU values (experimental summer test conditions).

From Figure 3.11 it can be seen that the experimental sensible effectiveness is only slightly dependent on NTU. As NTU was increased from 4.2 to 11.4, a maximum increase of 6% was observed. However, Figure 3.12 shows that the experimental and numerical latent effectivenesses are influenced by NTU. A maximum increase in latent effectiveness of nearly 20% was found when increasing NTU from 4.2 to 11.4. Therefore, in order to maximize the amount of moisture transfer it is important to keep NTU high. This can be done by optimizing the membrane characteristics (increasing water vapor permeability, decreasing thickness), increasing the surface area of the membrane, and by keeping the air flow rate low compared to the heat and mass transfer surface area in the exchanger.

Both sensible and latent experimental effectiveness results appear to be impacted by the flow maldistribution problem at low Cr* values, but they approach the numerical results at high Cr* values. The numerical model shows that the latent effectiveness is

not very dependent on Cr* for Cr*>3. However, the sensible effectiveness is impacted by different Cr* values, especially at higher NTU values. The simulations show that it is critical to keep Cr* as close as possible to 3 in order to maximize the sensible effectiveness. This is done by providing the proper desiccant flow rate for the given air flow rate. In a variable air flow system, a control system would be necessary to change the flow rate of the desiccant to keep Cr*=3 as the air flow rate changes.

The uncertainty in the experimental sensible effectiveness ranges from 2.1% at low NTU and Cr* values to 6.9% at high NTU and Cr* values. The uncertainty in the latent effectiveness ranges from 2.2% at low NTU and Cr* values to 6.2% at high NTU and Cr* values. The uncertainties in Cr* range from 0.2 at the lowest Cr* value to 2.3 at the highest Cr* value.

3.4 Chapter 3 Summary

In this chapter, the performance of the RAMEE system was investigated both numerically and experimentally. The transient performance of the RAMEE system was found to be important during system start-up, as long delays of up to several hours can occur before reaching quasi-steady state. Heat losses/gains between the RAMEE system and the environment were found to play a large role in the performance of the system. The heat losses/gains cause an imbalance in the amount of energy exchanged by the supply exchanger compared to the exhaust exchanger. Therefore, heat gains/losses should be minimized as much as possible by carefully insulating the system. The transient performances of the numerical and experimental RAMEEs were found to be in agreement, within experimental uncertainty. The maximum root mean square error was found to be 10% which implies good accuracy of the numerical model.

The quasi-steady-state performance of the RAMEE system was found to be influenced by two important factors; the number of heat transfer units (NTU), and the ratio of solution and air heat capacity rates (Cr*). The latent effectiveness was found to be heavily influenced by the NTU, as a higher NTU resulted in a higher latent effectiveness. Both the latent and sensible effectivenesses were found to be influenced by Cr*. The numerical model indicates that the effectiveness should increase with increasing Cr* until Cr*=3, at which point the effectiveness will decrease slightly to an asymptotic value for increasing Cr*. However, the experimental data shows a continuous increase in effectiveness with Cr*. The reason for this discrepancy between the numerical and experimental results at low Cr* values is believed to be due to maldistributed solution flow. The numerical and experimental results show good agreement at higher Cr* values, where the solution flow (and therefore the solution pressure) is increased.

CHAPTER 4

CONTROL STRATEGIES

4.1 Introduction

The purpose of this chapter is to use the numerical model to develop control strategies that can be used to minimize the transient time delays associated with both system start-up and changing outdoor weather conditions. The experimental and numerical comparison in Chapter 3 showed an example where the RAMEE took almost 5 hours to reach quasi-steady state. This chapter will show other conditions where the transient time is even longer (up to several days), and therefore even more critical. The control strategies that will be considered are solution and air flow control, air flow bypass, solution temperature control, and solution concentration control. In addition to start-up conditions, this chapter will also implement the control strategies to determine how the RAMEE system reacts to changing outdoor conditions.

4.2 Solution and Air Flow Control

The first control strategy that will be examined is solution and air flow control. Recall that the performance of the system is dependent on the ratio between the solution and air heat capacity rates (Cr*). The quasi-steady-state results shown in Chapter 3 revealed that the optimum effectiveness occurs when $Cr^* \approx 3$. Therefore it is important to maintain $Cr^* = 3$ when the system is at quasi-steady state. However, a higher solution flow rate, or a lower air flow rate can increase the amount of energy transferred between

the air and the solution for a single exchanger, even though it decreases the amount of energy transferred between the two air streams (system effectiveness). Therefore, increasing Cr* by increasing the solution flow rate and/or decreasing the air flow rate can result in lower transient times. The objective of this section is to determine how adjusting Cr* can reduce the transient time, while maintaining performance.

4.2.1 Initial Conditions

For this control strategy, it will be assumed that all the solution in the RAMEE system is initially at the same temperature as the exhaust inlet air (24°C for summer AHRI conditions) and the solution concentration begins at the average quasi-steady state concentration $\left(\Delta X_{Sol} = 0\right)$ as defined by equations (2.37) and (2.38). For these initial conditions, the solution must undergo a temperature change and only a slight concentration change in order to meet the desired conditions of each exchanger. The case of different initial concentrations will be considered in detail in section 4.5.

4.2.2 Methodology

The method of using flow control to decrease transient times is initiated from the fact that a single LAMEE is capable of transferring more energy between the air and the solution at higher Cr* values. Figure 4.1 shows this by examining the transient trend in total system effectiveness for two different Cr* values. Increasing Cr* from 3 to 15, reduces the transient time by 14 minutes (6%).

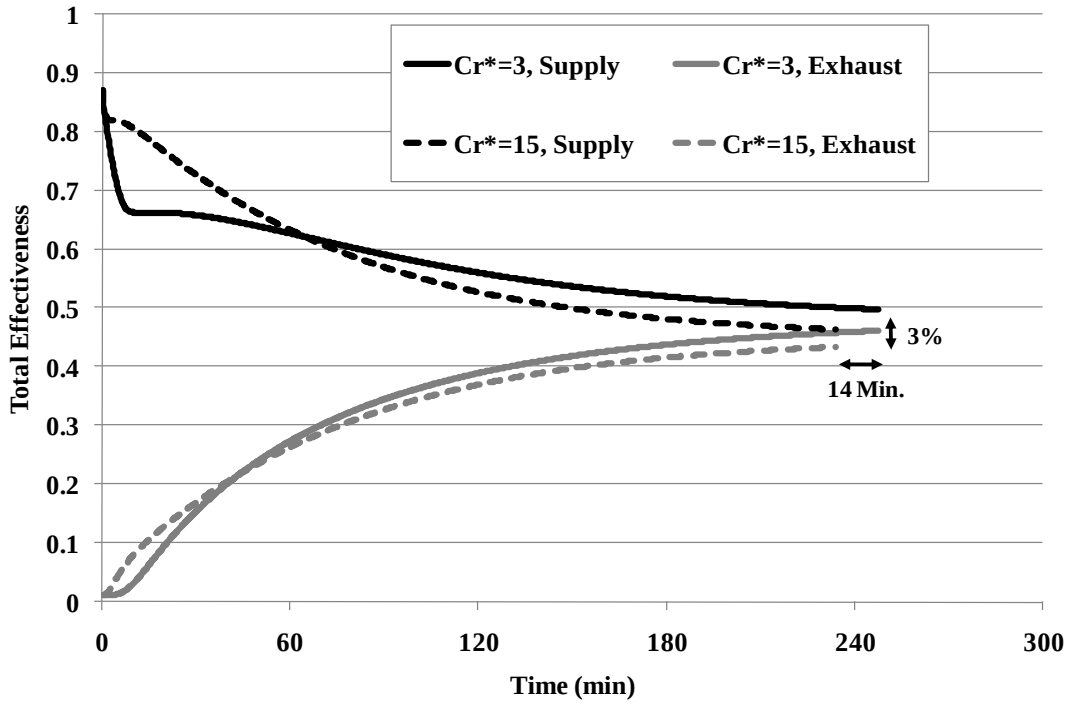

Figure 4.1: Total effectiveness over time for Cr*=3 and Cr*=15 (NTU=11.4, summer AHRI conditions, ΔX_{Sol}=0).

Unfortunately, the increase in Cr* also results in a 3% loss in overall RAMEE total effectiveness. Due to this behavior, it is desired to begin with the system operating at,

$$Cr^* = Cr^*_{Initial} > 3, \tag{4.1}$$

where:

$Cr^*_{Initial}$ is the Cr* value that is used at system start-up.

After the transient time is complete the system should return to,

$$Cr^* = Cr^*_{QSS} = 3, \tag{4.2}$$

where:

Cr^*_{QSS} is the optimal Cr* value that is used at quasi-steady state.

However, extra time will be needed for the RAMEE to reach quasi-steady state when Cr* is returned from $Cr^*_{Initial}$ to Cr^*_{QSS}. Figure 4.2 shows the extra transition time due to a

step change in Cr* from $Cr^*_{Initial}$ to Cr^*_{QSS}. For this case, the transition causes an increase in transient time of 90 minutes over the case when Cr* is held constant at $Cr^*_{QSS} = 3$.

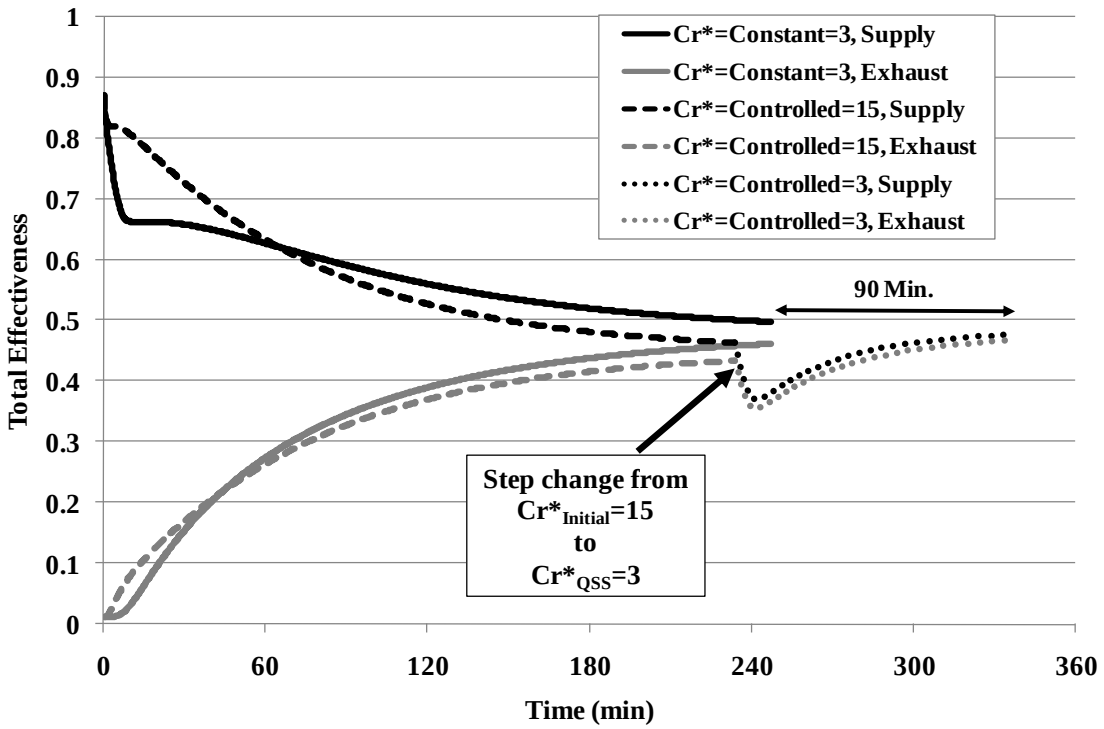

Figure 4.2: Total effectiveness over time for a constant Cr*=3 and a controlled Cr* undergoing a step change from Cr*=15 to Cr*=3. (NTU=11.4, summer AHRI conditions, ΔX_{Sol}=0).

It should be noted that the sudden, and brief, decrease in effectiveness when Cr* is initially reduced from $Cr^*_{Initial}$ to Cr^*_{QSS} is caused because the amount of energy transfer between the air and solution in each exchanger decreases as Cr* is reduced. This decrease in energy transfer results in a smaller air temperature change in both supply and exhaust exchangers, and therefore also results in a decrease in total effectiveness. When Cr* is initially reduced, the solution in each storage tank is still at the quasi-steady-state temperature for $Cr^*_{Initial}$, and must undergo a slight temperature change. For the case presented here, when $Cr^*_{Initial}$ is changed to Cr^*_{QSS}, the solution temperature in the storage tank located before the supply exchanger decreases, while the

solution temperature in the storage tank located before the exhaust exchanger increases. Therefore as the solution temperature changes, the RAMEE system effectiveness increases and eventually reaches the effectiveness corresponding to Cr^*_{QSS}. The higher the solution volume is in the system, the longer this temperature transition takes. Therefore, it is important to keep the solution volume to a minimum.

Due to the extra time required for the system to adjust to changing Cr* conditions, it may be advantageous to begin the transition from $Cr^*_{Initial}$ to Cr^*_{QSS} earlier. It may also be advantageous to use a slower rate of change (instead of a step change) from $Cr^*_{Initial}$ to Cr^*_{QSS} in order to allow the system more time to adjust. Therefore the flow control strategy developed will depend on four parameters, which will be discussed in detail throughout this section:

1) The initial ratio of heat capacity rates ($Cr^*_{Initial}$).
2) The time at which the initial ratio of heat capacity rates ($Cr^*_{Initial}$) should be reduced to the quasi-steady-state ratio of heat capacity rates ($Cr^*_{QSS} = 3$).
3) The rate of change in Cr* ($\partial Cr^* / \partial t$) during the transition between $Cr^*_{Initial}$ and Cr^*_{QSS}.
4) The time at which quasi-steady state is considered to be reached.

4.2.3 Flow Control Quasi-Steady-State Determination

The system is typically considered as having reached quasi-steady state when the mass convergence criterion (2.5%, Section 2.9), and the energy convergence criterion (3%, Section 2.9) have been met. However these criteria do not ensure that the system has returned to quasi-steady state conditions during the transition phase following the

change from $Cr^*_{Initial}$ to Cr^*_{QSS}. In order to ensure that the system has completed this adjustment phase, additional criteria must be met, which state that the effectiveness values for the supply exchanger must be within 2.5% of the quasi-steady-state effectiveness if Cr* was held constant with no flow control. The criteria are given by:

$$\varepsilon_{S,Sen,QSS} = \varepsilon_{S,Sen,QSS@Cr^*=3} \pm 2.5\% \tag{4.3}$$

$$\varepsilon_{S,Lat,QSS} = \varepsilon_{S,Lat,QSS@Cr^*=3} \pm 2.5\% \tag{4.4}$$

$$\varepsilon_{S,Tot,QSS} = \varepsilon_{S,Tot,QSS@Cr^*=3} \pm 2.5\% \tag{4.5}$$

where subscripts:

"$QSS@Cr^* = 3$" refers to the value at quasi-steady state if Cr* is not controlled, but rather held at a constant Cr*=3.

These criteria, along with equation (4.2), ensure that Cr* has not only returned to the quasi-steady-state value, but also that the system has finished adjusting to the change. A 2.5% range in effectiveness was chosen so that the air properties leaving the supply exchanger (temperature and humidity) would be the same as the properties at quasi-steady-state if Cr* was held at a constant Cr*=3, within the limits set by the governing mass convergence criteria in Chapter 2:

$$T_{QSS} = T_{QSS@Cr^*=3} \pm 0.2\,K, \text{ and} \tag{4.6}$$

$$RH_{QSS} = RH_{QSS@Cr^*=3} \pm 1\%. \tag{4.7}$$

4.2.4 Cr* Adjustment

If quasi-steady state is reached before adjusting $Cr^*_{Initial}$ to Cr^*_{QSS}, then the transient time will increase as shown in Figure 4.2. Changing from $Cr^*_{Initial}$ to Cr^*_{QSS}

earlier may reduce transient times. The mass convergence criterion will be used to determine when the air and/or solution flow rates should be returned to their optimal quasi-steady-state values corresponding to Cr*=3. When the mass convergence is less than a certain value, Cr* will begin to be reduced to reach Cr*=3. Therefore, Cr* will begin to decrease when:

$$m\_c < CC_{Cr^*} \,, \tag{4.8}$$

where:

m_c is the mass convergence equation given by Eq. (2.28), and

CC_{Cr^*} is the selected Cr* control criterion for mass convergence [%].

In addition to determining when Cr* should be returned to Cr^*_{QSS}, it is important to determine an appropriate rate of change for Cr* $\left(\partial Cr^* / \partial t\right)$.

Figure 4.3 presents results that show the effect of various Cr* control criteria for mass convergence $\left(CC_{Cr^*}\right)$ and rates of change of Cr* $\left(\partial Cr^* / \partial t\right)$ on the transient times of the RAMEE system. The transient times in Figure 4.3 are presented as a ratio of the transient time with flow control $\left(t_{QSS,FC}\right)$ to the transient time with no flow control $\left(t_{QSS,No\ FC}\right)$ for the case where $Cr^*_{Initial} = 15$. The rate of change of Cr* $\left(\partial Cr^* / \partial t\right)$ is normalized by the total change in Cr* that must occur before quasi-steady is reached ($Cr^*_{Initial} - Cr^*_{QSS}$).

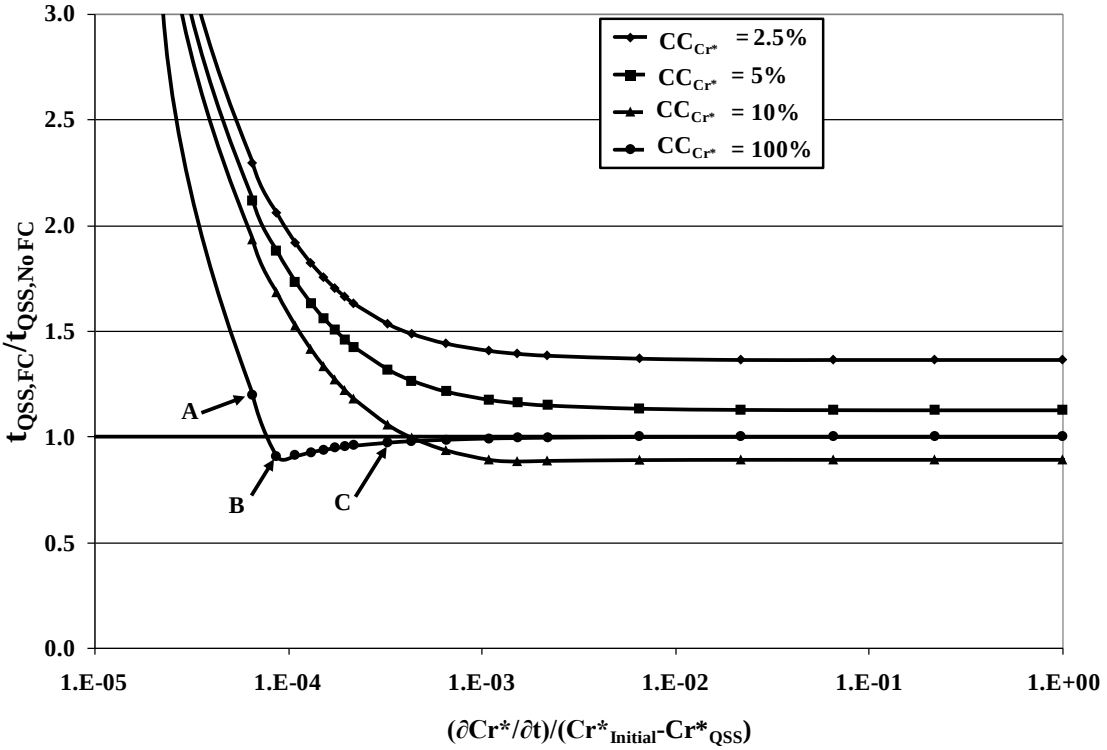

Figure 4.3: The ratio of transient time with Cr* control to the transient time without Cr* control versus the rate of change in Cr*, for four different Cr* convergence criteria (NTU=11.4, summer AHRI conditions, ΔX_{Sol}=0, $Cr^*_{Initial}$=15, Cr^*_{QSS}=3).

As Figure 4.3 shows, flow control reduces the transient times $\left(t_{QSS,FC}/t_{QSS,No\ FC}<1\right)$ for only a few combinations of CC_{Cr^*} and $\partial Cr^*/\partial t$ values. In fact, the improper selection of these Cr* reduction parameters can result in an increase in transient time $\left(t_{QSS,FC}/t_{QSS,No\ FC}>1\right)$. For example with $CC_{Cr^*}=2.5\%$ *or* 5% , the transient time is always larger than if no flow control is used $\left(t_{QSS}/t_{QSS@Cr^*=3}>1\right)$. Increasing the Cr* control criterion (i.e. starting to return from $Cr^*_{Initial}$ to Cr^*_{QSS} at an earlier time) results in a lower transient time and eventually results in a decrease in transient time compared to the case where no flow control is used. For example, a Cr* control criterion of 100% means that the Cr* begins to decrease immediately. For this control criterion, there is range of $\partial Cr^*/\partial t$ values that result in a lower transient time.

The change in Cr* during transient time is shown Figure 4.4, for three points on the curve indicated in Figure 4.2 (points A, B, and C).

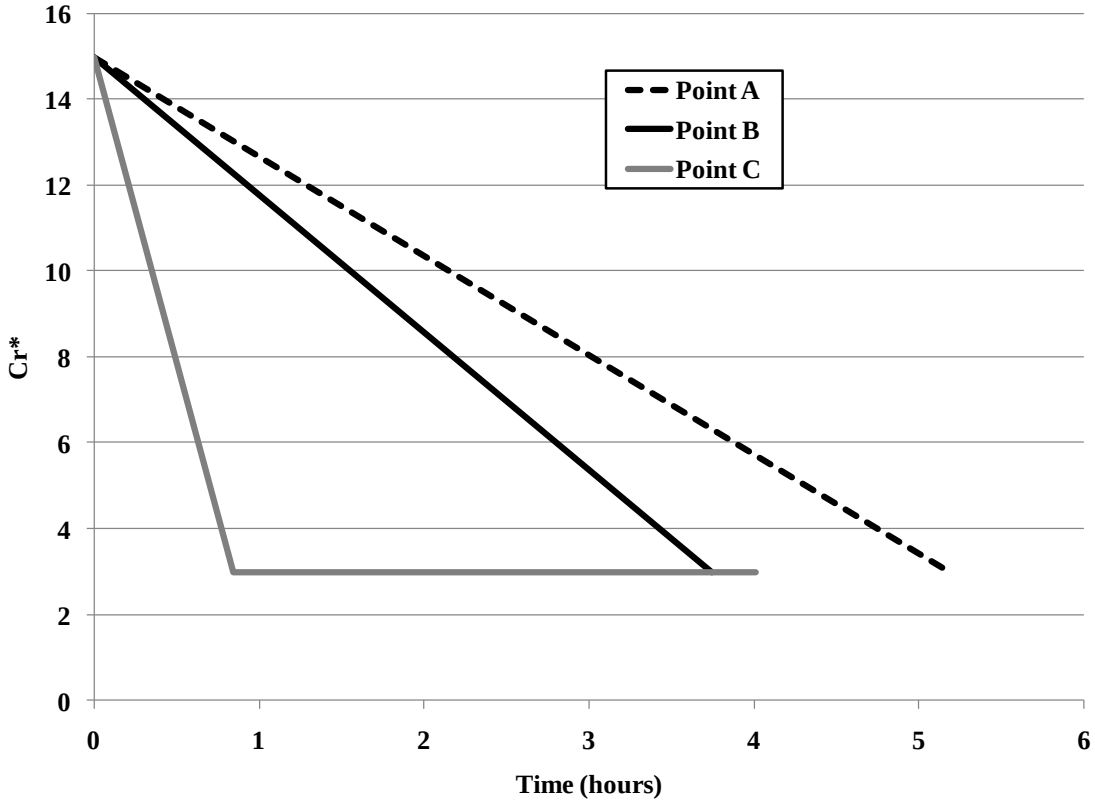

Figure 4.4: Cr* as a function of time for three select points from Figure 4.2 (NTU=11.4, summer AHRI conditions, ΔX_{Sol}=0, $Cr^*_{Initial}$=15, Cr^*_{QSS}=3).

Point A refers to a change in Cr* that is too slow, causing the adjustment in Cr* to take longer than the system requires to adjust and reach quasi-steady state. Point C refers to a change in Cr* that is too fast, causing the system to take longer to adjust compared to what is needed for Cr*=3 to be reached. For this case, only a slight reduction in transient time occurs. Point B represents the ideal rate of change in Cr*, which causes the adjustment in Cr* to be completed at the same time that the system converges to quasi-steady state. Therefore, point B results in the lowest possible transient time for this Cr* control criterion. However this rate of change in Cr* is very difficult to determine without the use of a simulation since the required rate of decrease

in Cr* and the corresponding transient time are dependent on each other. Also, as Figure 4.4 shows, a lower Cr* control criterion (such as 10%), and a higher rate of Cr* decrease can produce as low of a transient time and is simpler to use. Therefore, the rate of change in Cr* is chosen to be,

$$\frac{\partial Cr^*}{\partial t} = \left(Cr^*_{Initial} - Cr^*_{QSS}\right). \tag{4.9}$$

Figure 4.5 shows results for different NTU and $Cr^*_{Initial}$ values (NTU=5, $Cr^*_{Initial} = 9$) and confirms the rate of change in Cr* given by equation (4.9).

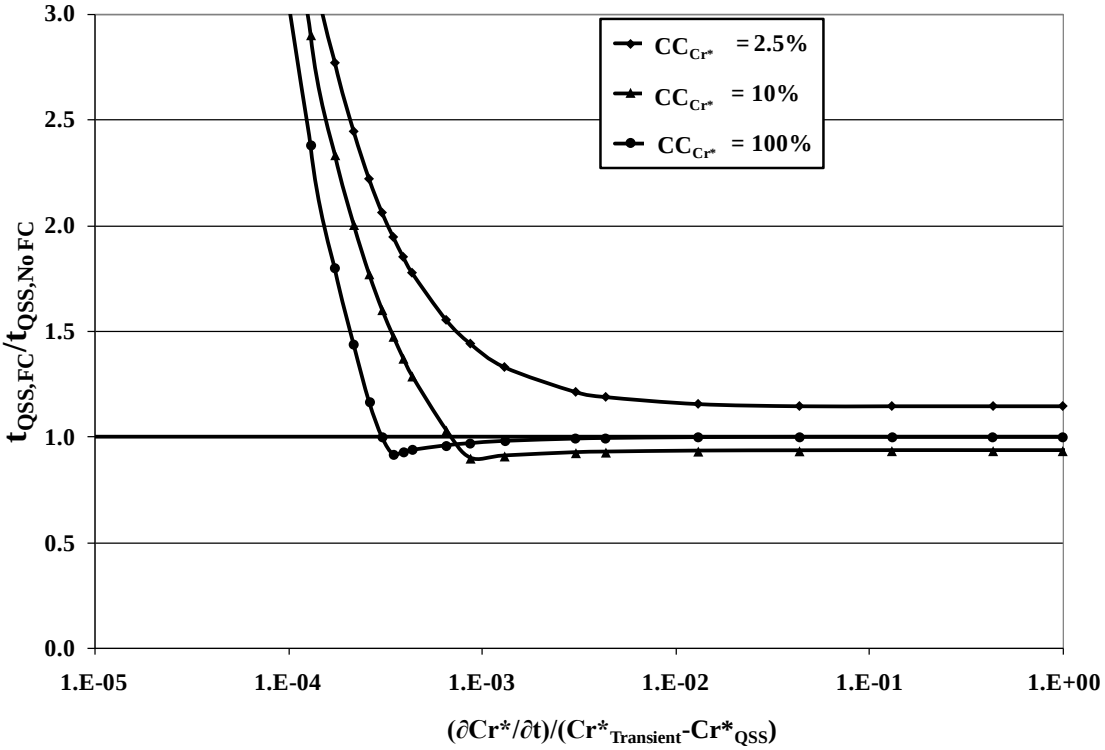

Figure 4.5: The ratio of transient time with Cr* control to the transient time without Cr* control versus the rate of change in Cr* for four different Cr* convergence criteria (NTU=5, summer AHRI conditions, $X_{Sol,Initial}$=2.1702 (ΔX_{Sol}=0), $Cr^*_{Initial}$=9, Cr^*_{QSS}=3)

Using the rate of decrease given by Eq. (4.9), the best Cr* control criterion $\left(CC_{Cr^*}\right)$ can be determined from Figure 4.6, which shows the ratio of the transient time with flow control $\left(t_{QSS,FC}\right)$ to the transient time with no flow control $\left(t_{QSS,No\ FC}\right)$ for

various CC_{Cr^*} values and two different NTU values. The optimum value of CC_{Cr^*} is found to be approximately 10% for NTU=11.4, and 6% for NTU=5.

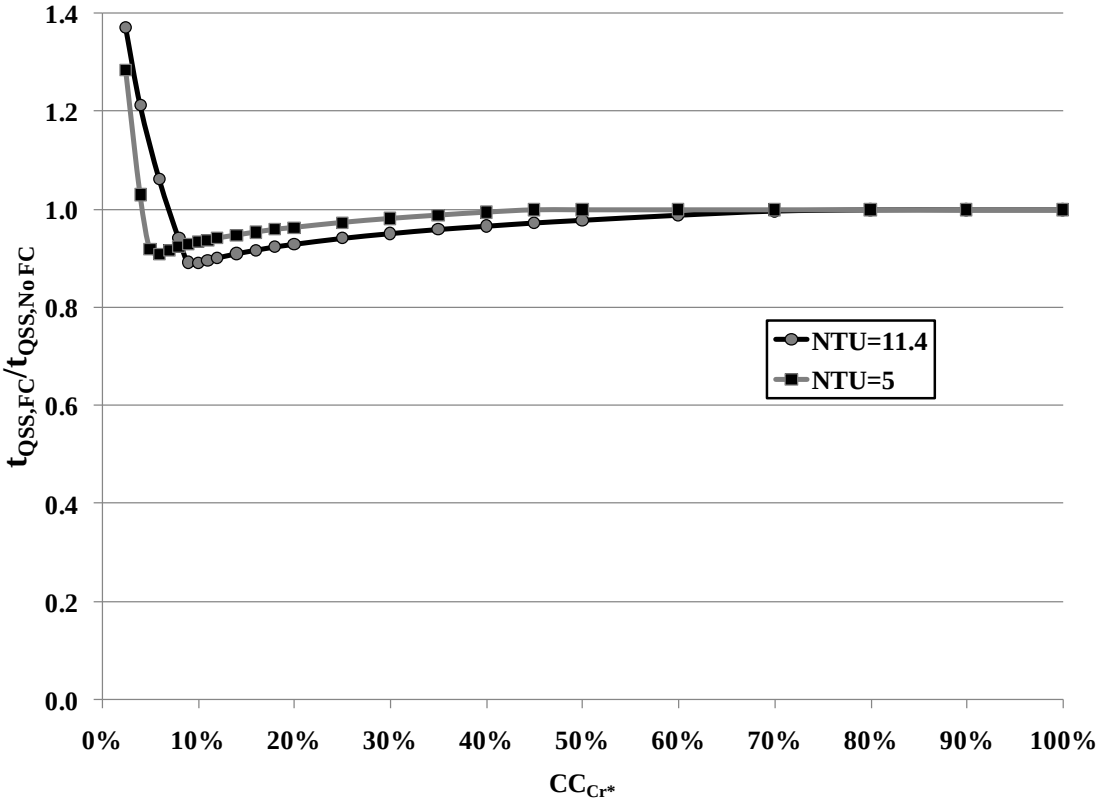

Figure 4.6: The ratio of transient time with Cr* control to the transient time without Cr* control versus the Cr* control criterion (CC_{Cr^*}), for two different NTU values (ΔX_{Sol}=0, $Cr^*_{Initial}$=9 for NTU=5 and $Cr^*_{Initial}$=15 for NTU=11.4) (summer AHRI conditions and Cr^*_{QSS}=3).

4.2.5 Initial Cr* Value

Using the rate of change in Cr* $\left(\partial Cr^* / \partial t\right)$ given by Eq. (4.9), and a Cr* control criterion $\left(CC_{Cr^*}\right)$ of 10% and 6% for NTU values of 11.4 and 5 respectively, the appropriate value of the initial Cr* $(Cr^*_{Initial})$ can be determined. Figure 4.7 shows the percent reduction in transient time for different $Cr^*_{Initial}$ values and two different NTU values.

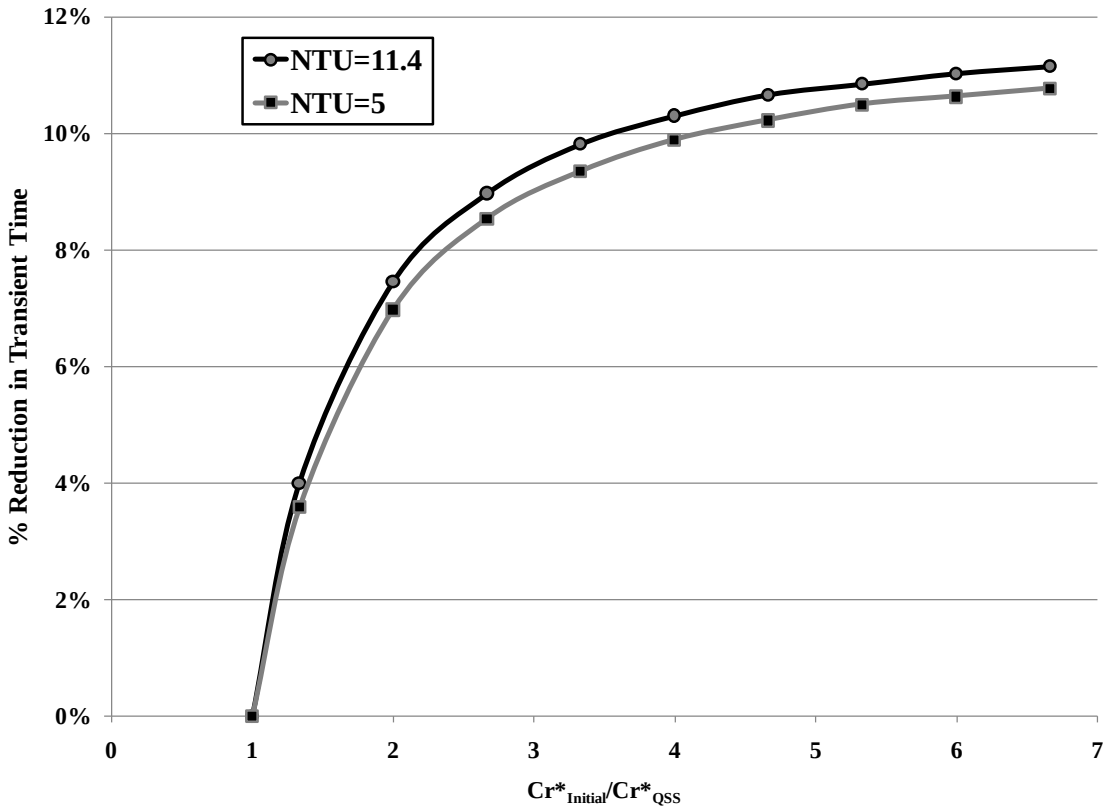

Figure 4.7: The percent reduction in transient time versus the ratio of the initial and quasi-steady-state Cr* for two different NTU values (summer AHRI conditions, ΔX_{Sol}=0, Cr^*_{QSS}=3).

Figure 4.7 shows that using a value of $Cr^*_{Initial}$ that is three times the quasi-steady-state value $\left(Cr^*_{QSS}\right)$ only provides a 9.4% reduction in transient time for the case of NTU=11.4 and a 8.9% reduction in transient time for the case of NTU=5. This initial Cr* value requires the solution flow rate to be three times higher than the required quasi-steady-state flow rate, which would increase both the capital cost of the system (larger pump) and the operating costs (higher power consumption). Alternatively, the air flow rate could be reduced to a third of the quasi-steady-state air flow rate. However, a decrease in air flow rate may result in poor indoor air quality if the air being provided by the system is required for ventilation purposes and not just space heating or cooling.

4.2.6 Solution and Air Flow Control Conclusion

Solution and air flow control have been found to provide a reduction in transient time of under 10% when providing either a solution flow rate that is three times more, or an air mass flow rate that is three times less than the required flow rate at quasi-steady-state. Increasing the solution flow rate by a factor of three is costly, while reducing the air flow by a factor of three jeopardizes indoor air quality and comfort. Therefore, based on these results it is concluded that the small reduction in transient time does not justify implementing flow control.

4.3 Air Flow Bypass

Another way to adjust the air flow without decreasing performance or indoor air quality is to bypass the supply or exhaust air streams around the LAMEE, as shown in Figure 4.8. Bypassing one exchanger allows the solution to exchange energy with only one air stream, without any regenerative energy transfer with the other air stream. For example, the solution can be heated and humidified by a hot and humid supply air stream without having to transfer the energy back into the colder and dryer exhaust air stream. This can reduce the time required to get the solution up to operating temperature and concentration.

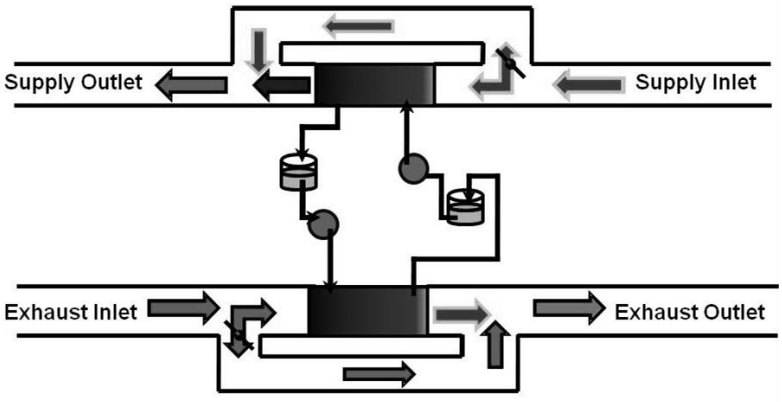

Figure 4.8: Schematic of a RAMEE system with an air flow bypass option.

4.3.1 Initial Conditions

To investigate the possible benefits of using air flow bypass, summer AHRI indoor and outdoor test conditions will be used. The desiccant solution is assumed to begin initially at the indoor air temperature ($T_{Sol,Initial}$=24°C) and at the average quasi-steady state concentration $(\Delta X_{Sol} = 0)$. For these initial conditions, the solution must undergo a temperature change and only a slight concentration change before reaching quasi-steady state. The case of different initial concentrations will be considered in detail in section 4.5.

4.3.2 Methodology

The LAMEE that should be bypassed depends on both the solution temperature and the supply inlet air temperature. Table 4.1 shows four different bypass control strategies used to determine which LAMEE should be bypassed depending on the solution and outdoor air conditions. Controllable dampers can be used to control the air bypass based on these strategies. As noted in Table 4.1, some of these bypass control strategies will decrease the transient time, but will also decrease the performance of the RAMEE. These strategies should be avoided in the practical application of air flow bypass.

Table 4.1: Bypass control strategies.

Criteria	Control Strategy
$T_{Sol,S,in} < T_{Sol,S,in,QSS}$ and $T_{Air,S,in} > T_{Sol,S,in}$	Bypass Exhaust Exchanger*
$T_{Sol,S,in} < T_{Sol,S,in,QSS}$ and $T_{Air,S,in} < T_{Sol,S,in}$	Bypass Supply Exchanger
$T_{Sol,S,in} > T_{Sol,S,in,QSS}$ and $T_{Air,S,in} < T_{Sol,S,in}$	Bypass Exhaust Exchanger*
$T_{Sol,S,in} > T_{Sol,S,in,QSS}$ and $T_{Air,S,in} > T_{Sol,S,in}$	Bypass Supply Exchanger

* For these conditions, bypassing will result in a decrease in RAMEE Performance.

Both exchangers can be bypassed if part-load conditions occur, where the outside air does not need to be conditioned as much as the RAMEE provides. During these part-load conditions, an uncontrolled RAMEE can over heat/cool and over humidify/dehumidify the supply air, resulting in other HVAC equipment having to re-condition the air, wasting energy in the process. Bypassing air also reduces the air flow pressure drop resulting in a savings in fan energy, especially if the fan is equipped with a variable frequency drive. Part-load conditions will not be considered in detail in this section.

4.3.3 Results

Figure 4.9 shows the time required for the solution to reach quasi-steady state for different amounts of air bypass during AHRI summer conditions. As shown in Figure 4.9, a higher amount of air bypass yields a higher reduction in transient time. Therefore, a 100% bypass of the appropriate exchanger provides the greatest reduction in transient time. For the AHRI summer test conditions and the initial conditions presented in this section, a 16% reduction in transient time is achievable.

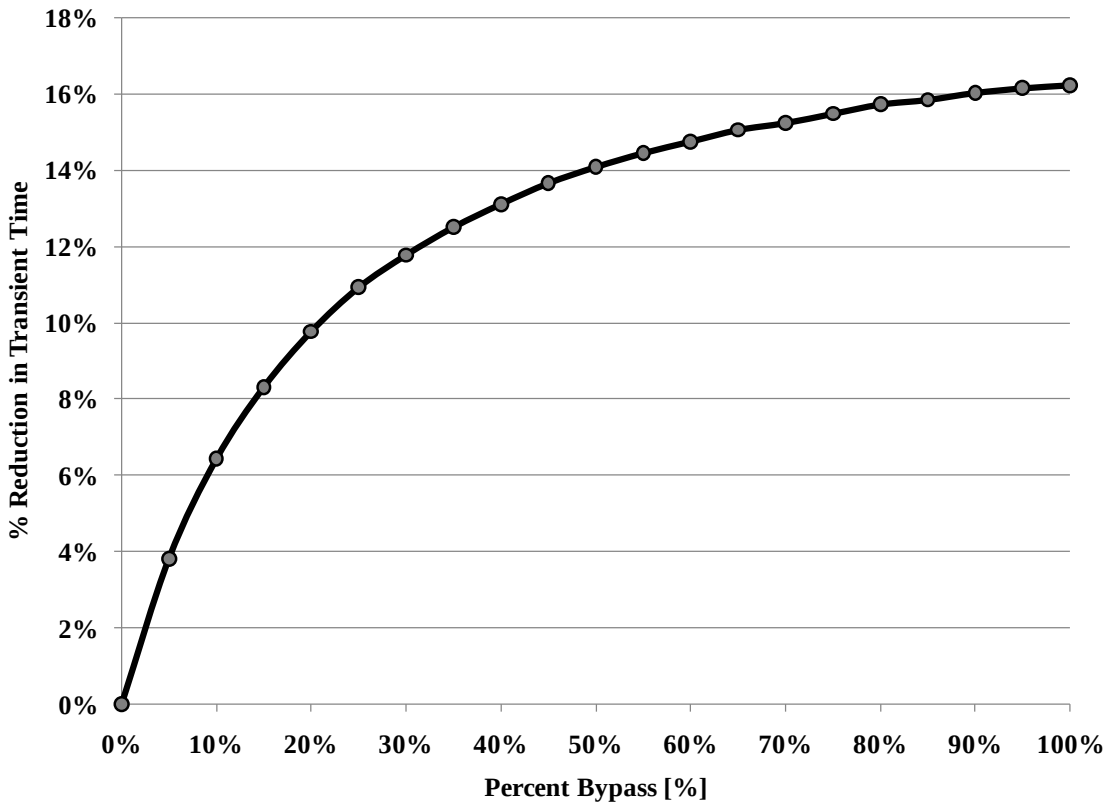

Figure 4.9: Reduction in transient time for different amounts of air flow bypass (NTU=11.4, Cr*=3, ΔX_{Sol}=0, summer AHRI conditions).

4.3.4 Air Flow Bypass Conclusion

Air flow bypass is capable of providing a 16% reduction in transient time. Therefore, air flow bypass is a more viable control strategy compared to flow control, since it provides a higher reduction in transient time (16% with air flow bypass versus 11% with flow control at the same operating conditions) without reducing the amount of fresh air being supplied to the building or increasing pumping costs. However a decrease of 16% may not be sufficient for a RAMEE in a practical HVAC system that needs to react within a few hours. Therefore air flow bypass should not be a primary control strategy, but rather an option that could further reduce transient times in conjunction with a more suitable primary method of control (such as temperature control or concentration control in subsequent sections). Air flow bypass is also recommended

as a possible method to control the system during part load conditions (requires further investigation).

4.4 Temperature Control

The transient time delays that result because the desiccant needs to be heated or cooled to the proper temperature can be significant if the initial solution temperature (usually at the indoor or outdoor temperature) is much different than the quasi-steady-state solution temperature (which will be between the indoor and outdoor temperatures). The focus of this section will be on the thermal transients corresponding to the time required for the solution to reach quasi-steady-state temperature. The mass transients corresponding to the time required for the desiccant to reach quasi-steady-state concentration will be considered in section 4.5. The thermal transient time $\left(t_{thermal}\right)$ will not be determined by using the mass and energy convergence criterion (since this includes mass and thermal transients), but rather be determined as the time it takes the solution to reach the quasi-steady-state temperature given by,

$$T_{Sol,S,in} = T_{Sol,S,in,QSS} \pm 0.2\,K, \tag{4.14}$$

where:

$T_{Sol,S,in}$ is the solution temperature entering the supply exchanger [K], and

$T_{Sol,S,in,QSS}$ is the solution temperature entering the supply exchanger at quasi-steady state (determined using mass and energy convergence criteria) [K].

4.4.1 Initial Conditions

In order to examine thermal transients and the possible advantage of using temperature control, the indoor air will be kept at constant AHRI summer indoor conditions. However the outdoor air temperature will be varied, while keeping the

relative humidity at a constant 50%. The solution will begin in equilibrium with the indoor air temperature and humidity, resulting in $T_{Sol,Initial}$=24°C and $C_{Salt,Initial}$=31.8% $\left(\Delta X_{Sol} = -0.02\ kg/kg\right)$.

4.4.2 Methodology

The time required for the solution to reach quasi-steady-state temperature is dependent on the difference between the initial solution temperature and the quasi-steady-state solution temperature, which can be expressed as,

$$\Delta T_{Sol} = \left| T_{Sol,Initial} - T_{Sol,QSS} \right|, \tag{4.15}$$

where:

ΔT_{Sol} is the difference between the initial solution temperature and the quasi-steady-state solution temperature [K],

$T_{Sol,Initial}$ is the average between the entering and leaving initial solution temperatures for the supply exchanger [K],

$T_{Sol,QSS}$ is the average between the entering and leaving quasi-steady-state solution temperatures for the supply exchanger [K],

Figure 4.10 shows that as the difference between the initial and quasi-steady-state temperatures increase, the thermal transient time ($t_{thermal}$) increases.

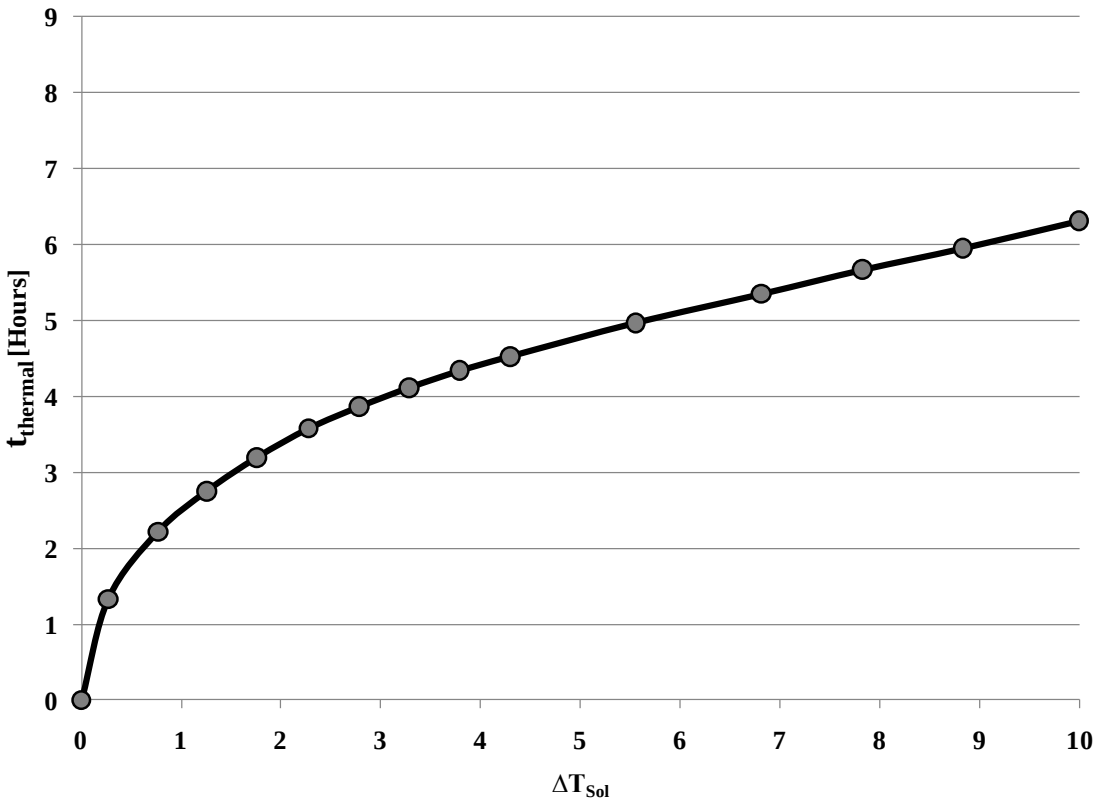

Figure 4.10: The thermal transient time at different values of ΔT_{Sol} (NTU=11.4, Cr*=3, ΔX_{Sol}=-0.02kg/kg).

The goal of solution temperature control is to get the desiccant solution to the operating temperature as quickly as possible, thus reducing the thermal transient time. This can be done by heating/cooling the solution before it enters the supply exchanger. The solution can also be heated/cooled before entering the exhaust exchanger in order to speed up the process. However, having two external solution heating/cooling systems is redundant and generally more costly than a single larger system capable of heating/cooling the solution at the same rate. Therefore, only one heater/cooler will be placed before the supply exchanger. An electric, gas, or hydronic heater can be used to heat the solution, while a small refrigeration compressor/coil can be used to cool the solution. Alternatives include heat pumps and geothermal systems. It is assumed that the concentration of the solution does not change as the solution temperature changes.

The amount of heating/cooling required not only depends on the difference between the initial and quasi-steady-state solution temperatures, but also depends on the size of the system. A larger system will have a higher solution flow rate and therefore requires a larger external heat transfer rate. The capacity of the external heating/cooling system can be normalized with respect to the cooling/heating capacity of the RAMEE, and can be expressed as,

$$q^* = \frac{q_{Extemal,Sol}}{q_{RAMEE,QSS}}, \tag{4.16}$$

where:

$q_{Extemal,Sol}$ is the heating/cooling capacity of the external solution temperature control system [W], and

$q_{RAMEE,QSS}$ is the amount of energy transferred between the supply and exhaust air streams by the RAMEE at quasi-steady state [W].

Therefore, a higher q* means that the external solution heating/cooling system has a higher capacity relative to the RAMEE.

4.4.3 Results

Figure 4.11 shows the thermal transient time for different values of ΔT_{Sol} and q*. Figure 4.11 shows that a higher q* results in a lower thermal transient time. In fact a value of q*=1 results in the complete elimination of the thermal transient time for an initial and quasi-steady-state solution temperature difference of up to (and over) 10°C. This difference in solution temperature corresponds to a difference between the outdoor and indoor air temperature of 20°C (when the solution begins at either indoor or outdoor air temperature). Even a value of q*=0.1 is capable of reducing the thermal transient

time by up to 47%. Therefore, the external solution heating/cooling system should be sized based on the desired reduction in thermal transient time, as well as the financial feasibility of providing the temperature control.

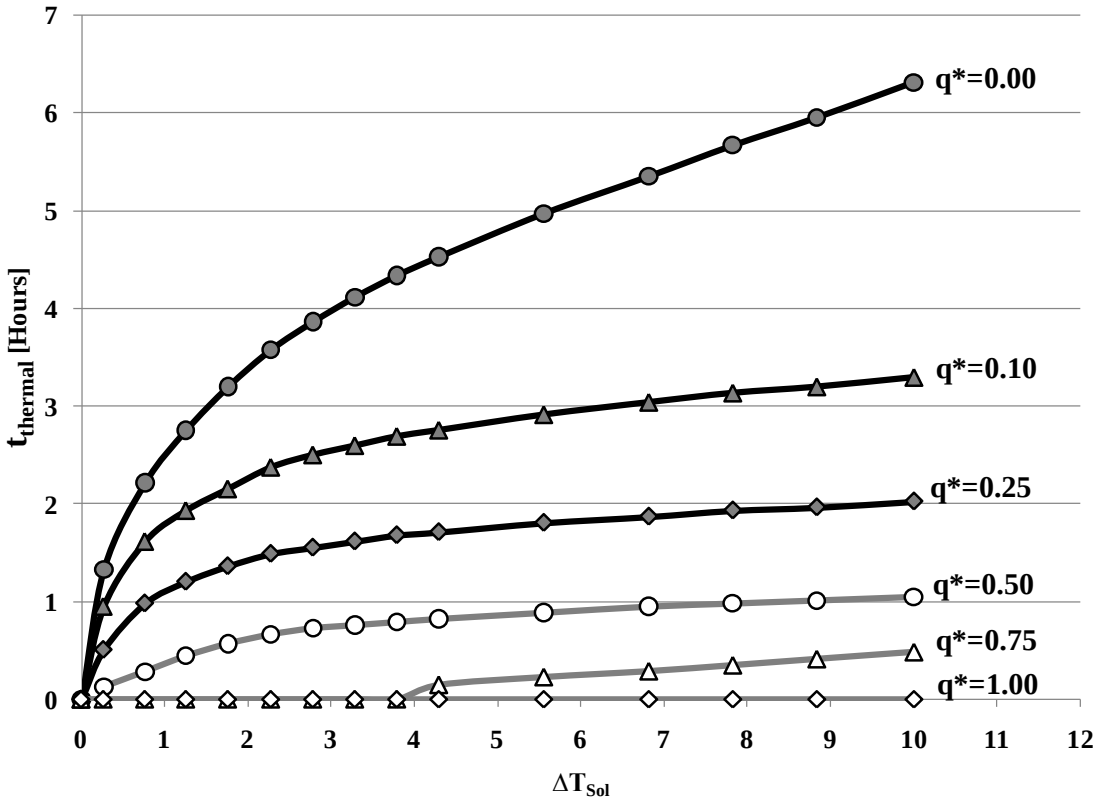

Figure 4.11: The thermal transient time at different values of ΔT_{Sol} values for six different q* temperature control values (NTU=11.4, Cr*=3, ΔX_{Sol}=-0.02kg/kg).

Temperature control is used to help reduce thermal transients. However, the operating conditions may require the solution to undergo a change in both temperature (thermal transients) and concentration (moisture transients). Figure 4.12 shows the percent reduction in both thermal and total (thermal and moisture) transient times during initial start-up at AHRI conditions, where $\Delta T_{Sol} = 3.2°C$ and $\Delta X_{Sol} = -0.02\ kg/kg$. For these conditions, temperature control can be used to eliminate up to 15% of the overall (thermal and moisture) transients if q* is chosen high enough as shown in Figure 4.12. The remaining transient time is due to moisture transients that occur due to

the change in desiccant concentration over time. Therefore even if the thermal transients are eliminated, the system still undergoes long transient times due to even a small required change in solution concentration.

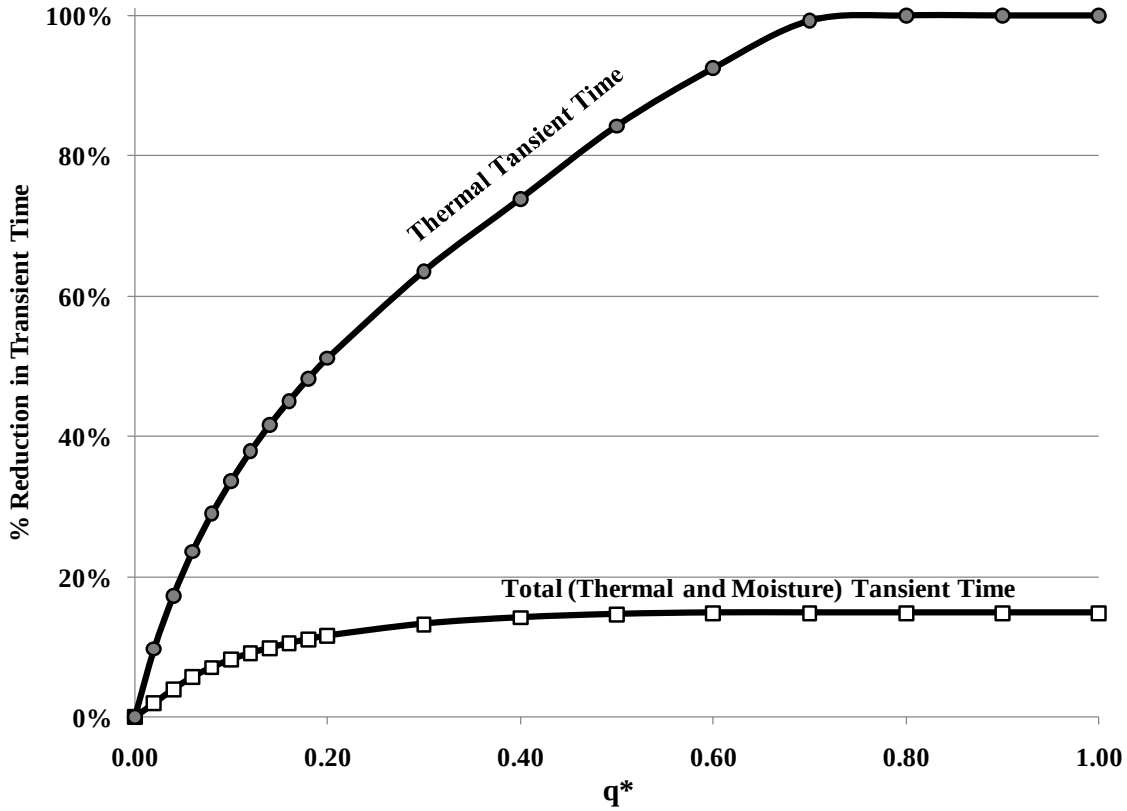

Figure 4.12: The percent reductions in thermal transient time and total transient time at different q* temperature control values (summer AHRI conditions, NTU=11.4, Cr*=3, ΔX_{Sol}=-0.02kg/kg).

4.4.4 Temperature Control Conclusion

Temperature control was found to be very advantageous in reducing thermal transients. An external solution heating/cooling system that is capable of transferring as much energy as the RAMEE transfers at quasi-steady state (q*=1) is capable of eliminating all thermal transients for temperature differences of over 6°C between the initial and quasi-steady-state solution temperatures. Even a much smaller system where q*=0.1 is capable of reducing the thermal transients by up to 47%. However, thermal transients are found to be a minor contributor to the overall transient time for cases even

when $\Delta X_{Sol} \neq 0$. Therefore, temperature control only reduces the total (thermal and moisture) transients by up to 15%. Temperature control is recommended, but only in conjunction with a better control method that is capable of reducing moisture transients.

4.5 Concentration Control

Both sections 2.10 and 4.4 showed that the transient time required for the solution to reach quasi-steady state is largely dependent on the difference between the initial solution concentration and the desired quasi-steady-state concentration. Figure 4.13 recalls how even a small difference between the initial and quasi-steady-state mass fraction, ΔX_{Sol} (inversely proportional to concentration), can cause a large increase in transient time (t_{QSS}).

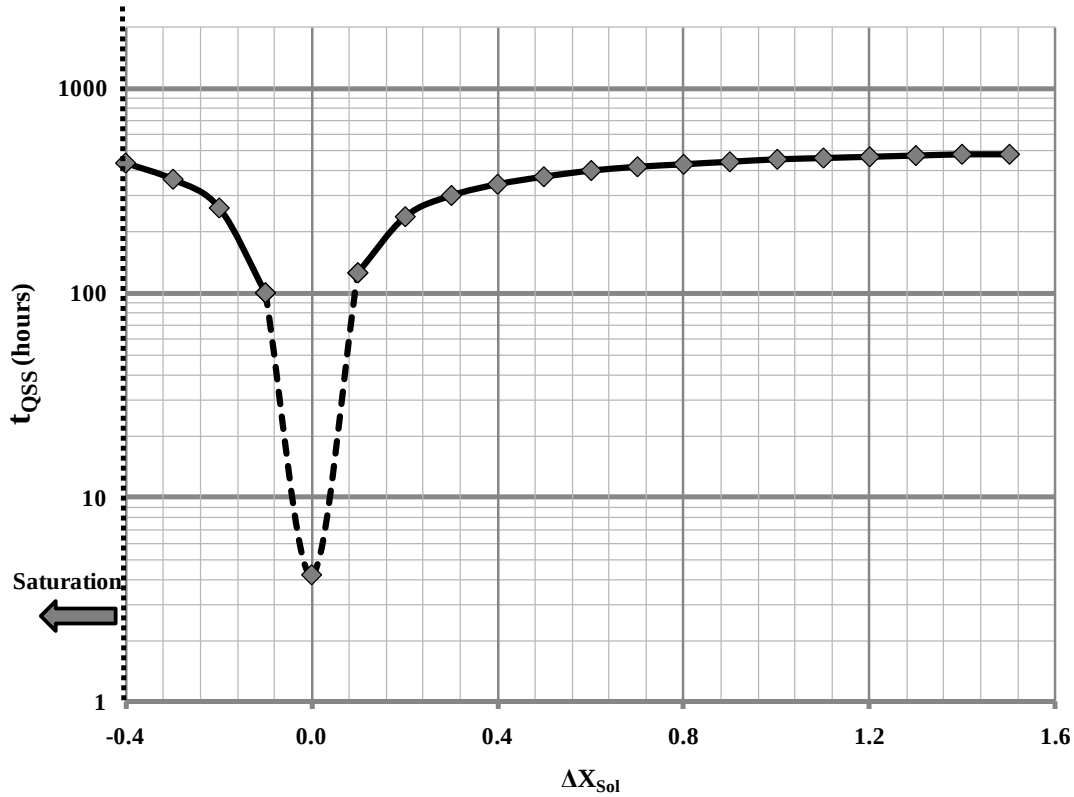

Figure 4.13: Time required to reach quasi-steady state at various initial solution concentrations that are ΔX_{Sol} away from the quasi-steady-state concentration (NTU=11.4, Cr*=3, summer AHRI conditions, $X_{Sol,QSS}$=2.1692, mass convergence=2.5%).

Figure 4.13 shows, a value of $\Delta X_{Sol} = +1$ can result in a transient time of over 18 days. This is not an unrealistic starting condition, as shown in Figure 4.14 which shows several lines of constant ΔX_{Sol} superimposed on a psychometric chart. For the example of AHRI summer conditions, the point labeled "Sol,QSS" represents the quasi-steady-state solution condition. As Figure 4.14 shows, it is possible for the solution to begin at conditions of $\Delta X_{Sol} = +1$ or higher, especially if the solution were to be initially at outdoor conditions in a very hot and humid climate.

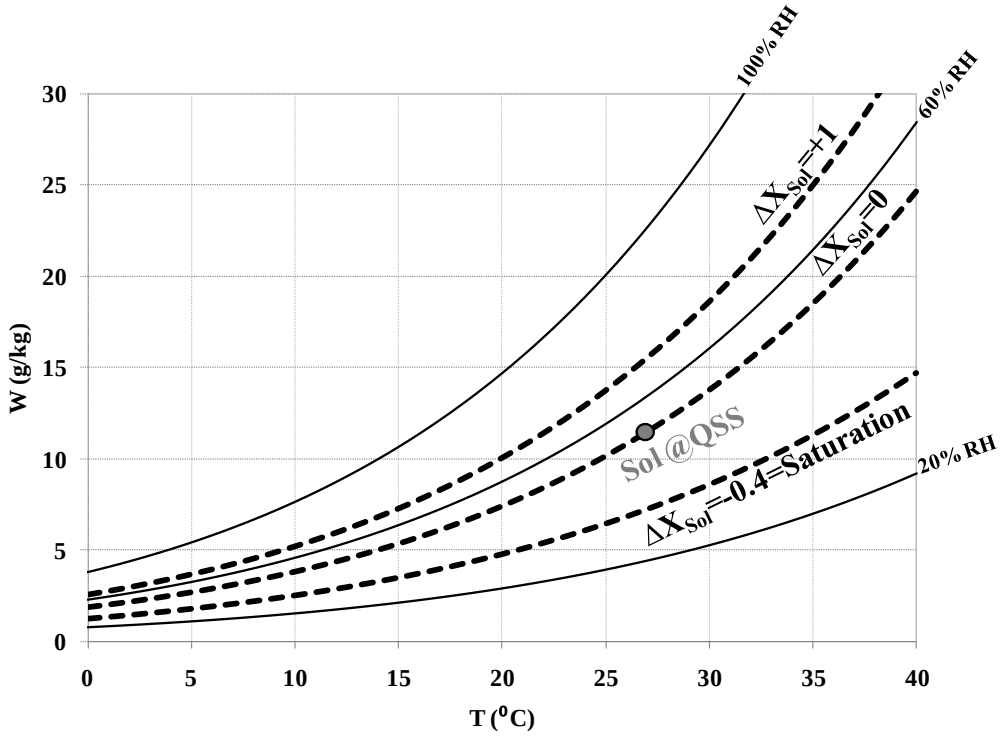

Figure 4.14: Lines of ΔX_{Sol} superimposed on a psychrometric chart for the case where point "Sol@QSS" represents the quasi-steady-state mass fraction for AHRI summer indoor and outdoor conditions (NTU=11.4, Cr*=3).

4.5.1 Initial Conditions

For concentration control, both the indoor and outdoor air will be held at constant AHRI conditions. The solution will begin at the indoor temperature ($T_{Sol,initial}$=24°C), but the initial concentration will be varied to provide conditions where

$\Delta X_{Sol} \neq 0$. Therefore, the primary cause of transient delays will be due to the required change in solution concentration.

4.5.2 Methodology

The goal of concentration control is to reduce the transient time by adding or removing water from the solution. The water addition/removal will occur at the storage tank located just before the inlet of the supply exchanger, as this is the easiest location for practical application. The water addition/removal could also occur at the storage tank located before the exhaust exchanger. The use of two addition/removal points ensures that the concentration before each exchanger is controlled independently, thus further reducing the transient time. However, the advantages of using two concentration control systems may not be worth the additional cost. Therefore water addition/removal will only be considered as occurring in the storage tank located before the supply exchanger inlet. The amount of water addition/removal required can be normalized with respect to the size of the system by considering the amount of moisture exchanged by the RAMEE at quasi-steady state conditions. This can be defined as

$$\dot{m}^* = \frac{\dot{m}_{addition/removal}}{\dot{m}_{RAMEE,QSS}} \tag{4.17}$$

where:

$\dot{m}_{addition/removal}$ is the rate of water addition/removal using concentration control [kg/s], and

$\dot{m}_{RAMEE,QSS}$ is the rate of water transfer by the RAMEE at quasi-steady state [kg/s].

4.5.3 Results

Figure 4.15 shows the transient time required to reach quasi-steady state using different values of $\dot{m}^*$ and ΔX_{Sol}. A higher $\dot{m}^*$ results in a lower transient time. However for large ΔX_{Sol} values the reduction in transient time for a given $\dot{m}^*$ is smaller than at low ΔX_{Sol} values.

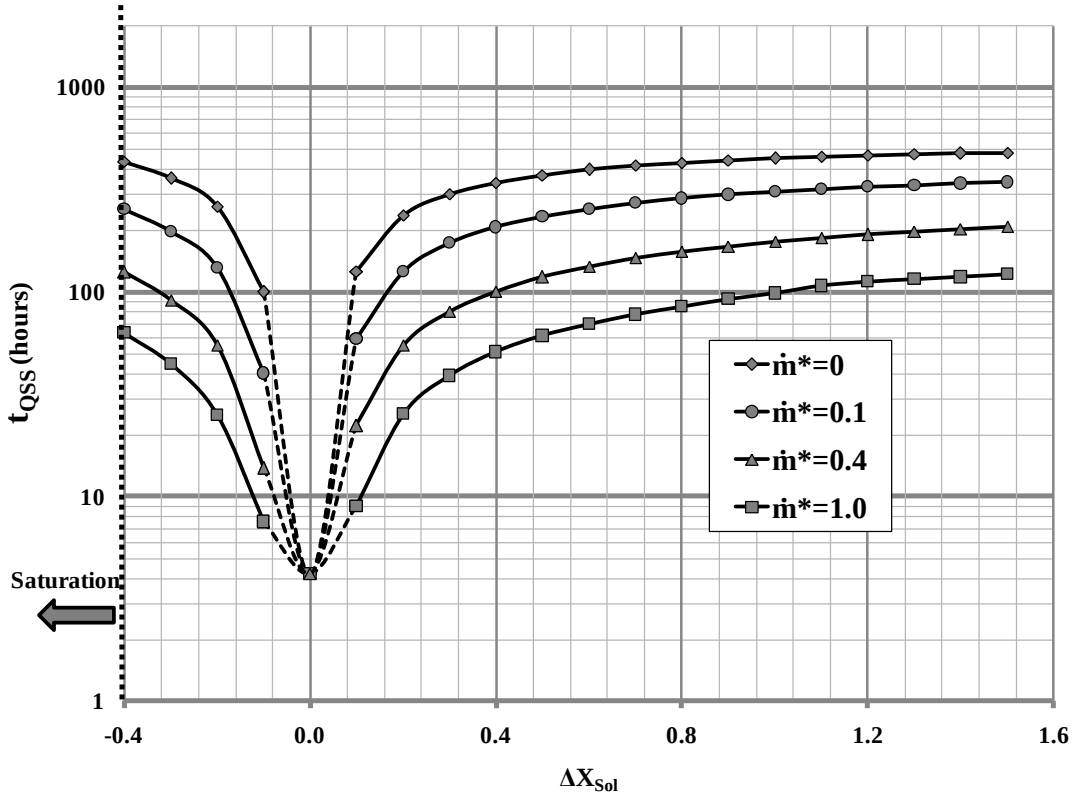

Figure 4.15: Time required to reach quasi-steady state at various initial solution concentrations that are ΔX_{Sol} away from the quasi-steady-state concentration and for different values of $\dot{m}^*$ (NTU=11.4, Cr*=3, summer AHRI conditions, $X_{Sol,QSS}$=2.1692, mass convergence=2.5%).

The proper selection of $\dot{m}^*$ depends on the range of solution concentrations that the system will encounter, and how much of a decrease in transient time is desired. Figure 4.16 shows how the transient time is decreased with increasing $\dot{m}^*$ for the cases where $\Delta X_{Sol} = -0.1$ and $\Delta X_{Sol} = +1.0$. For both of these examples an optimum value

of $\dot{m}^*$ is reached, where any further increase in $\dot{m}^*$ no longer provides any further advantage. This optimum $\dot{m}^*$ value is dependent on the value of ΔX_{Sol}.

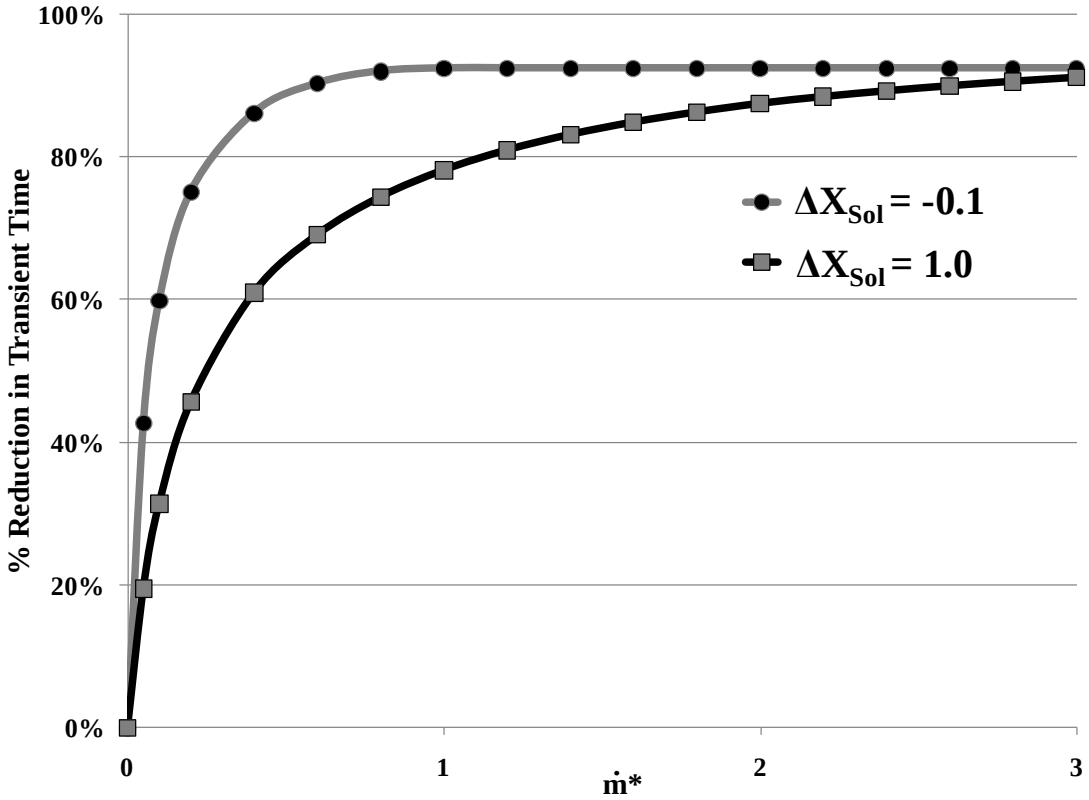

Figure 4.16: The percent reduction in transient time versus $\dot{m}^*$ for two values of ΔX_{Sol} (NTU=11.4, Cr*=3, summer AHRI conditions, $X_{Sol,QSS}$=2.1692) .

As both examples in Figure 4.16 show, concentration control is capable of providing over a 90% reduction in transient times. The reduction in transient time is also significant at lower values of $\dot{m}^*$, indicates that it may be worthwhile to implement concentration control.

4.5.4 Practical Implementation of Concentration Control

The practical implementation of concentration control is more complex than the other control systems studied thus far. Adding water to the solution is as simple as installing a water supply pipe leading into the storage tank located before the supply exchanger and utilizing a flow control valve to control the rate of water addition. It

should be noted that deionized water should be used to ensure that water contaminates do not impact the desiccant performance. A large reservoir of deionized water can be used, or a water deionizing and filtering system can be installed beside the RAMEE system. Although adding water is relatively simple, removing water is much more difficult.

There are two practical methods to remove water from the solution. The first is to evaporate the moisture by heating up the desiccant in an open environment. However, this method would require either a large surface area of desiccant open to the environment (and contaminants), or a large amount of heat input to evaporate the moisture. The second, preferred method is to simply heat up the desiccant in the storage tank before the exhaust exchanger. By doing this, the desiccant temperature increases, while the concentration remains constant (or relatively constant if tank is open to the external environment). This increases the humidity ratio (W) as shown in Figure 4.17, which shows an example of the solution condition a short time after initial start-up before being heated ($Sol_{No\ Heat}$) and after being heated (Sol_{Heated}). As Figure 4.17 shows, as the desiccant is heated up, it follows the constant concentration line and the potential for moisture transfer (ΔW) between the solution and the exhaust air (point E) increases. Therefore, as the heated solution passes through the exhaust exchanger, more moisture is transferred from the solution into the air stream, thus increasing the solution concentration.

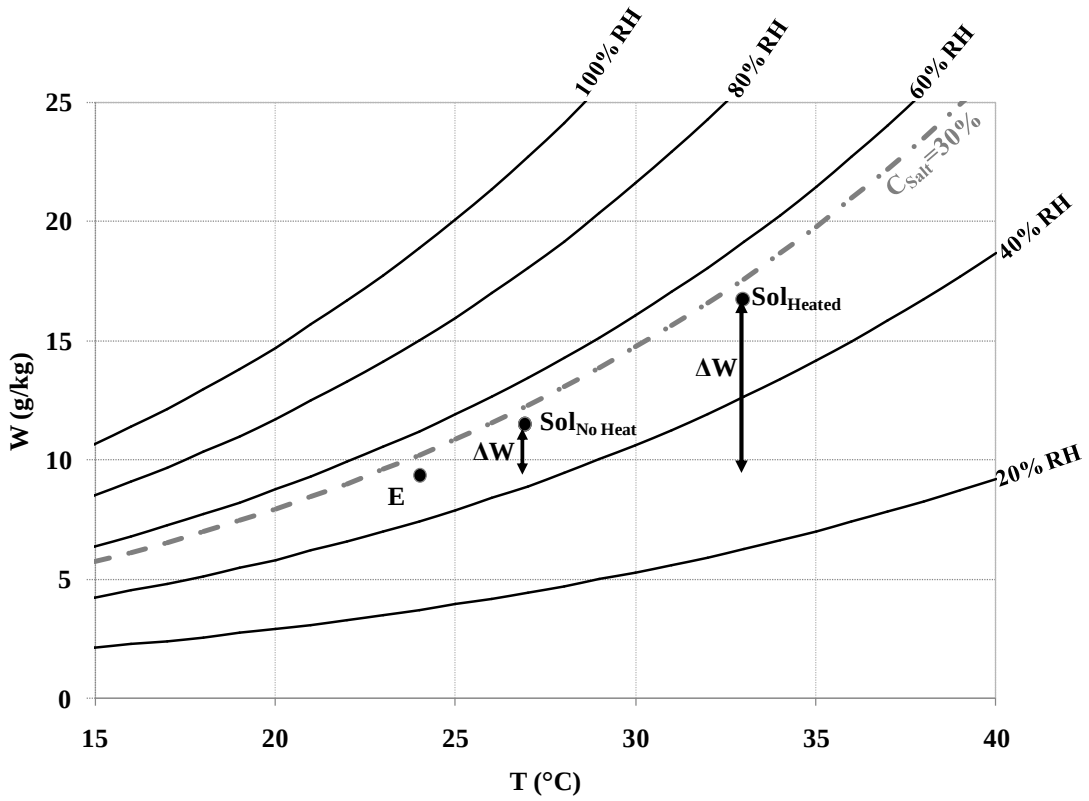

Figure 4.17: The solution conditions superimposed on the psychrometric chart before ($Sol_{No\ Heat}$) and after (Sol_{Heated}) being heated, and their moisture transfer potential (ΔW) with the exhaust air (E).

The amount of heat required to change the equilibrium humidity ratio for concentration of the solution depends on both ΔX_{Sol} and the size of the system. This amount of heating can be normalized with respect to the systems energy transfer capacity and can be expressed as,

$$q^{*}_{concentration} = \frac{q_{concentration,heating}}{q_{RAMEE,QSS}}, \tag{4.18}$$

where:

$q_{concentration,heating}$ is the heating/cooling capacity of the external solution concentration control system [W].

$q_{RAMEE,QSS}$ is the amount of energy transferred between the supply and exhaust air streams by the RAMEE at quasi-steady state [W].

Heating up the solution before the exhaust exchanger helps increase the solution equilibrium humidity ratio (W) which changes the concentration, but also results in a higher solution temperature entering the supply exchanger. During summer cooling condition, this decreases the RAMEE performance. Therefore, the solution should be re-cooled before it enters the supply exchanger. The amount of heat required before the exhaust exchanger should be controlled based on the concentration of the solution entering the supply exchanger, while the amount of cooling required before the supply exchanger should be controlled based on the temperature of the solution entering the supply exchanger. Since the solution temperature entering the supply exchanger will be controlled, this method of concentration control also provides the same method of temperature control discussed in section 4.4. Therefore this control method will be referred to as a concentration and temperature control. A schematic of this control method is shown in Figure 4.18.

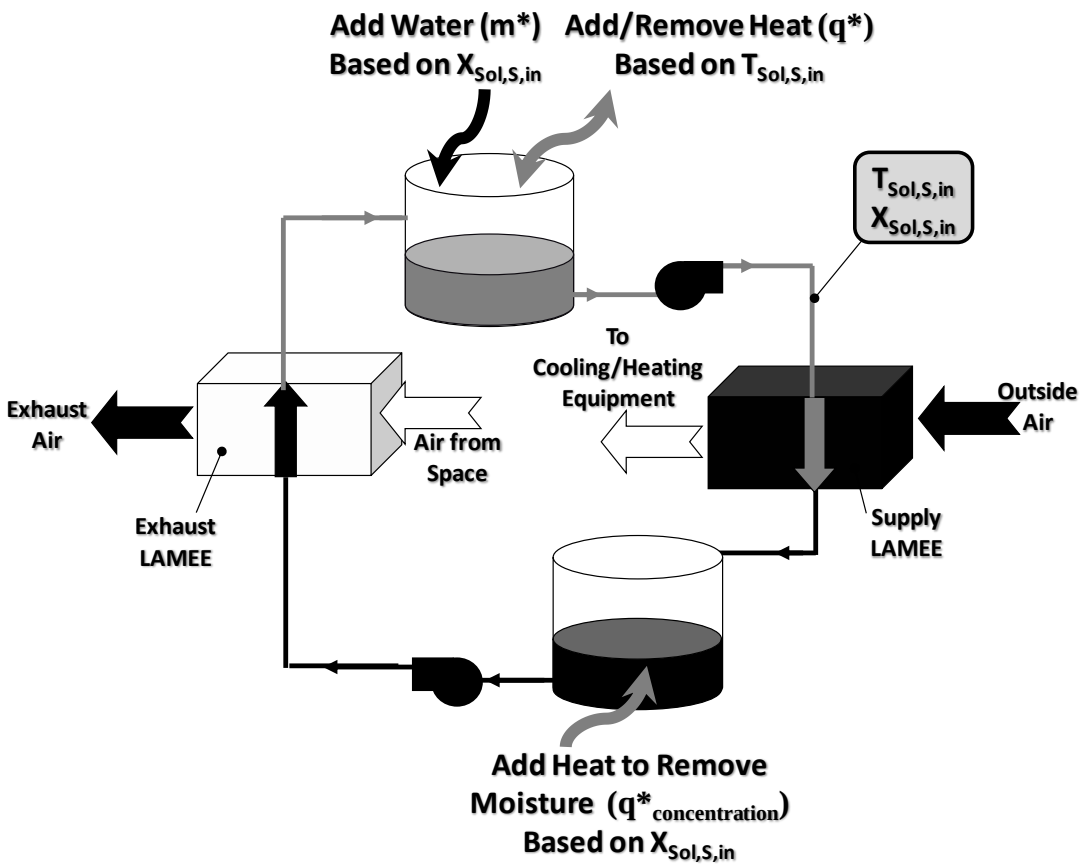

Figure 4.18: Schematic of a RAMEE with concentration and temperature control points.

A heat pump is one method that could be used to heat the solution before the exhaust exchanger and then re-cool the solution before the supply exchanger. Alternatively, a solar regeneration system is capable of providing the heat required, while a ground source geothermal loop could provide most of the cooling required. These are just a few examples of how this type of concentration and temperature control can be implemented.

Figure 4.19 shows the reduction in transient time for various values of $q^*_{concentration}$ and positive ΔX_{Sol} values that require an increase in concentration. For these results, the amount of cooling provided to the solution before the supply exchanger is assumed

to be controlled independent of $q^*_{concentration}$. The external solution cooling capacity is chosen to be:

$$q^*=1.0, \tag{4.19}$$

as defined by equation (4.16). Therefore the temperature control is capable of re-cooling the solution by over 10°C (from Figure 4.11).

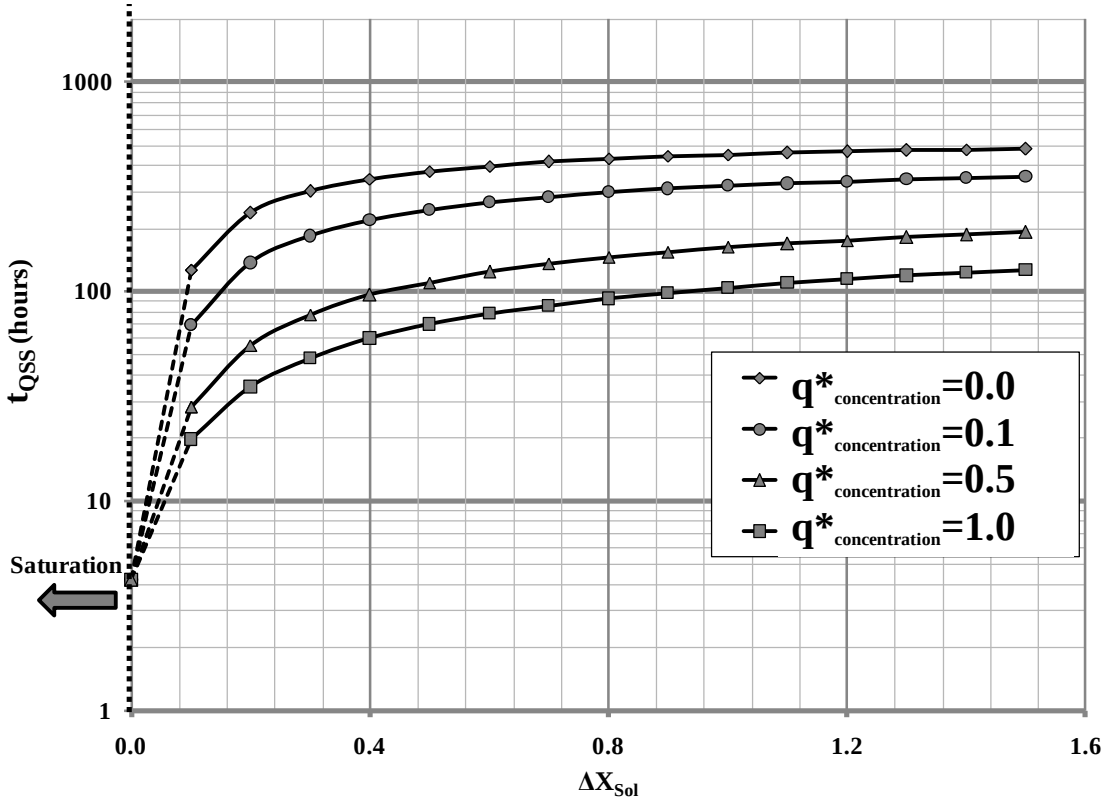

Figure 4.19: : Time required to reach quasi-steady state at various initial solution concentrations that are ΔX_{Sol} away from the quasi-steady-state concentration, for different values of $q^*_{concentration}$ (NTU=11.4, Cr*=3, summer AHRI conditions, $X_{Sol,QSS}$=2.1692, mass convergence=2.5%).

Figure 4.19 shows that using an external heating system with a higher $q^*_{concentration}$ results in a lower transient time. Even a relatively small heating system capable of providing 10% as much energy as the RAMEE system can recover $\left(q^*_{concentration} = 0.1\right)$ results in an average decrease in transient time of 31% over the range of shown in Figure 4.19. Increasing the capacity of the external solution heating system so that

$q^*_{concentration} = 0.5$ increases the average reduction in transient time to 63%, while a value of $q^*_{concentration} = 1.0$ increases the average reduction to 74%. Figure 4.20 shows how the percent reduction in transient time changes with $q^*_{concentration}$ for two values of ΔX_{Sol}.

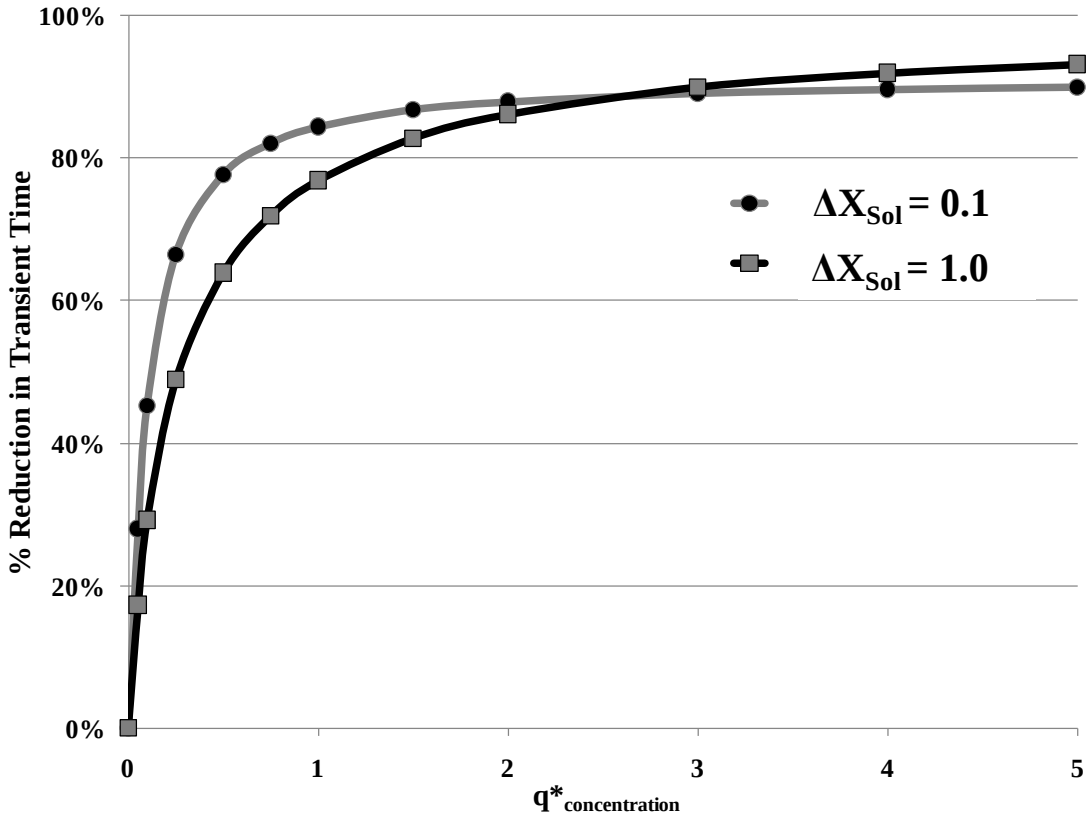

Figure 4.20: The percent reduction in transient time versus $q^*_{concentration}$ for two values of ΔX_{Sol} (NTU=11.4, Cr*=3, summer AHRI conditions, $X_{Sol,QSS}$=2.1692).

As Figure 4.20 shows, the percent reduction in transient time increases with $q^*_{concentration}$, and the maximum percent reduction depends on the initial concentration of the solution (ΔX_{Sol}) condition exists. However, for both small and large values of ΔX_{Sol}, the possible reduction in transient time is over 90%, and occurs at large values of $q^*_{concentration}$. However even with a 90% reduction, transient times can still be a few days long. The proper selection of $q^*_{concentration}$ depends on the expected range of ΔX_{Sol}

encountered by the system, the desired reduction in transient time, and the cost of providing and controlling $q^*_{concentration}$.

4.5.5 Concentration Control Conclusion

The initial concentration of the solution has been found to largely impact the transient time of the system. An initial solution concentration that is different from the quasi-steady-state concentration can cause the transient time of the system to be over 18 days. Ideal concentration control, where water is both added and removed from the solution without external heating/cooling, has been found to eliminate up to 90% of the transient time. The practical method of concentration control which also implements the temperature control studied in section 4.4, was also found to reduce transient times by over 90% and should be capable of providing these reductions for almost any initial solution temperature and concentration values. Therefore, the practical method of concentration and temperature control studied in section 4.5.4 should be implemented to reduce the RAMEE transient times associated with the initial system start-up.

4.6 Application of Control Strategies

This section will examine how the control strategies developed in section 4.5 can be used to eliminate unwanted transients during system operation, and increase the RAMEE performance. This will include both system start-up as well as variable outdoor conditions. The practical method of concentration and temperature control studied in section 4.5.4 will be used, while flow control and air flow bypass will be neglected due to their poor performance.

4.6.1 Outdoor Conditions

Both variable summer (cooling) and winter (heating) outdoor conditions will be examined in this section. A 24 hour sinusoidal temperature wave is chosen for both summer and winter conditions and these are shown in Figure 4.21. The humidity ratios of the inlet air are assumed to be constant throughout the 24 hour period as shown in Figure 4.22. These outdoor conditions will be repeated for a 7 day period in order to get an in depth look at the system behavior upon start-up and changing weather conditions.

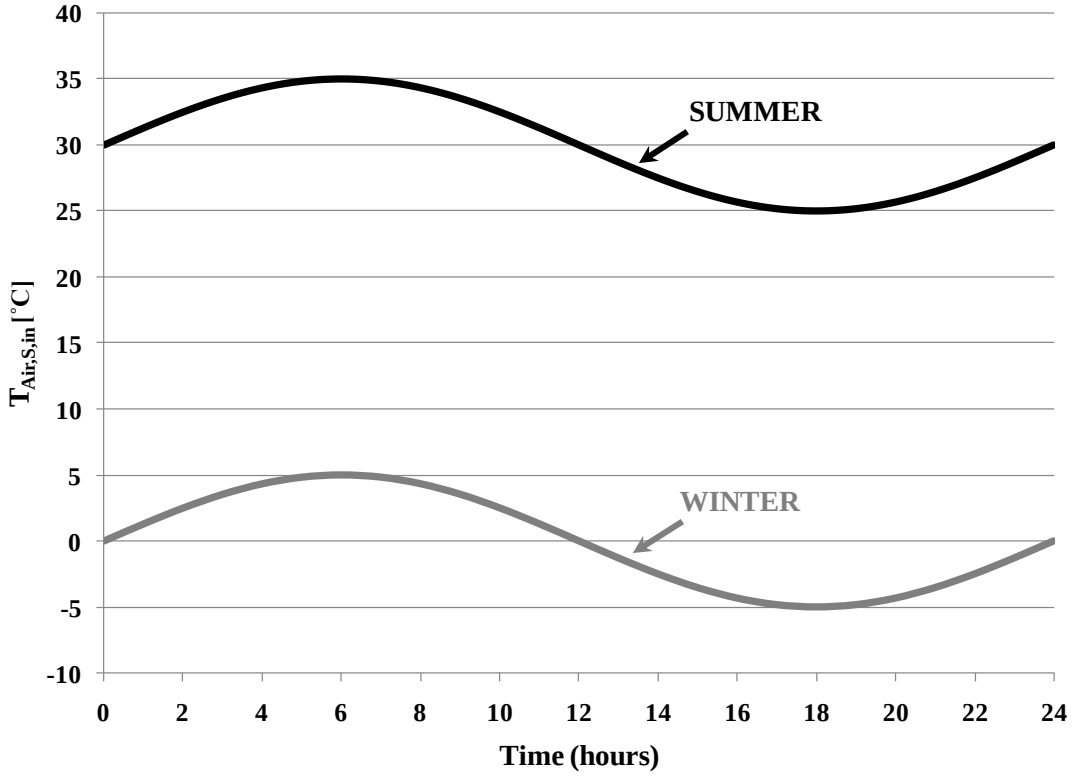

Figure 4.21: Outdoor air temperature ($T_{Air,S,in}$) during a 24 hour period for both summer (cooling) and winter (heating) conditions.

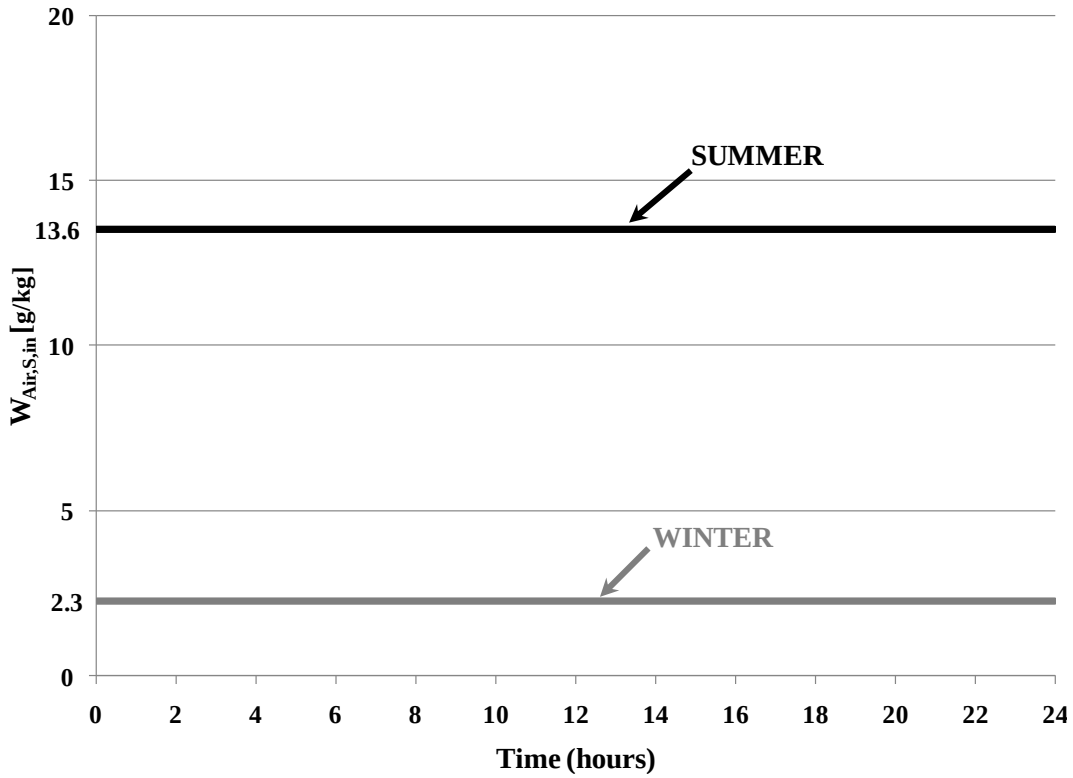

Figure 4.22: Outdoor air humidity ratio ($W_{Air,S,in}$) during a 24 hour period for both summer (cooling) and winter (heating) conditions.

4.6.2 Indoor Conditions

In a practical application, the indoor conditions may vary slightly with changing outdoor conditions. However for this study, it is assumed that the HVAC system is capable of maintaining constant indoor conditions throughout the 24 hour cycle. The indoor air conditions will be chosen as constant AHRI summer conditions during variable outdoor summer (cooling) conditions, and constant AHRI winter conditions during variable outdoor winter (heating) conditions. These conditions are shown in Table 2.3.

4.6.3 Initial Solution Conditions

There are two typical options for the initial solution start-up conditions. If the RAMEE system is installed in an HVAC system that is located primarily inside the building (e.g. a mechanical room), then the solution will most likely begin at

equilibrium with the indoor air conditions. Alternatively, if the HVAC system is located on the roof, then the solution may initially begin at equilibrium with the outdoor air conditions. Both of these initial solution condition possibilities are shown in Table 4.2.

Table 4.2: Indoor and outdoor initial solution conditions for both summer and winter.

		Solution Conditions	
		Indoor System	**Roof-Top System**
Summer	Initial Temperature: $T_{Sol,Initial}$	24 ºC	30 ºC
	Initial Mass Fraction: $X_{Sol,Initial}$	2.1447 kg/kg	2.1373 kg/kg
Winter	Initial Temperature: $T_{Sol,Initial}$	21 ºC	0 ºC
	Initial Mass Fraction: $X_{Sol,Initial}$	1.9586 kg/kg	2.7130 kg/kg

The initial condition of the solution will largely impact the performance of the RAMEE during the transient time. Figure 4.23 shows the air temperature leaving the supply exchanger ($T_{Air,S,out}$) for both indoor and outdoor initial solution conditions during summer operation, with no implemented transient control strategies.

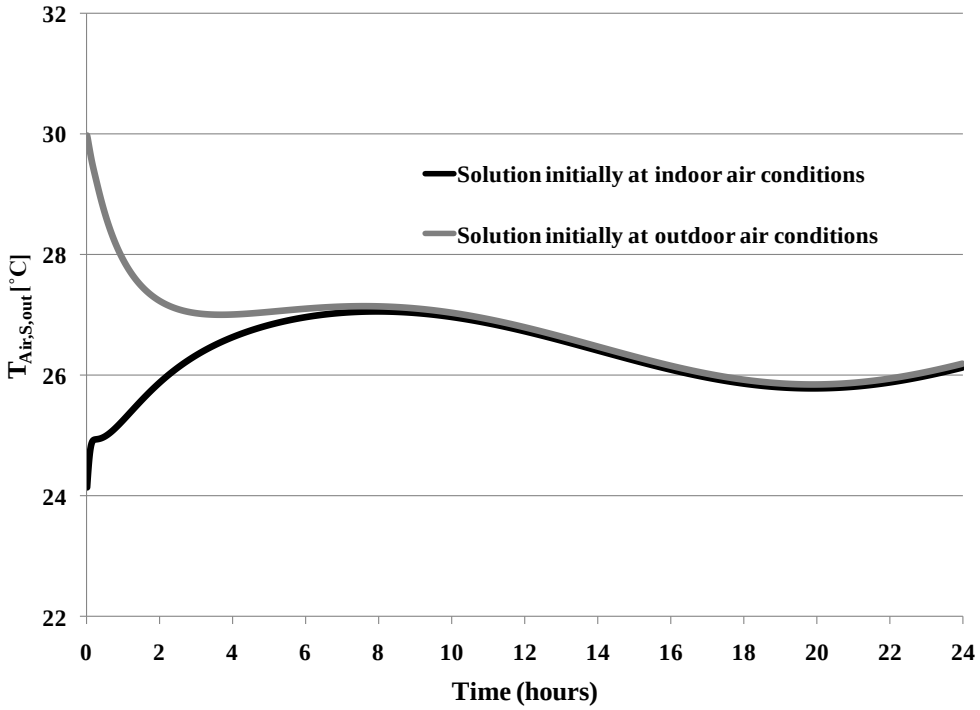

Figure 4.23: Air temperature leaving the supply exchanger ($T_{Air,S,out}$) for both indoor and outdoor initial solution conditions during summer operation with no implemented control strategies (summer AHRI indoor conditions, NTU=11.4, Cr*=3).

Initially starting with the solution at the indoor conditions, results in a lower and more desirable temperature. This is because the solution begins at a temperature much cooler than the outdoor air and is capable of significantly decreasing the air temperature. As the solution warms up, the potential for energy transfer between the solution and outside air decreases and the supply outlet air also warms up. If the solution begins at outdoor conditions, there is no potential to cool the outdoor air initially (t=0). However, the solution temperature will decrease over time due to the cool exhaust air stream. Therefore, the solution will begin to cool the outdoor air over time, as shown in Figure 4.23 by the decreasing supply outlet air temperature. However as Figure 4.23 shows, starting with the solution at outdoor temperature results in a much higher supply outlet air temperature during the first few hours, which results in a decrease in the performance of the RAMEE during this time.

The supply outlet humidity ratio ($W_{Air,S,out}$) also depends on the initial solution conditions. Figure 4.24 shows that if the solution begins at indoor conditions, the resulting supply outlet humidity ratio is initially lower due to the potential for mass transfer between the outdoor air and the solution. If the solution begins at outdoor conditions, then the moisture transfer between the outdoor air and the solution is initially zero until the solution changes temperature and concentration. Therefore for summer conditions, it is beneficial to have the solution begin at equilibrium with the indoor air conditions.

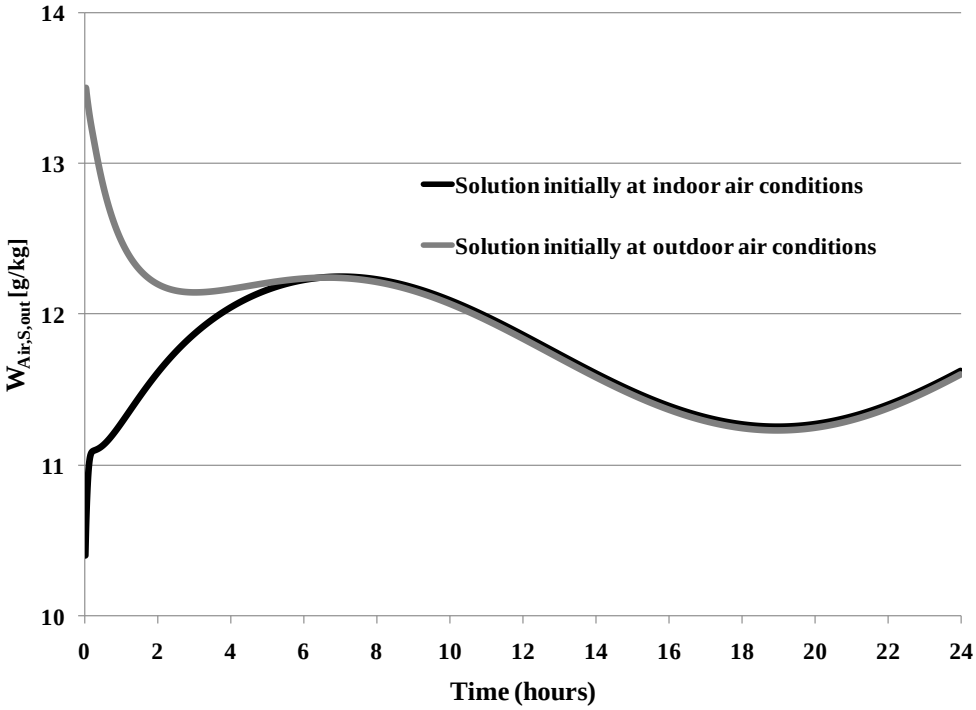

Figure 4.24: Air humidity ratio leaving the supply exchanger ($W_{Air,S,out}$) for both indoor and outdoor initial solution conditions during summer operation, with no implemented control strategies (summer AHRI indoor conditions, NTU=11.4, Cr*=3).

A similar behavior occurs during winter conditions. Figure 4.25 shows the air temperature ($T_{Air,S,out}$) and Figure 4.26 shows the air humidity ratio leaving the supply exchanger, for both indoor and outdoor initial solution conditions during winter operation with no implemented transient control strategies.

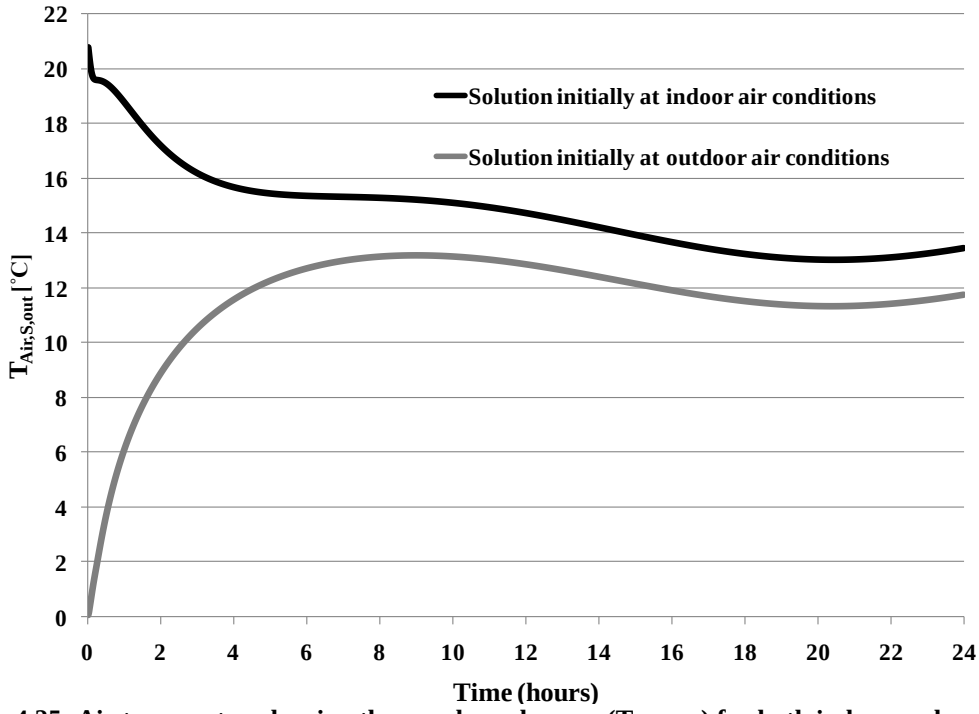

Figure 4.25: Air temperature leaving the supply exchanger ($T_{Air,S,out}$) for both indoor and outdoor initial solution conditions during winter operation, with no implemented control strategies (winter AHRI indoor conditions, NTU=11.4, Cr*=3).

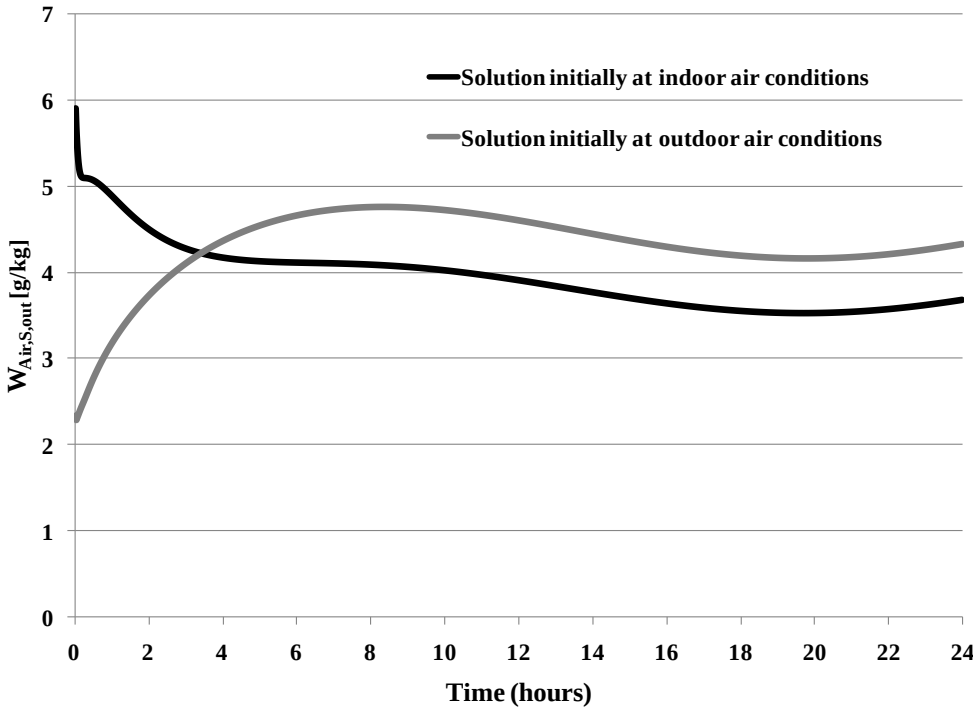

Figure 4.26: Air humidity ratio leaving the supply exchanger ($W_{Air,S,out}$) for both indoor and outdoor initial solution conditions during winter operation, with no implemented control strategies (winter AHRI indoor conditions, NTU=11.4, Cr*=3).

Once again, beginning with the solution at equilibrium with the indoor air conditions results in better performance (higher supply outlet temperature and humidity) during the first few hours, since the potential for both thermal and moisture transfer between the outdoor air and solution are greater. However after a few hours, and for the remainder of the 24 hour period, the supply outlet humidity ratio is more favorable if the solution begins at the outdoor condition. Both the temperature and humidity depend on the initial solution condition over the entire 24 hour period. This is unlike the summer conditions in which the temperature and humidity converged to the same trend after 6 hours. The reason for this difference is due to the difference in initial solution mass fraction. Figure 4.27 shows the solution mass fraction entering the supply exchanger ($X_{Sol,S,in}$) over a 7 day period, when the 24 hour cycle is repeated.

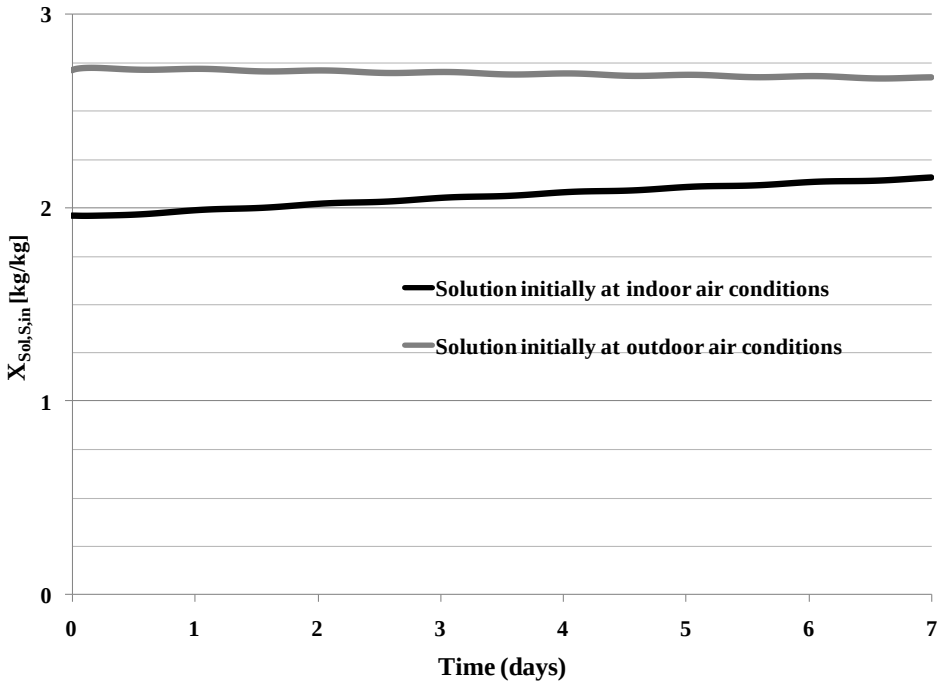

Figure 4.27: Solution mass fraction entering the supply exchanger ($X_{Sol,S,in}$) for both indoor and outdoor initial solution conditions during winter operation, with no implemented control strategies (winter AHRI indoor conditions, NTU=11.4, Cr*=3).

When the solution begins at outdoor conditions, the solution mass fraction needs to decrease to reach the quasi-steady-state value. However if the solution begins at

indoor conditions, the mass fraction must increase to reach the quasi-steady-state value. As Figure 4.27 shows, the change in mass fraction has yet to be complete after 7 days, and would most likely take several more days or weeks to converge to a constant value. Due to this moisture transient, different outlet air conditions occur for the entire week, depending on the initial solution condition as shown in Figures 4.28 and 4.29. Starting the solution at indoor air conditions results in a higher (and more desirable) supply outlet temperature during the entire week time. Figure 4.29 shows that starting the solution at indoor conditions results in a lower (and less desirable) supply outlet humidity ratio during the week, except for the initial 3 hours. Over the week, the trends in both temperature and humidity ratio which result from indoor and outdoor initial solution conditions approach each other. During winter conditions, it is likely more beneficial to maintain a higher supply outlet temperature versus a higher outlet humidity ratio. Therefore for the remainder of this study, the solution will be assumed to start at indoor conditions.

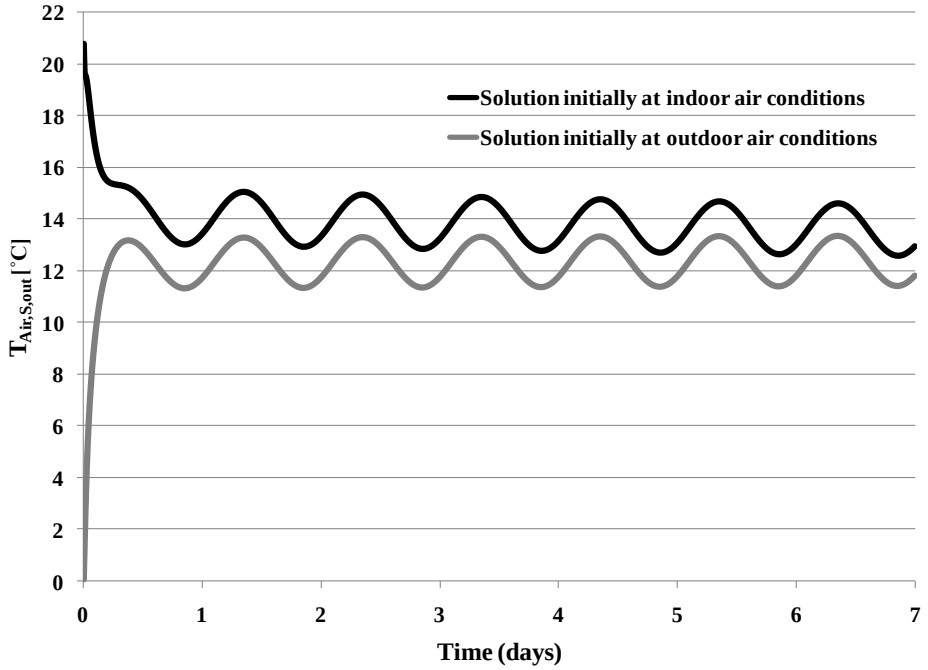

Figure 4.28: Air temperature leaving the supply exchanger ($T_{Air,S,out}$) for both indoor and outdoor initial solution conditions during winter operation, over a week (7 day) time period (winter AHRI indoor conditions, NTU=11.4, Cr*=3).

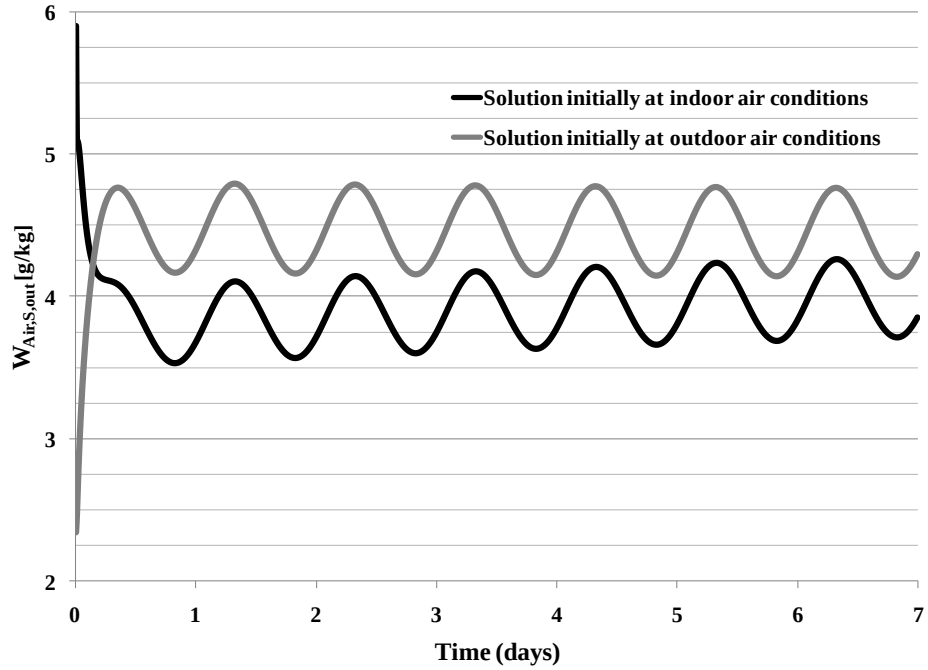

Figure 4.29: Air humidity ratio leaving the supply exchanger ($W_{Air,S,out}$) for both indoor and outdoor initial solution conditions during winter operation, over a week (7 day) time period (winter AHRI indoor conditions, NTU=11.4, Cr*=3).

4.6.4 Control Capacities

The capacities chosen for both temperature and concentration control are shown in Table 4.3. These are the maximum capacities that the external systems can provide during any outdoor condition and are normalized by the amount of energy or mass transferred by the RAMEE at quasi-steady state for summer and winter AHRI conditions. AHRI summer and winter conditions are used for the normalization, to ensure that the external control capacities are normalized to a constant standard for each RAMEE system, regardless of outdoor operating conditions. The RAMEE quasi-steady-state energy $\left(q_{RAMEE,QSS}\right)$ and mass $\left(\dot{m}_{RAMEE,QSS}\right)$ transfer rates used for normalization are given in Table 4.3 for summer and winter conditions. Large control capacities were chosen in order to demonstrate the maximum potential of using temperature and concentration control.

Table 4.3: RAMEE system capacities and control capacities for summer and winter conditions.

	Summer	Winter
$q_{RAMEE,QSS}$	99 W	111 W
q^*	2	2
$q^*_{concentration}$	2	2
$\dot{m}_{RAMEE,QSS}$	2.18×10^{-6} kg/s	1.36×10^{-6} kg/s
$\dot{m}^*$	2	2

4.6.5 Appropriate Transient Control

As shown previously, there are times when the air conditions leaving the supply exchanger are more favorable during transient operation than during quasi-steady-state operation. Therefore it is often desirable to allow the system to maintain a transient operation as long as possible. The conditions at which temperature and concentration control should be avoided in order to maintain performance are given in Table 4.4 below, and will be used during this study. For example, increasing the solution

temperature entering the supply exchanger should be avoided if the outdoor air temperature is warmer than the indoor air temperature, but cooler than the solution temperature (row 1 in Table 4.4). Increasing the solution temperature during these conditions would result in a warmer air temperature leaving the supply exchanger.

Table 4.4: Conditions at which temperature and concentration control should be avoided.

AVOID	IF
Increasing $T_{Sol,S,in}$	$T_{Sol,S,in} < T_{Air,Outdoor}$ AND $T_{Air,Outdoor} > T_{Air,Indoor}$
Decreasing $T_{Sol,S,in}$	$T_{Sol,S,in} > T_{Air,Outdoor}$ AND $T_{Air,Outdoor} < T_{Air,Indoor}$
Increasing $X_{Sol,S,in}$	$W_{Sol,S,in} < W_{Air,Outdoor}$ AND $W_{Air,Outdoor} > W_{Air,Indoor}$
Decreasing $X_{Sol,S,in}$	$W_{Sol,S,in} > W_{Air,Outdoor}$ AND $W_{Air,Outdoor} < W_{Air,Indoor}$

4.6.6 Results

Figure 4.30 shows the transient behavior of the supply outlet air temperature with and without transient control, for 7 days at summer conditions. During times when the outdoor temperature is increasing, no transient control is used. This is because it is more beneficial for the solution to remain cooler and keep the resulting supply air temperature lower. Therefore, initially, the system behaves the same with or without transient control. However when the outdoor temperature begins to decrease, transient control is used to lower the temperature of the solution quicker. This control results in a faster rate of decrease in the supply outlet air temperature. Since the outlet air temperature decreases at a fast rate with transient control, it is able to reach a lower temperature (over 1°C lower) before the outdoor air begins to increase again.

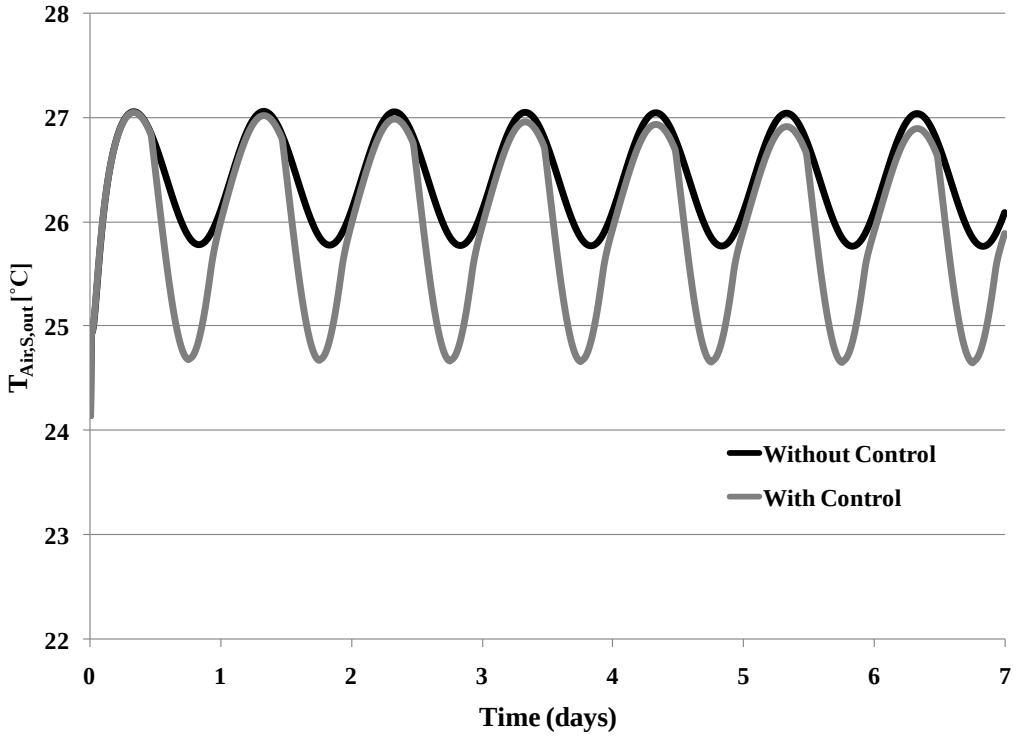

Figure 4.30: The transient behavior of the supply outlet air temperature with and without transient control for a 7 day period during summer conditions (NTU=11.4, Cr*=3).

The average supply outlet air temperature over the 7 day period is reduced by 0.5°C with the use of transient controls. It should be noted that the peak supply outlet air temperature decreases very slowly over time. Although this trend is nearly impossible to see for the case without transient control, it is visible with transient control in Figure 4.30. This trend exists because the system is always transient due to the ever changing outdoor conditions. However, these changing outdoor conditions are cyclic and repeating over time. Therefore, the system will also reach a consistent cyclical performance. However, the system has yet to reach its steady-state cyclical performance during the 7 day period. Therefore the system has a certain step response (time constant) and a frequency response (amplitude and phase shift) which depends on how it is controlled.

Using transient control reduces the time required to reach the steady-state cyclical performance. Therefore the daily average in supply outlet air temperature decreases over time as shown in Figure 4.31. Transient control results in a faster decrease, and therefore a faster convergence to steady-state cyclical performance.

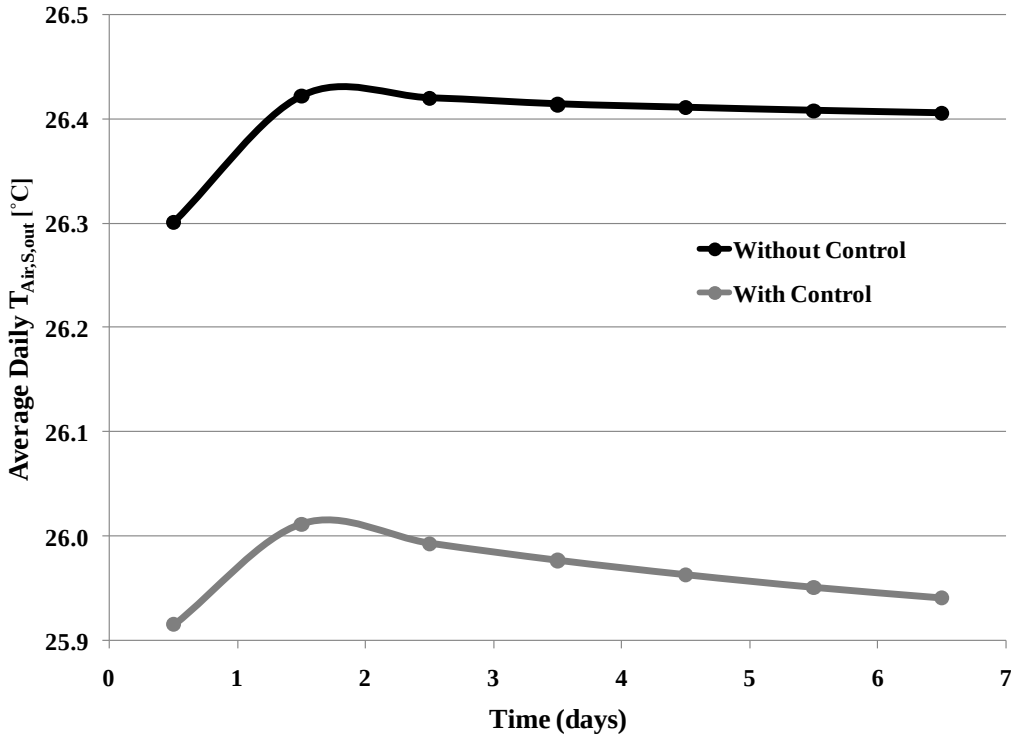

Figure 4.31: The transient behavior of the daily average supply outlet air temperature with and without transient control, for 7 days at summer conditions (NTU=11.4, Cr*=3).

The supply outlet humidity ratios with and without transient control are shown in Figure 4.32 during the 7 day period. During periods where transient controls are used, the resulting supply outlet humidity ratio decreases faster. This allows a lower humidity ratio to be achieved, before the outdoor temperature and relative humidity increase again. Over the 7 day period, the average supply outlet humidity ratio is decreased by 0.12 g/kg with the use of transient controls. As discussed earlier, the use of transient control decreases the time required to reach the systems steady-state cyclical

performance. This is visible in Figure 4.32 where the peak outlet air humidity ratio is increasing quicker with transient control.

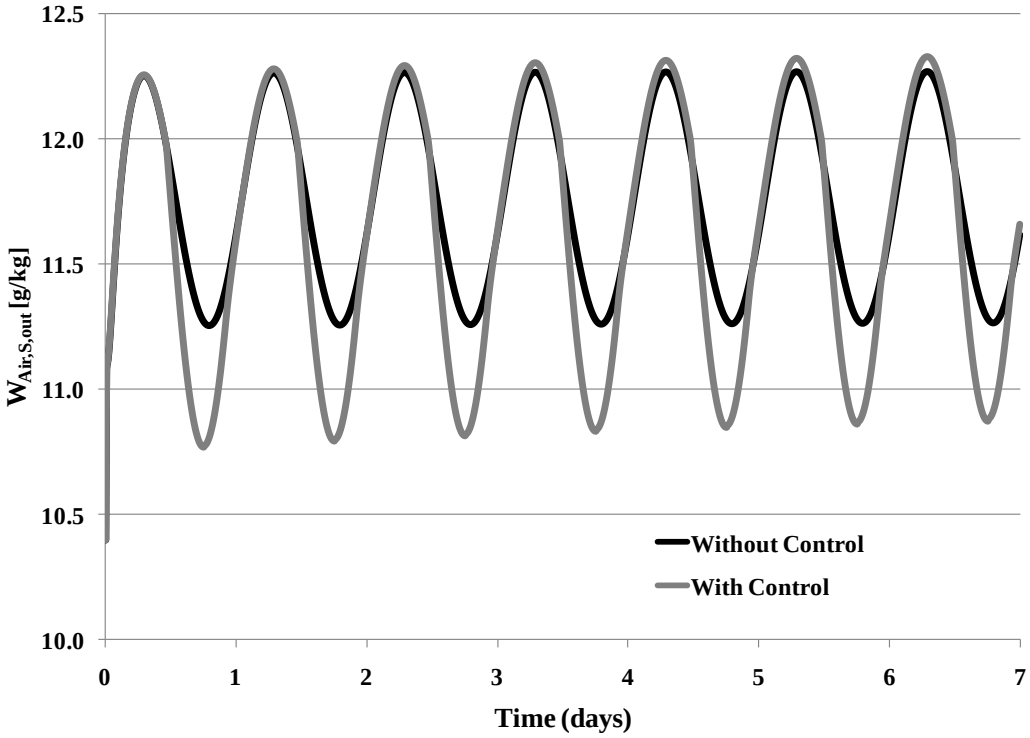

Figure 4.32: The transient behavior of the supply outlet air humidity ratio with and without transient control, for 7 days at summer conditions (NTU=11.4, Cr*=3).

The resulting supply total effectiveness is shown in Figure 4.33. The use of transient control keeps the effectiveness from decreasing as low, and results in an increase of 6% in the average supply total effectiveness over the 7 day period. Therefore for summer conditions, the use of transient control during changing outdoor weather conditions is beneficial.

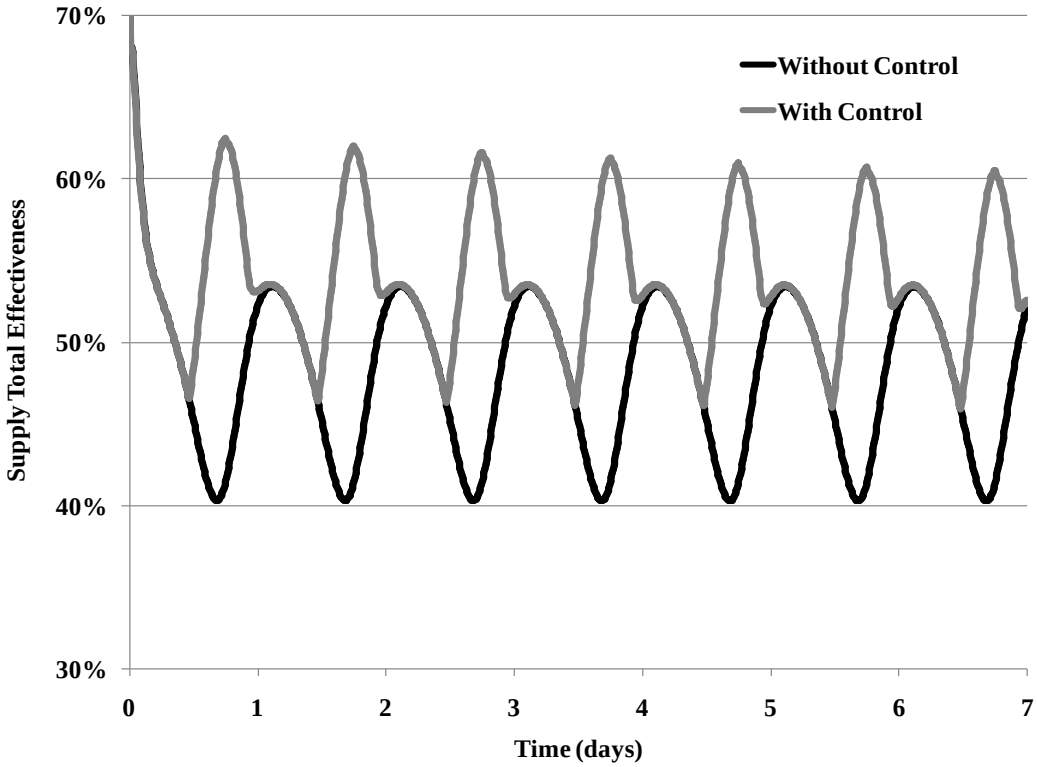

Figure 4.33: The transient behavior of the supply total effectiveness with and without transient control, for 7 days at summer conditions (NTU=11.4, Cr*=3).

For winter conditions, the supply outlet air temperature is shown in Figure 4.34 with and without transient control. Transient control causes the supply outlet air temperature to increase more rapidly when the outdoor temperature increases. However, it also causes a decrease in the minimum temperature. This is due to the system trying to reach the steady-state periodic temperature (which is lower) quicker. As Figure 4.34 shows, minimum (and therefore also average) outlet temperature reached decreases over time for both cases with and without transient control. However, the average outlet temperature decreases faster over time with the use of transient control, therefore providing a lower (and less desirable) temperature sooner. However, Figure 4.35 shows that during this same time, the peak (and therefore also average) supply outlet humidity ratio increases to a more desirable value sooner with transient control. Therefore, transient control will cause the system to reach steady-state cyclical performance

quicker, but the net effect of transient control on the performance will depend on the change in effectiveness during this time.

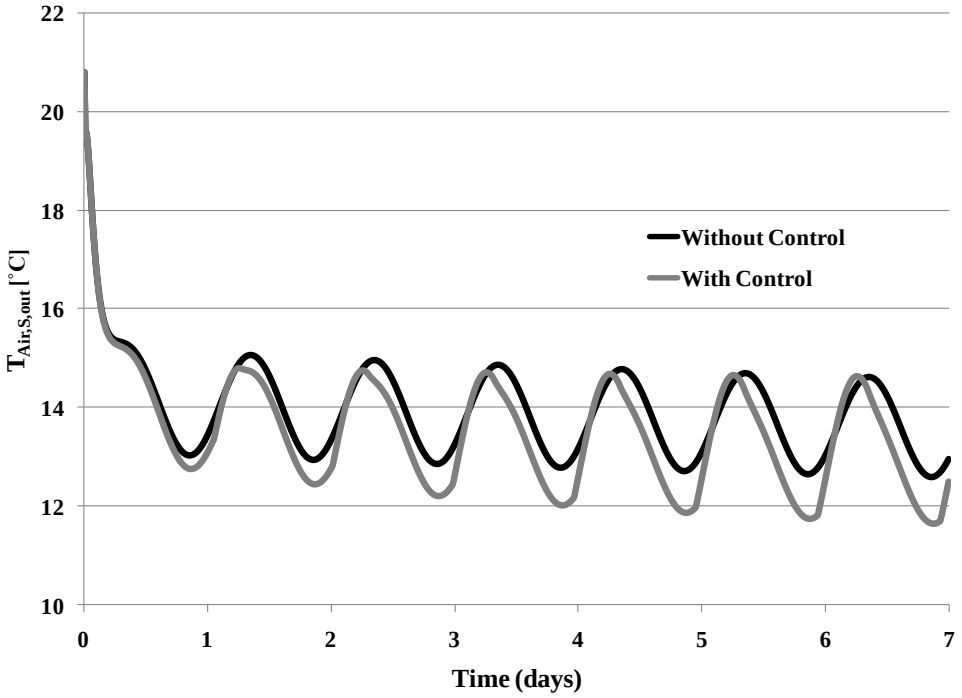

Figure 4.34: The transient behavior of the supply outlet air temperature with and without transient control, for 7 days at winter conditions (NTU=11.4, Cr*=3).

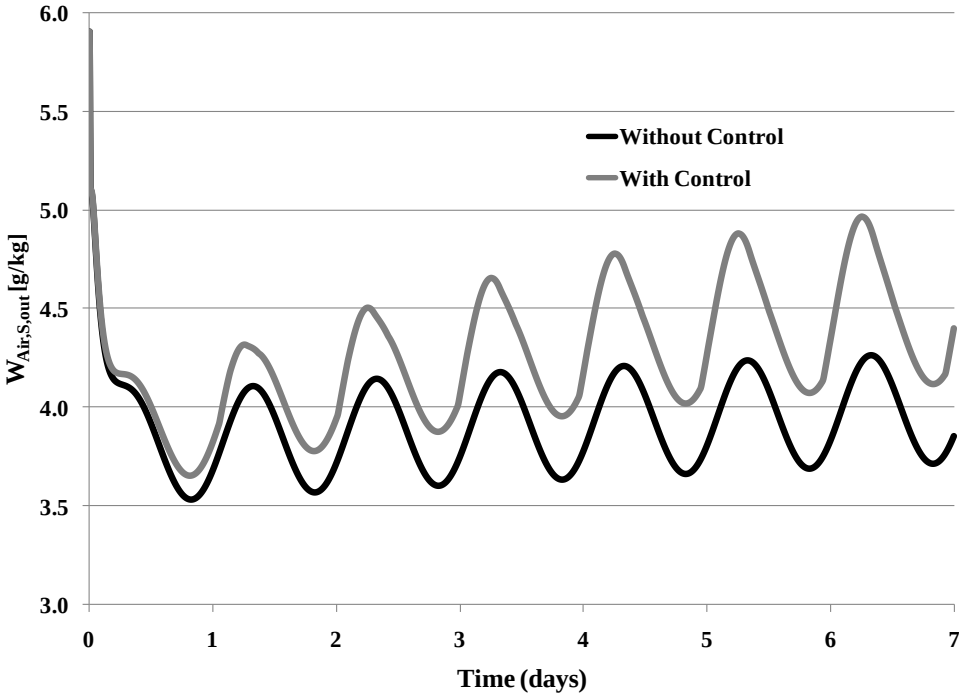

Figure 4.35: The transient behavior of the supply outlet air humidity ratio with and without transient control, for 7 days at winter conditions (NTU=11.4, Cr*=3).

Figure 4.36 shows the supply total effectiveness with and without transient control, during winter conditions. As Figure 4.36 shows that the transient control results in an increase in effectiveness during times when control is used. Therefore, even though the average supply outlet air temperature is decreased with transient control, the average humidity ratio is substantially increased such that the net energy transfer is greater.

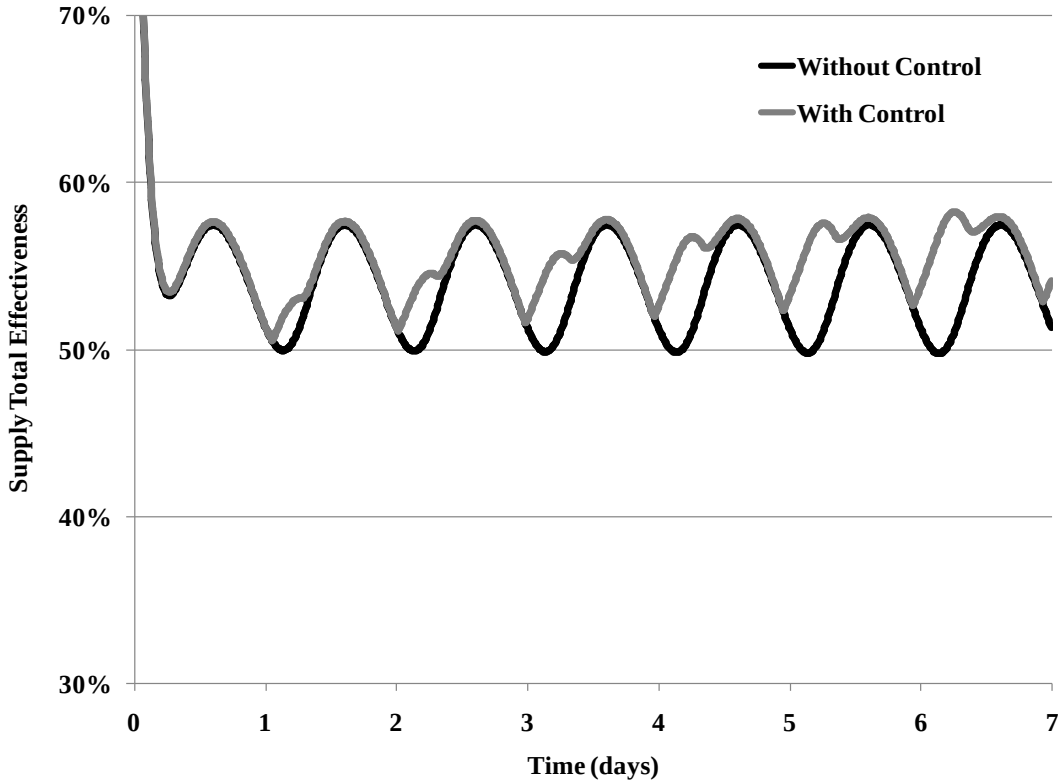

Figure 4.36: The transient behavior of the supply total effectiveness with and without transient control, for 7 days at winter conditions (NTU=11.4, Cr*=3).

Transient control provides a 1.5% increase in the average supply total effectiveness, over the week long period. The increase in effectiveness due to transient control is small during the first few days but increases with time. Figure 4.37 shows the average daily effectiveness values with and without transient control.

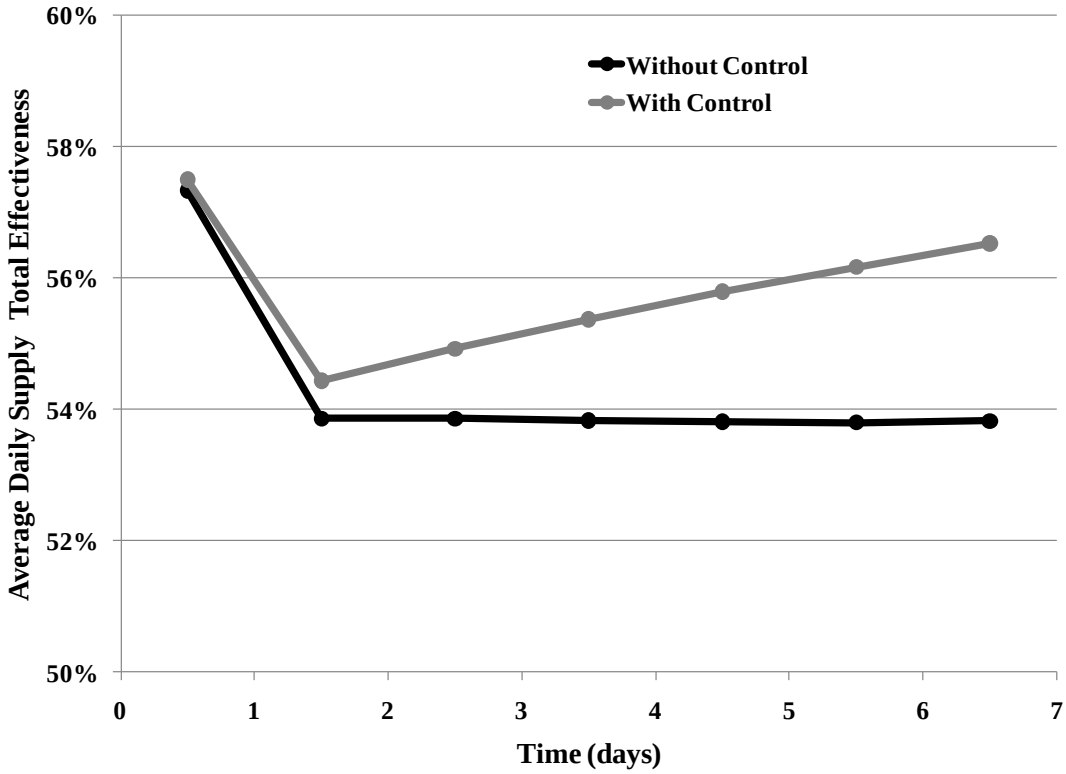

Figure 4.37: The transient behavior of the daily average supply total effectiveness with and without transient control, for 7 days at winter conditions (NTU=11.4, Cr*=3).

The daily average effectiveness with transient control is increasing over time, and would become even more beneficial than without transient control in future days. Therefore transient control is beneficial during the changing winter outdoor conditions.

4.6.7 Application of Control Strategies Conclusion

The practical application of the control strategies developed throughout this chapter, showed the importance of understanding when transients are beneficial or harmful to the RAMEE performance. By implementing transient control only when it is appropriate, allows for both the reduction in transient time and an increase in performance. Transient control was found to be beneficial for both summer and winter variable outdoor conditions. Not only does transient control reduce the time required to

reach steady-state cyclical performance, but it also provides an increase in effectiveness. Therefore, it is recommended that transient control be used during variable outdoor conditions.

4.7 Chapter 4 Summary

The purpose of this chapter was to investigate control strategies that could be used to minimize the transient time delays associated with both system start-up and changing outdoor weather conditions. The control strategies considered were solution and air flow control, air flow bypass, solution temperature control, and solution concentration control. Solution and air flow control were found to provide a reduction in transient time of 10%, and required either a solution flow rate that is three times more, or an air mass flow rate that is three times less than the required flow rate at quasi-steady-state. Increasing the solution flow rate by a factor of three is costly, while reducing the air flow by a factor of three jeopardizes indoor air quality and comfort. Therefore, based on these results, flow control is not recommended as a viable control strategy.

Air flow bypass was found to be a more viable alternative to solution and air flow control as it is capable of providing a reduction in transient time of over 16% without reducing the amount of fresh air being supplied to the building or increasing pumping costs. However a 16% decrease is not substantial enough for air flow bypass to be the primary method of transient control. Therefore, air flow bypass is recommended as an option that could further reduce transient times in conjunction with a more suitable primary method of control. Air flow bypass is also recommended as a possible method to control the system during part load conditions.

Temperature control was found to be capable of reducing thermal transients. An external solution heating/cooling system that is capable of transferring as much energy as the RAMEE transfers at quasi-steady state ($q^*=1$) is capable of eliminating the thermal transients for temperature differences of over 10°C between the initial and quasi-steady-state solution temperature. This temperature difference corresponds to a 20°C temperature difference between the indoor and outdoor air temperatures (if the solution begins at either indoor or outdoor air temperature). However, thermal transients were found to be a minor contributor to the overall transient time for cases where the initial solution concentration is different than the quasi-steady state concentration. As such, temperature control only reduces the total (thermal and moisture) transients by up to 15%. Therefore, temperature control is recommended, but only in conjunction with concentration control.

Concentration control was investigated as a possible method to reduce the transient times that occur when the initial solution concentration is different from the quasi-steady-state concentration. These transient times can be as long as 18 days. Controlling the concentration by adding or removing water from the solution was found to reduce transient times by up to 90%, and therefore is a vital control strategy.

A practical method of concentration control, which also implements temperature control, was developed. This control strategy adds water when the solution concentration needs to be decreased. When the solution concentration needs to be increased, heat is added to the exhaust storage tank (tank located before the exhaust exchanger), so that more moisture is transferred from the solution to the exhaust air. In order to cool the solution back down, temperature control is utilized. This practical

method of control can reduce the transient time by 90%, and therefore is recommended as a proper control strategy. This practical transient control method was also tested during variable outdoor conditions. It was found that the transient control not only decreases the time required for the RAMEE to reach quasi-steady-state operating conditions, but also provides an increase in system effectiveness during variable outdoor conditions. Therefore, the practical method of concentration and temperature control studied in section 4.5.4 is recommended as a suitable method to reduce transient times associated with the initial system start-up, and increase the RAMEE performance during variable outdoor conditions.

CHAPTER 5

SUMMARY, CONCLUSIONS AND RECCOMMENDATIONS

5.1 Summary

The objective of this study was to investigate the performance and control of a run-around membrane energy exchanger (RAMEE), by considering both experimental and numerical methods. The RAMEE prototype and evaluation methods (numerical and experimental) were presented in Chapter 2, including a discussion on the membrane and desiccant solution used. In addition, the experimental test apparatus and corresponding experimental uncertainties were presented. The uncertainties in quasi-steady-state total effectiveness range from 1.8% at NTU=4.2 and low Cr* values, to 5.1% at NTU=11.4 and high Cr* values. Higher NTU values create a higher uncertainty due to the lower air flow rate, which are difficult to measure accurately using the orifice plate pressure drop.

The numerical model was compared to the experimental data in Chapter 3. The quasi-steady-state performance of the RAMEE system was found to be influenced by two important factors; the number of heat transfer units (NTU) and the ratio of solution and air heat capacity rates (Cr*). The latent effectiveness was found to be greatly influenced by the NTU, as a higher NTU resulted in a higher latent effectiveness. Both the latent and sensible effectivenesses were found to be influenced by Cr*, with the maximum effectiveness occurring at Cr*=3. A discrepancy between the numerical and experimental data was found to occur at low solution flow rates (low Cr* values), which

suggested that a flow maldistribution problem occurred in the experimental prototype, which caused the solution flow to be non-uniform throughout the exchanger. This discrepancy was not found at high solution flow rates, where the pressure inside the solution channel is high enough to increase flow distribution. Therefore at high solution flow rates, the experimental and numerical data agrees within experimental uncertainty. At low Cr* values, the maximum difference in total effectiveness between the numerical and experimental data is 11% (NTU=11.4, Cr*=3.3), which is higher than the corresponding experimental uncertainty of 5%. More research should be completed on flow maldistribution in order to determine strategies to better avoid problems. Heat losses/gains between the RAMEE system and the environment were found to play a large role in the performance of the system, and should be minimized as much as possible by carefully insulating the system.

The transient performances of the numerical and experimental RAMEEs were found to agree within experimental uncertainty. The maximum root mean square error was found to be 10% which implies good accuracy of the numerical model. The transient performance of the RAMEE system was found to be important during system start-up, as long time delays of up to several hours can occur before reaching quasi-steady state. Transient times as long as 18 days occur if the solution begins at a concentration that is different than the desired quasi-steady-state concentration.

Chapter 4 focused on multiple control strategies that can be implemented to minimize the transient delays of the RAMEE system. Control strategies studied include: solution and air flow rate control, air flow bypass, solution temperature control, and solution concentration control.

Flow control was found to reduce the transient time by up to 11% for start-up conditions. However, this small reduction in transient time may not be worth the additional pumping costs (capital and energy costs) required to providing the increased solution flow rate, and it may not be worth decreasing the air flow rate because it will reduce the indoor air quality.

Air flow bypass was found to be a better alternative to flow control, as the transient time could be reduced by 16%, without having to increase the solution flow rate, or decrease the air flow rate being supplied to the building.

Solution temperature control was found to decrease the thermal transients by up to 100%, but depends on the capacity of auxiliary heating/cooling equipment. Nevertheless, thermal transients were found to be only a small portion of the total transient time when the solution concentration is different than the quasi-steady-state concentration. For these cases, temperature control was found to only reduce the total transient time by 15%.

Solution concentration control is able to reduce transient times associated with the solution having to change concentration by up to 90%, but requires a practical means of adding and removing moisture from the solution. A practical method of control which integrates both concentration control and temperature control was developed. This method adds water to the solution when the concentration needs to be reduced, but adds heat to the solution before the exhaust exchanger if the solution concentration needs to be increased. By adding heat to the solution before it enters the exhaust exchanger, more moisture is transferred out of the solution and into the exhaust air. Therefore, the solution loses moisture and increases concentration. The solution is then

cooled back down before entering the supply exchanger to maintain performance. This practical method of control was found to eliminate over 90% of the total transient time. Applying this practical control strategy during variable weather conditions was found to not only reduce transients, but also increase the effectiveness of the system. Therefore, the practical method of temperature and concentration control is suggested as a feasible method of reducing transient times and increasing performance both during initial system start-up and variable outdoor conditions.

5.2 Conclusions

The following conclusions can be made from the research presented in this thesis:

1. The numerical model of Seyed-Ahmadi (2008) accurately predicts both the transient and steady-state performance of the RAMEE prototype which was experimentally tested.
2. The quasi-steady-state performance of the RAMEE system was found to be influenced by both the number of heat transfer units (NTU), and the ratio of solution and air heat capacity rates (Cr*). The latent effectiveness was found to be heavily influenced by the NTU, as a higher NTU resulted in a higher latent effectiveness. Both the latent and sensible effectivenesses were found to be influenced by Cr*.
3. The numerical model indicates that the effectiveness should increase with increasing Cr* until Cr*=3, at which point the effectiveness will decrease slightly to an asymptotic value for increasing Cr*. However, the experimental data shows a continuous increase in effectiveness with Cr*. The reason for this

discrepancy between the numerical and experimental results at low Cr* values is believed to be due to maldistributed solution flow. Therefore, the numerical and experimental total effectiveness results only agree within experimental uncertainties at high Cr* values. At low Cr* values, the maximum difference in total effectiveness between the numerical and experimental data is 11% (NTU=11.4, Cr*=3.3).

4. Heat losses/gains between the RAMEE system and the environment were found to play a large role in the performance of the system. Therefore, heat gains/losses should be minimized as much as possible by carefully insulating the system, including the exchangers, piping, and storage tank.
6. The numerical and experimental performances of the RAMEE were found to be in agreement, within experimental uncertainty. The maximum root mean square error between the numerical and experimental data was found to be 10%.
7. Both experimental and numerical results showed that large transient delays (of up to several days) can occur upon initial system start-up.
8. Transient delays increase if the solution concentration is different than the desired steady-state concentration. These transient delays can become as long as 18 days, which is too long for a practical system.
9. Control strategies can be used to decrease the transient delays:
    i. Solution and air flow control can be used to decrease transient times. However, an increase in solution flow rate, or a decrease in air flow rate of 300% only reduces the transient times by less than 10%. The small reduction in transient time may not justify the additional pumping costs

(capital and energy costs) associated to providing the increased solution flow rate, and may not justify a decrease in the air flow rate which results in poor indoor air quality.

ii. Air flow bypass proves to be a more feasible alternative to solution and air flow control and can reduce transient times of up to 16% compared to the case of no control. This control method does not require an increase in operating costs, does not reduce the amount of ventilation air entering the space, and only requires a small increase in capital expenses for dampers, damper controls, and a small bypass duct.

iii. Solution temperature control was found to be able to entirely eliminate the thermal transient time required for the solution to reach quasi-steady-state temperature, but requires an auxiliary heating/cooling source capable of providing the same amount of energy that is transferred by the RAMEE at quasi-steady-state. The feasibility of such a control strategy would depend on the application.

iv. Solution concentration control is able to significantly reduce the transient time, especially for cases where the solution concentration is different than the desired quasi-steady-state concentration. The transient time can be reduced by up to 90% but requires an auxiliary method of adding/removing moisture from the desiccant. Adding moisture can be done by simply adding deionized water to the system, but removing moisture will require the solution to be heated before the exhaust exchanger, and then re-cooled before the supply exchanger. This

practical method of control provides both concentration and temperature control, and reduces the transient time by over 90%. The feasibility of this control strategy must be determined based on the size of the system and its application.

10. When variable outdoor conditions exist, the practical method of concentration and temperature control is capable of both reducing transient times and increasing effectiveness.
11. The practical method of concentration and temperature control is recommended as a suitable method to reduce transient times and increase performance during both system start-up and variable outdoor operating conditions.

5.3 Recommendations for Future Work

There are many topics that can be studied to optimize the design and control of a run-around membrane energy exchanger (RAMEE). Some of these topics that are suggested based on the results of this research are:

1. The effect of solution maldistributed flow should be investigated in order to determine how to better optimize the solution and air flow channels.
2. The system design should be optimized based on both cost and performance.
3. The performance and control strategies discussed in this thesis should also be considered for a counter flow or counter/cross flow exchanger arrangement.
4. The economical feasibility of the control strategies discussed should be determined.
5. The response of the RAMEE system should be quantified in order to better control the system. This includes determining the RAMEE system response time

(time constant) and frequency response (amplitude and phase shift) when controlled at different operating conditions. By quantifying the system behavior, the control methods discussed in this thesis can be applied more effectively without having overshoot or undershoot in the output response of the system.

6. An active system that uses the practical method of solution temperature and concentration control to control the leaving supply air temperature and humidity should be studied. This system would not only provide energy recovery, but also heating, cooling, humidifying, and dehumidifying, which would eliminate the need for additional HVAC equipment downstream of the RAMEE. In order to control the system based on leaving air properties (instead of entering solution properties), the RAMEE behavioral response to energy and moisture inputs must first be quantified, as described in the previous point.
7. The impact of salt solution crystallization on the performance of the RAMEE system should be studied, including the solution behavior during transient times.
8. The behavior of salt solutions other than $MgCl_2$ should be examined, including mixtures of desiccants. Cost, performance, transient delays, and crystallization should all be considered when selecting a desiccant.

REFERENCES

Afshin, M., Simonson, C.J., Besant, R.W., 2009. Crystallization limits of LiCl-Water and $MgCl_2$-Water salt solutions as operating liquid desiccant in the RAMEE system. Submitted for publication in ASHRAE Transactions. ASHRAE, Atlanta.

AHRI. 2005. ANSI/ARI Standard 1060, Standard for Rating Air-to-Air Exchangers for Energy Recovery Ventilation Equipment. Arlington, VA: Air-Conditioning & Refrigeration Institute.

Ali, A., Vafai, K. and Khaled, A.-R.A., 2004. Analysis of heat and mass transfer between air and falling film in a cross flow configuration, International Journal of Heat and Mass Transfer 47, 743-755.

ANSI/ASHRAE Standard 55-2004, Thermal Environmental Conditions for Human Occupancy. Atlanta: ASHRAE.

ANSI/ASHRAE, 2008. ANSI/ASHRAE Standard 84 Method of Testing Air-to-Air Heat Exchangers. ASHRAE, Atlanta.

ANSI/ASHRAE STANDARD 62.1-2004, Ventilation for acceptable indoor air quality. Atlanta: ASHRAE.

ASHRAE, 1985. 1985 Fundamentals Handbook, Ch 8: Physiological Principles For Comfort and Health. ASHRAE, Atlanta.

ASHRAE, 2000. 2000 HVAC Systems and Equipment Handbook, Ch 44: Air-to-Air Energy Recovery. ASHRAE, Atlanta.

Asiedu, Y., Besant, R.W. and Simonson, C.J., 2005. Cost effective design of dual heat and energy recovery exchangers for 100% ventilation air in HVAC cabinet units, ASHRAE Transactions., 111(1), 857-872.

Asiedu, Y., Besant, R.W. and Simonson, C.J., 2004. Wheel selection for heat and energy recovery in simple HVAC ventilation design problems, ASHRAE Transactions. 110(1), 381-398.).

ASME Performance Test Code 19.1-1998, Test Uncertainty: Instruments and Apparatus, New York, NY.

Bennett, I.J.D., Besant, R.W., Schoenau, G.J. and Johnson, A.B., 1994a.
Procedure for optimizing coils in a run-around heat exchanger system. ASHRAE Transactions, 100(1), 442-451.

Bennett, I.J.D., Besant, R.W., Schoenau, G.J. and Johnson, A.B., 1994b. Validation of a run-around heat recovery system model. ASHRAE Transactions, 100(1), 230-237.

Charles, N.T. and D.W. Johnson, 2008. The occurrence and characterization of fouling during membrane evaporative cooling, Journal of Membrane Science, 319, 44–53.

Cisternas, L.A. and Lam, E.J., 1991. An analytical correlation for the vapor pressure of aqueous and non-aqueous solutions of single and mixed electrolytes, Part II: Application and extension. Fluid Phase Equilibrium, 62, 11–27.

D & R International. 2009. 2008 Buildings Energy Data Book. The Buildings Technologies Program, Energy Efficiency and Renewable Energy, U.S. Department of Energy.

Fan, H., Simonson, C.J., Besant, R.W. and Shang, W., 2006. Performance of a Run-Around System for HVAC Heat and Moisture Transfer Applications Using Cross-Flow Plate Exchangers Coupled with Aqueous Lithium Bromide, HVAC&R Research Vol. 12, No. 2, April 2006.

Fan, H., Simonson, C.J., Besant, R.W. and Shang, W., 2005. Run-around heat recovery system using cross-flow flat-plate heat exchangers with aqueous ethylene glycol as the coupling fluid, ASHRAE Trans., 111(1), 901-910.

Fan, H., 2005. Modelling a Run-Around Heat And Moisture Recovery System, MSc. Thesis, Department of Mechanical Engineering, University of Saskatchewan. Saskatoon, Saskatchewan.

Fang, L., Clausen, G. and Fanger, P.O., 2000. Temperature and humidity: important factors for perception of air quality and for ventilation requirements. ASHRAE Transactions, 106, 503-510.

Fauchoux, M., Simonson, C.J. and Torvi, D.A., 2007. The effect of energy recovery on perceived air quality, energy consumption and economics of an office building, ASHRAE Transactions, 113(2), 437-449.

Forsyth, B.I. and Besant, R.W., 1988a. The design of a run-around heat recovery system. ASHRAE Transactions, 94(2), 511-531.

Forsyth, B.I. and Besant, R.W., 1988b. The performance of a run-around heat recovery system using aqueous glycol as a coupling liquid, ASHRAE Transactions, 94(2), 532-545.

Greenspan, L., 1977. Humidity fixed points of binary saturated aqueous solutions, Journal of Research of the National Bureau of Standards – A. Physics and Chemistry. Vol 81A, No. 1, January-February 1977, 89–96.

Gryta, M., Influence of polypropylene membrane surface porosity on the performance of membrane distillation process, Journal of Membrane Science, 287, 67-78.

Incropera, F.P. and DeWitt, D.P., 2002. Fundamentals of heat and mass Transfer. Fifth edn. New York: John Wiley & Sons.

ISKRA, C., 2007. Convective mass transfer between a hydrodynamically developed airflow and liquid water with and without a vapor permeable membrane, MSc. Thesis, Department of Mechanical Engineering, University of Saskatchewan. Saskatoon, Saskatchewan.

ISO. 1991. ISO Standard 5167-1, Measurement of Fluid Flow by Means of Pressure Differential Devices. International Organization for Standardization

Johnson, A.B., R.W. Besant, and G.J. Schoenau. 1995. Design of multi-coil run-around heat exchanger systems for ventilation air heating and cooling. ASHRAE Transactions 101(2): 967–78.

Keep Right Refrigeration. 2009. Keep Right Refrigeration Run Around Heat Recovery, www.keeprightrefrigeration.com/products/kra.htm, Accessed June 2009.

Kosonen, R. and Tan, F., 2004. The effect of perceived indoor air quality on productivity loss. Energy and buildings, 36(10), 981-986.

Larson, M.D., Besant, R.W and Simonson, C.J., 2008. The effect of membrane deflections on flow rate in cross flow air-to-air exchangers, HVAC&R Research, 14(2), 275-288.

Larson, M.D., Simonson, C.J., Besant, R.W. and Gibson, P.W., 2007. The elastic and moisture transfer properties of polyethylene and polypropylene membranes for use in liquid-to-air energy exchangers. Journal of membrane science, 302(1), 136-149.

Larson, M.D., 2006. The performance of membrane in a newly proposed run-around heat and moisture exchanger, MSc. Thesis, Department of Mechanical Engineering, University of Saskatchewan. Saskatoon, Saskatchewan.

Linke, W.F. 1965. Solubilities: Inorganic and Metal-Organic Compounds K-Z. Vol II, Fourth Edition. American Chemical Society, Washington, D.C.. page 480.

London, A.L. and Kays, W.M., 1951. Liquid-coupled indirect-transfer regenerator for gas-turbine plants. Transactions of the American Society of Mechanical Engineers, 73(5), 529-542.

Mahmud, K. 2009. Design and testing of a laboratory RAMEE system with counter flow exchangers to transfer heat and water vapor between supply and exhaust air flows. MSc. Thesis, Department of Mechanical Engineering, University of Saskatchewan. Saskatoon, Saskatchewan.

Mathur, G.D., 1990. Long-term performance prediction of refrigerant charged flat plate solar collector of a natural circulation closed loop. ASME HTD 157:19-27. American Society of Mechanical Engineers, New York.

McDonald, T.W. and Shivprasad. 1989. Incipient nucleate boiling and quench study. Proceedings of CLIMA 2000 1:347-352. Sarajevo, Yugoslavia.

Mesquita, L.C.S., Harrison, S.J. and Thomey, D., 2006. Modeling of heat and mass transfer in parallel plate liquid –desiccant dehumidifiers, Solar Energy, 80, 1475-1482.

Mishra, M., Das, P.K. and Sarangi, S., 2004. Transient behavior of crossflow heat exchangers with longitudinal conduction and axial dispersion. Journal of heat transfer, 126(3), 425-433.

Oakley, D. 1972. Natural Radiation Exposure in the United States, ORP/SID Report., 72-1, U.S. EPA, Washington, DC.

Park, M.S., Howell, J.R., Vliet, G.C. and Peterson, J., 1994. Numerical and experimental results for coupled heat and mass transfer between a desiccant film and air in cross flow, International Journal of Heat and Mass Transfer 37(Suppl. 1), 395–402.

Romie, F.E., 1983. Transient response of gas-to-gas crossflow heat exchangers with neither gas mixed. Journal of heat transfer, 105(3), 563-570.

Seyed-Ahmadi, M. 2008. Modeling the Transient Behavior of a Run-around Heat and Moisture Exchanger System. MSc. Thesis, Department of Mechanical Engineering, University of Saskatchewan. Saskatoon, Saskatchewan.

Seyed-Ahmadi, M., Erb, B., Simonson, C., Besant, R.W. 2008a. Modeling and Simulation of the Transient Behavior of Run-around Heat and Moisture Exchanger System, Part I: Model Formulation and Verification. Submitted for publication in the International Journal of Heat and Mass Transfer.

Seyed-Ahmadi, M., Erb, B., Simonson, C., Besant, R.W. 2008b. Modeling and Simulation of the Transient Behavior of Run-around Heat and Moisture Exchanger System, Part II: Sensitivity Studies for a Range of Initial conditions. Submitted for publication in the International Journal of Heat and Mass Transfer.

Shang, W. and Besant, R.W. 2008. Theoretical and Experimental Methods for the Sensible Effectiveness of Air-to-Air Energy Recovery Wheels, HVAC&R Research., Volume 14, Number 3, 373-396.

Simonson, C.J., 2007. Heat and energy wheels, Encyclopedia of Energy Engineering and Technology, Volume 2, Edited by Barney Capehart, CRC Press, Boca Raton, FL, 794-800.

Spiga, G. and Spiga, M., 1987. Two-dimensional transient solutions for crossflow heat exchangers with neither gas mixed. Journal of heat transfer, 109(2), 281-286.

Srihari, N. and Das, S.K., 2008. Experimental and theoretical analysis of transient response of plate heat exchangers in presence of nonuniform flow distribution. New York, N.Y.: American Society of Mechanical Engineers.

Student. 1908. The Probable Error of a Mean. Biometrika (6), 1-25.

Vali, A. 2009. Modeling a Run-around Heat and Moisture Exchanger System Using Two Counter/Cross Flow Exchangers. MSc. Thesis, Department of Mechanical Engineering, University of Saskatchewan. Saskatoon, Saskatchewan.

Venmar CES. 2009. Venmar CES Inc. Cost-Effective Commercial Ventilation Product Website. www.venmarces.com/products., Accessed June 2009.

Wu, X.P., Johnson, P. and Akbarzadeh, A., 1997. Application of heat pipe heat exchangers to humidity control in air-conditioning systems. Applied thermal engineering, 17(6), 561-568.

Zhang, L.Z. and Niu, J.L., 2002. Effectiveness correlations for heat and moisture transfer processes in an enthalpy exchanger with membrane cores, *ASME J. Heat Transfer*, 124, 922-929.

Zhang, G., Zhang, Y.F., Fang, L. 2008. Theoretical study of simultaneous water and VOCs adsorption and desorption in a silica gel rotor, Indoor Air., 18, 37-43.

Zaytsev, I.D. and Aseyev, G.G., 1992. Properties of Aqueous Solutions of Electrolytes. CRC Press, Inc.